Editorial

〔Lab Med Int 2024; 3(3): 59-60〕

Extracellular vesicles control both coagulation and fibrinolysis to promote deep venous thrombosis

*Munekazu Yamakuchi, MD, PhD**

* Department of Laboratory and Vascular Medicine, Graduate School of Medical and Dental Sciences, Kagoshima University, 8-35-1 Sakuragaoka, Kagoshima 890-8544, Japan. E-mail: munekazu@m.kufm.kagoshima-u.ac.jp

See article volume 3(3): 95-107

Venous thromboembolism (VTE) is a disease concept that combines deep venous thrombosis (DVT) and pulmonary embolism (PE). Various pathological conditions can cause DVT, which is generated by Virchow's triad: stasis of blood flow, damage to vascular endothelial cells, and hypercoagulable states[1]. Although DVT is primarily characterized by swelling and pain in the lower extremities, many cases are asymptomatic, which can lead to PE and sudden death; therefore, prompt and accurate diagnosis is required. However, no clear diagnostic biomarkers are available for diagnosis. Echocardiography is suitable for identifying thrombi, and D-dimer is the most commonly used blood test. Although D-dimer levels within the reference range have diagnostic value as a rule-out test, even a high value has low disease specificity[2]. What are the alternative biomarkers for D-dimer levels?

Shiotsu et al. focused on large extracellular vesicles (LEVs) in blood to answer this question. Extracellular vesicles (EVs) are lipid bilayer membrane vesicles that encapsulate functional molecules such as proteins and nucleic acids and are secreted in various sizes. The minimal information for studies of extracellular vesicles 2018 (MISEV 2018) recommended referring to EVs separately according to their size and density, such as medium/large EVs (m/lEV) and small EVs (sEV); however, their functional differences are not well understood[3]. They included 28 patients with DVT, most of whom had carcinoma. In cancer-associated thrombosis, EVs derived from cancer cells promote thrombogenesis[4]. This is mainly due to the enhancement of the coagulation system by tissue factor on the EV membrane surface and promotion of platelet aggregation by podoplanin on the membrane[5]. They found that CD31 and CD61 positive LEVs, which are considered platelet-derived, increased in patients with DVT.

One important aspect of the study by Shiotsu et al. is that not only the membrane component of LEV, but also miR-4485, which is contained in LEV, was significantly increased in DVT patients. Receiver operating characteristic analysis indicates that miR-4485 could be a potential biomarker for DVT. Although various DVT-related miRNAs have been proposed[6], new miRNAs can be added to the list. Another important aspect was the identification of tissue plasminogen activator (tPA) as a target gene of miR-4485. LEVs from patients with DVT suppressed tPA expression in human umbilical vein endothelial cells (HUVECs). tPA is secreted from the Weibel-Palade bodies of endothelial cells and is present in the blood, mostly in complex with its specific inhibitor, plasminogen activator inhibitor 1 (PAI-1). tPA converts plasminogen into plasmin and initiates fibrinolytic reactions. Therefore, miR-4485 may promote DVT by decreasing tPA levels and delaying the fibrinolytic reaction. They found that LEV containing miR-4485 must be platelet-derived, indicating a novel phenomenon in which platelets regulate the fibrinolytic system.

Several points need to be addressed. First, platelet-derived LEVs increase in patients with DVT due to thrombus formation and platelet activation, and can this be a predictor of DVT, changes in this miRNA as DVT progresses, and whether the number of LEVs correlate with the degree of DVT are unknown. Second, although miR-4485 in LEVs is endocytosed by endothelial cells and inhibits tPA expression, in vivo data are required to demonstrate that the prothrombotic effects of LEVs are mediated by miR-4485. Furthermore, miR-4485 may have many other target genes besides tPA, and a comprehensive evaluation of the miRNAs encapsulated in LEVs is required based on the results of a comprehensive analysis of these genes. Finally, could the regulation of LEVs

or miR-4485 be a therapeutic target? As described, the increase in miR-4485 in platelets and endothelial cells appears to be associated with mitochondrial function; however, the underlying mechanism has not been elucidated. Although further studies are needed, this study reveals a novel role for platelet-derived LEVs in the pathogenesis of DVT and is a valuable clue for future research.

References

1) Stone J, Hangge P, Albadawi H, et al. Deep vein thrombosis: pathogenesis, diagnosis, and medical management. Cardiovasc Diagn Ther. 2017 ; 7:S276-S84. doi: 10.21037/cdt.2017.09.01.

2) Lim W, Le Gal G, Bates SM, et al. American Society of Hematology 2018 guidelines for management of venous thromboembolism: diagnosis of venous thromboembolism. Blood Adv. 2018 ; 2:3226-56. doi: 10.1182/bloodadvances.2018024828.

3) Thery C, Witwer KW, Aikawa E, et al. Andriantsitohaina R, et al. Minimal information for studies of extracellular vesicles 2018 (MISEV2018): a position statement of the International Society for Extracellular Vesicles and update of the MISEV2014 guidelines. J Extracell Vesicles. 2018 ; 7:1535750. doi: 10.1080/20013078.2018.1535750.

4) Tatsumi K. The pathogenesis of cancer-associted thrombosis. Int J Hematol. 2024 ; 119:495-504. doi: 10.1007/s12185-024-03735-x.

5) Hisada Y, Mackman N. Cancer-associated pathways and biomarkers of venous thrombosis. Blood. 2017 ; 130:1499-506. doi: 10.1182/blood-2017-03-743211.

6) Fang C, Huang F, Yao M, et al. Advances in microRNA regulation of deep vein thrombosis through venous vascular endothelial cells (Review). Mol Med Rep. 2024; 29: doi: 10.3892/mmr.2024.13220.

Review

Associations between preoperative fibrinogen levels and clinicopathological factors in oral squamous cell carcinoma: A meta-analysis

Akemi Inoue, Toshihide Matsumoto*, Yuka Ito*, Zehao Jiang*, †Hiroyuki Takahashi**

†Correspondence: Kitasato University School of Allied Health Sciences, 1-15-1 Kitazato Minimi-ku, Sagamihara, Kanagawa 252-0373, Japan
E-mail: hitakaha@med.kitasato-u.ac.jp
Received October 12, 2023; accepted July 1, 2024
* Kitasato University, School of Allied Health Sciences

ABSTRACT

Objectives: There is a lack of consensus among researchers regarding the relationship between preoperative fibrinogen levels and clinicopathological factors in oral squamous cell carcinoma (OSCC). The aim of this meta-analysis was to evaluate and clarify these associations in OSCC.
Methods: The PubMed, Web of Science, and Embase databases were examined for studies that evaluated the relationships between preoperative fibrinogen level and clinicopathological factors until October 12, 2023.
Results: Three studies comprising a total of 509 patients were included in the analysis. No correlations between preoperative fibrinogen levels and gender (odds ratio [OR], 0.93; 95% confidence interval [CI], 0.34–2.55; I^2=78%; p=0.89), the pT category (OR, 2.52; 95% CI, 0.75–8.46; I^2=81%; p=0.13), lymph node metastasis (OR, 0.75; 95% CI, 0.37–1.51; I^2=52%; p=0.41), and TNM stage (OR,1.59; 95% CI, 0.64-3.93; I^2=73%; p=0.32) were observed in the meta-analysis. However, the heterogeneity was found to be high or very high. The influence of publication bias was considered in this analysis.
Conclusion: Preoperative fibrinogen levels were not related to gender, the pT category, lymph node metastasis, or TNM stage in OSCC. The lack of sufficient data may render the data integration unreliable. Therefore, additional studies with larger sample sizes and similar cut-off values are required to validate the findings of this study.
〔Lab Med Int 2024; 3(3): 61-65〕

Key Words
Oral squamous cell carcinoma, fibrinogen, clinicopathological parameters, meta-analysis

I. Introduction

In Japan, oral cancer accounts for almost 1% of all cancers [1] and an increasing number of cancer-related deaths [2]. Oral squamous cell carcinoma (OSCC) is the most common type of oral cancer, and surgical resection is the most common treatment for this disease. Patients with advanced cancer have a significantly worse quality of life than those with early cancer [3].

Several methods, including assessments of the preoperative fibrinogen level, have been tested for the early detection and prognostic prediction of oral cancer [4)–6)]. There is a lack of consensus among studies on the relationship between preoperative fibrinogen levels and clinicopathological factors in OSCC. Therefore, this study meta-analysis was conducted to evaluate and clarify the aforementioned associations in OSCC.

II. Materials and methods

Search strategy

This meta-analysis was performed in accordance with the 2020 Preferred Reporting Items for Systematic Re-

views and Meta-analyses Statement [7]. The PubMed, Web of Science, and Embase databases were searched to identify articles on the relationship between preoperative fibrinogen levels and clinicopathological factors in OSCC, published until August 3, 2023. The following search keywords were used: "oral squamous cell carcinoma" [AND] "fibrinogen." We searched all fields in the literature. Additionally, the reference lists of the included papers were examined. Studies published in languages other than Japanese or English, those that used cultured cells or animal experiments, case reports, and articles lacking data on the relationships between clinicopathological factors and preoperative fibrinogen level were excluded from this study.

Statistical analysis

Statistical analysis was performed using Review Manager 5.4 (Cochrane Collaboration, Oxford, UK) to combine the data and the effect estimate. A random effects model was used due to the presumed population differences among the included studies. The effect estimates are presented with their 95% confidence intervals (CIs). The intervention effects were measured using odds ratios (ORs), and the heterogeneity among studies was calculated using the I^2 values. Publication bias was assessed using funnel plots for the primary endpoint.

III. Results

Study selection

A total of 50, 24, and 69 studies were identified from the PubMed, Web of Science, and Embase databases (**Figure 1**). In the primary screening, the titles and abstracts were examined to exclude review articles, studies with

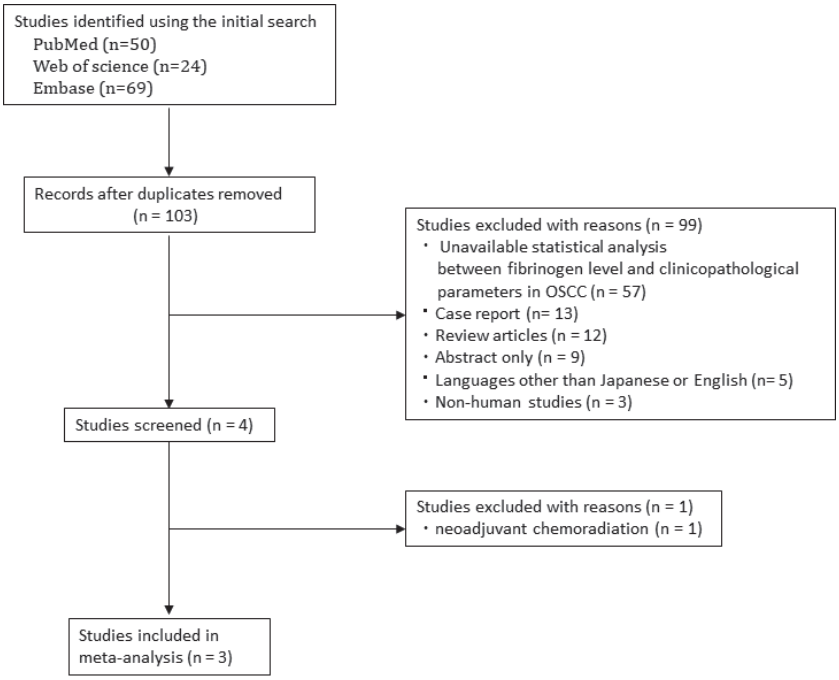

Figure 1 Flow chart for the selection of studies in this meta-analysis. OSCC, oral squamous cell carcinoma.

Table 1 Characteristics of the studies included in this meta-analysis.

No.	First author	Journal (year)	Population	Hospital facility	Period	No. of cases.	FIB cut-off
1	Liang YJ	BMC Cancer. (2021)	China	Guanghua Hospital of Stomatology	January 2015 - December 2018	202	3.33 (g/L)
2	Caruntu A	Cancers (Basel). (2021)	Romania	Carol Davila Central Military Emergency Hospital	2016 - 2019	223	525 (mg/dL)
3	Inoue A	Hum Pathol. (2022)	Japan	Kitasato University Hospital	2014 - 2016	84	342 (mg/dL)

no., number; FIB, fibrinogen.

inappropriate research designs, non-human studies, and those published in languages other than Japanese and English. Of the five studies remaining after primary screening, two were excluded due to cases of advanced cancer or treatment by neoadjuvant chemoradiation. Finally, three articles with a total of 509 patients were included in the analysis (**Table 1**). Relationships between clinicopathological factors and preoperative fibrinogen levels.

The preoperative fibrinogen levels were not associated with gender (OR, 0.93; 95% CI, 0.34–2.55; I^2=78%; p=0.89; **Figure 2A**), the pT category (OR, 2.52; 95% CI, 0.75–8.46; I^2=81%; p=0.13; **Figure 2B**), which indicates the size or local extent of the primary tumor, lymph node metastasis (OR, 0.75; 95% CI, 0.37–1.51; I^2=52%; p=0.41; **Figure 2C**), and TNM stage (OR, 1.59; 95% CI, 0.64–3.93; I^2=73%; p=0.32; **Figure 2D**). Associations between fibrinogen levels and other clinicopathological factors, such as age and tumor differentiation, could not be analyzed due to a lack of data. The heterogeneity, demonstrated by the I^2 values, was high or very high. The funnel plots for gender, the pT category, lymph node metastasis, and TMN stage demonstrated asymmetry, suggesting the possibility of publication bias (**Figure 3**).

IV. Discussion

Fibrinogen is a blood coagulation factor produced in the liver; it is converted into fibrin by thrombin to form fibers and strong fibrin clots [8) 9)]. The expression of this classic acute phase reactant is considerably increased in the liver and blood during inflammatory conditions [10)]. In addition, hyperfibrinogenemia and a cancer-associated systemic inflammatory response are strongly associated with cancer progression and prognosis [11)]. A meta-analysis of 17 studies revealed that higher pretreatment plasma fibrinogen levels predicted poor overall survival (OS) and disease- or progression-free survival in patients with

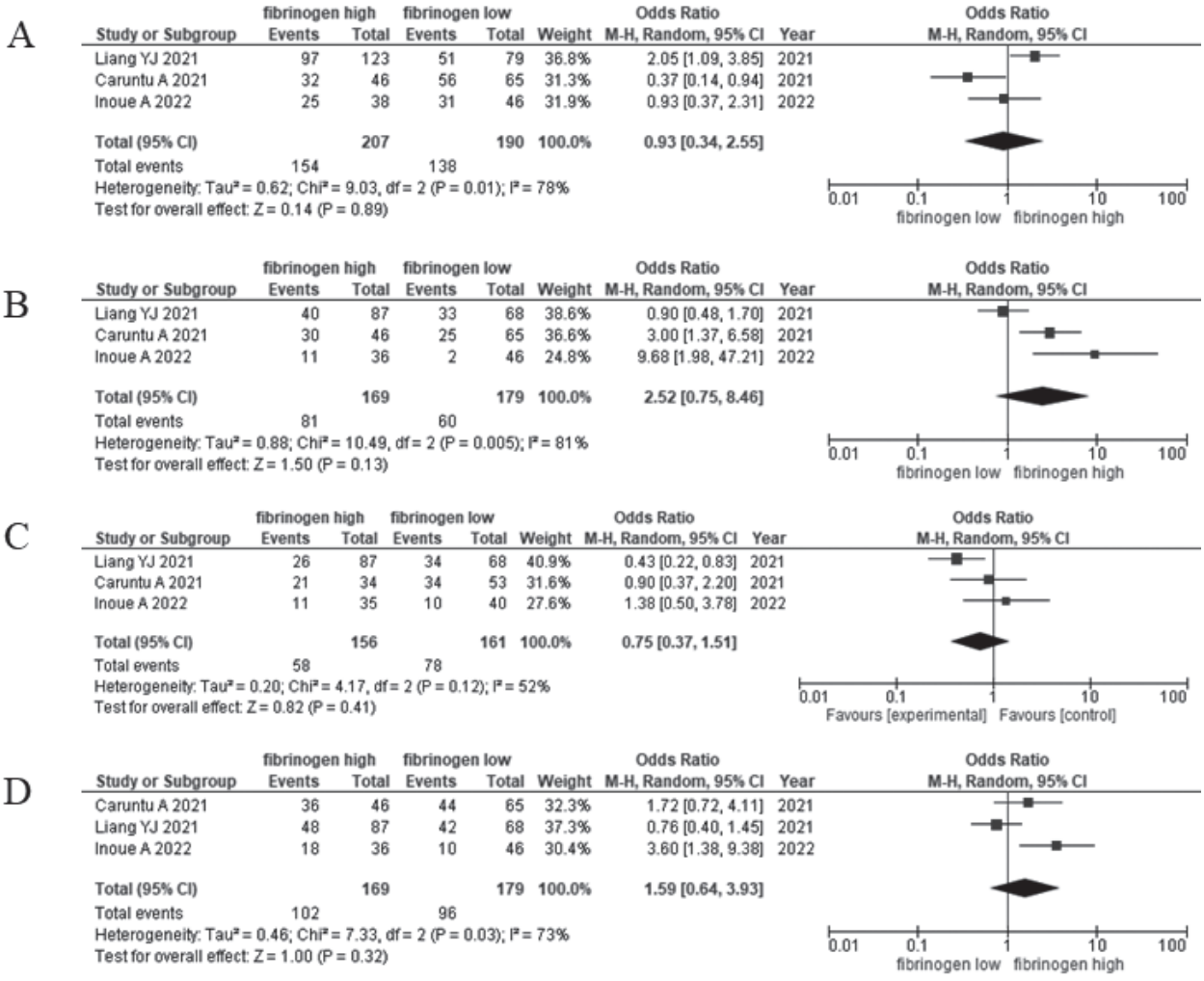

Figure 2 Meta-analysis for the fibrinogen level and clinicopathological parameters in OSCC. Forest plots showing the correlations between fibrinogen levels and gender (A), the pT category (B), lymph node metastasis (C), and TNM stage (D) in OSCC.

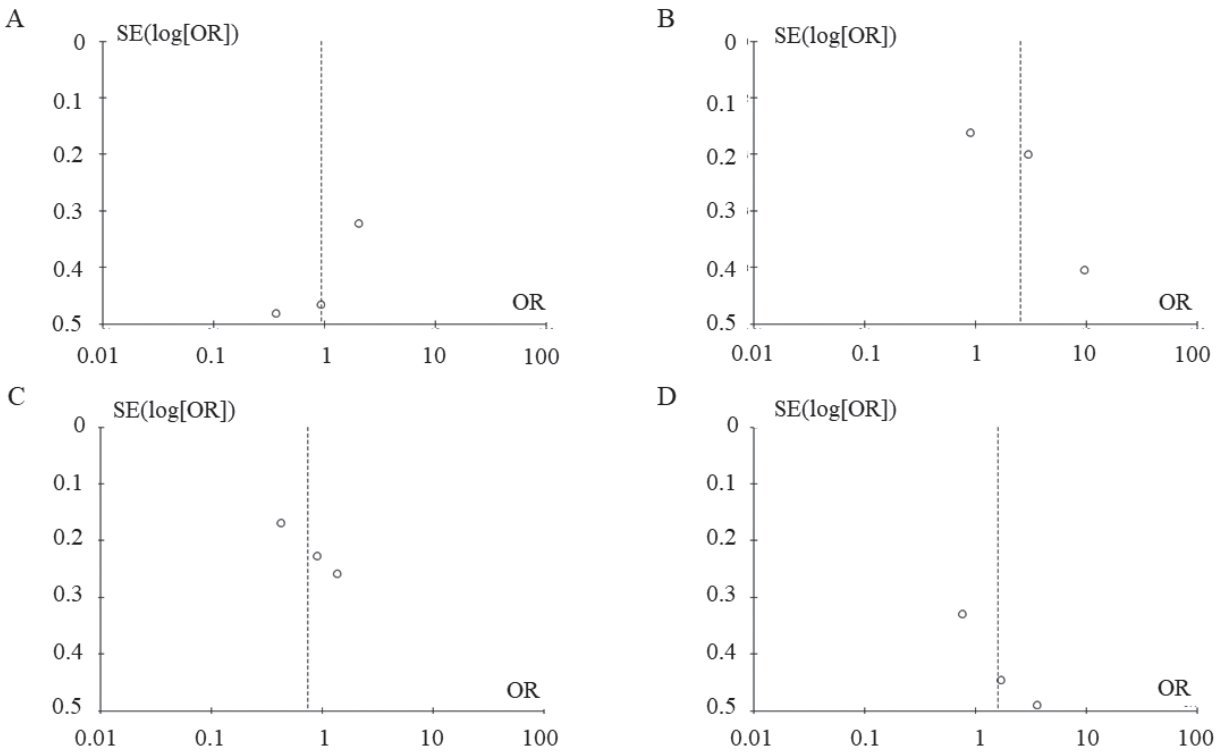

Figure 3 Funnel plots for the fibrinogen levels. (A) gender, (B) pathological pT category, (C) lymph node metastasis, and (D) TNM stage.

lung cancer [12]. In a recent study, preoperative fibrinogen levels in colorectal cancer were correlated with several clinicopathological factors, including age, tumor differentiation status, tumor location, pT category, and TNM stage; moreover, an elevated fibrinogen level was independently correlated with poor OS and cancer-specific survival [13]. However, no clear conclusions regarding the relationship between preoperative fibrinogen values and clinicopathological factors in OSCC have been reached.

In the current study, the preoperative fibrinogen levels were not associated with the clinicopathological features of OSCC. Inoue et al. and Caruntu et al. reported high preoperative fibrinogen levels and the pT category in OSCC [5,6]. High preoperative fibrinogen levels were detected in many patients with advanced TNM stages in the studies by Liang et al.; additionally, several cases of lymph node metastasis due to the high preoperative fibrinogen levels were reported [4]. Furthermore, according to Liang et al. [4], high levels of preoperative fibrinogen were more common in men, but no significant difference based on sex was observed in the studies by Inoue et al. and Caruntu et al. [5,6]. Despite the concordant and inconsistent reports on the relationship between preoperative fibrinogen levels and clinicopathological factors, the I^2 statistics in all studies showed high or very high heterogeneity in OSCC.

One of the limitations of the current meta-analysis was the difference in the cut-off values that separated the high and low fibrinogen values in each study. Moreover, the number of articles included in this meta-analysis was low, resulting in high heterogeneity and publication bias. Nevertheless, our results indicate that preoperative fibrinogen measurement may not be useful in determining the treatment strategy. Additional studies using similar cut-off values and larger sample sizes are necessary to validate the findings of this study.

Abnormalities in the blood coagulation and fibrinolysis system are frequently observed in patients with malignant tumors, and these abnormalities are linked to the progression of DIC and thrombosis [14]. In addition, the fibrinolysis system affects the growth and metastasis of malignant tumors [15]. Several thrombin-related factors, such as plasminogen activator inhibitor-1 polymorphism [16], the low-production allele of the VEGF +936C/T polymorphism [17], coagulation factor XIII [18], and the 1040C/T polymorphism influencing thermal stability and activity of thrombin activatable fibrinolysis inhibitor [19], have been linked to oral carcinogenesis. As previously described, there are few reports on the relationships of the blood coagulation and fibrinolysis system with ma-

lignancy, including studies on fibrinogen in malignant tumors of the oral region.

V. Conclusions

Despite the limitations of this study, no associations of fibrinogen levels with gender, the pT category, lymph node metastasis, or TNM stage were observed. Nonetheless, further studies on the blood coagulation and fibrinolysis system, including fibrinogen, are required to confirm these findings in OSCC.

Conflicts of interest: none.

Funding source: This research did not receive any specific grant from funding agencies in the public, commercial, or not-for-profit sectors.

References

1) Japan Society of Clinical Oncology. Clinical Practice guideline (2019). Available from: http://www.jsco-cpg.jp/oral-cavity-cancer/guideline/#II (Accessed on: July 22, 2023).
2) Almangush A, Mäkitie AA, Triantafyllou A, et al. Staging and grading of oral squamous cell carcinoma: An update. Oral Oncol 2020; 107: 104799. doi: 10.1016/j.oraloncology.2020.104799.
3) Bschorer M, Schneider D, Goppold K, et al. Quality of life and survival rate after primary surgical treatment of oral squamous cell carcinoma: A retrospective study with 18 years of follow-up. J Craniomaxillofac Surg 2022; 50 (2): 170–7. doi: 10.1016/j.jcms.2021.09.016.
4) Liang YJ, Mei XY, Zeng B, et al. Prognostic role of preoperative D-dimer, fibrinogen and platelet levels in patients with oral squamous cell carcinoma. BMC Cancer 2021; 21 (1): 122. doi: 10.1186/s12885-021-07841-5.
5) Inoue A, Matsumoto T, Ito Y, et al. TP53 positivity combined with high fibrinogen expression defines a subtype of oral squamous cell carcinoma with an unfavorable prognosis. Hum Pathol 2022: 130: 25-35. doi: 10.1016/j.humpath.2022.10.008.
6) Caruntu A, Moraru L, Lupu M, et al. The Hidden Treasures of Preoperative Blood Assessment in Oral Cancer: A Potential Source of Biomarkers. Cancers (Basel) 2021; 13 (17): 4475. doi: 10.3390/cancers13174475.
7) Page MJ, McKenzie JE, Bossuyt PM, et al. The PRISMA 2020 statement: An updated guideline for reporting systematic reviews. BMJ 2021; 372: n71. doi: 10.1136/bmj.n71.
8) Zhang X, Long Q. Elevated serum plasma fibrinogen is associated with advanced tumor stage and poor survival in hepatocellular carcinoma patients. Medicine (Baltimore) 2017; 96 (17): e6694. doi: 10.1097/MD.0000000000006694.
9) Levy JH, Welsby I, Goodnough LT. Fibrinogen as a therapeutic target for bleeding: a review of critical levels and replacement therapy. Transfusion 2014; 54 (5): 1389-405. doi: 10.1111/trf.12431.
10) Castell JV, Gómez-Lechón MJ, David M, et al. Interleukin-6 is the major regulator of acute phase protein synthesis in adult human hepatocytes. FEBS Lett 1989; 242 (2): 237–9. doi: 10.1016/0014-5793 (89) 80476-4.
11) Wang PX, Wang HJ, Liu JH, et al. A nomogram combining plasma fibrinogen and systemic immune-inflammation index predicts survival in patients with resectable gastric cancer. Sci Rep 2021; 11 (1): 10301. doi: 10.1038/s41598-021-89648-9.
12) Zhang Y, Cao J, Deng Y, et al. Pretreatment plasma fibrinogen level as a prognostic biomarker for patients with lung cancer. Clinics (Sao Paulo) 2020; 75: e993. doi: 10.6061/clinics/2020/e993.
13) Sun Y, Han W, Song Y, et al. Prognostic value of preoperative fibrinogen for predicting clinical outcome in patients with nonmetastatic colorectal cancer. Cancer Manag Res 2020; 12: 13301-9.
14) Zacharski LR, Wojtukiewicz MZ, Costantini V, et al. Pathways of coagulation/fibrinolysis activation in malignancy. Semin Thromb Hemost 1992; 18 (1): 104-16. doi: 10.1055/s-2007-1002415.
15) Lindahl AK, Odegaard OR, Sandset PM, et. al. Coagulation inhibition and activation in pancreatic cancer. Changes during progress of disease. Cancer 1992; 70 (8): 2067-72. doi: 10.1002/1097-0142 (19921015) 70:8<2067::aid-cncr2820700809>3.0.co;2-a.
16) Vairaktaris E, Yapijakis C, Serefoglou Z, et al. Plasminogen activator inhibitor-1 polymorphism is associated with increased risk for oral cancer. Oral Oncol 2006; 42 (9): 888-92. doi: 10.1016/j.oraloncology.2005.12.005.
17) Yapijakis C, Vairaktaris E, Vassiliou S, et al. The low VEGF production allele of the +936C/T polymorphism is strongly associated with increased risk for oral cancer. J Cancer Res Clin Oncol 2007; 133 (10): 787-91. doi: 10.1007/s00432-007-0240-y.
18) Vairaktaris E, Vassiliou S, Yapijakis C, et al. Increased risk for oral cancer is associated with coagulation factor XIII but not with factor XII. Oncol Rep 2007;18 (6): 1537-43.
19) Vairaktaris E, Yapijakis C, Nkenke E, et al. The 1040C/T polymorphism influencing thermal stability and activity of thrombin activatable fibrinolysis inhibitor is associated with risk for oral cancer. Am J Hematol 2007; 82 (11): 1010-2.

Case Report

A patient with partial E phenotype expressing alloanti-E antibody after transfusion with platelet concentrates

Marie Yamada[*1], Naotomo Yamada*[*1], †Yasushi Kubota*[*2,3], Emi Takahashi*[*4], Mami Nakao*[*1], Toru Miyazaki*[*4], Shinichiro Sato*[*4], Hideaki Nakamura*[*1], Shinya Kimura*[*2], †Eisaburo Sueoka*[*5]*

†Correspondence: Department of Transfusion and Cell Therapy, Saitama Medical Center, Saitama Medical University, 1981 Kamoda, Kawagoe 350-8550, Japan. E-mail: kubotay@saitama-med.ac.jp.
Department of Clinical Laboratory Medicine, Faculty of Medicine, Saga University, 5-1-1 Nabeshima, Saga 849-8501, Japan.
E-mail: sueokae@cc.saga-u.ac.jp
Received November 27, 2023; accepted July 18, 2024
*1 Department of Transfusion Medicine, Saga University Hospital, 5-1-1 Nabeshima, Saga 849-8501, Japan.
*2 Division of Hematology, Respiratory Medicine and Oncology, Department of Internal Medicine, Faculty of Medicine, Saga University, 5-1-1 Nabeshima, Saga 849-8501, Japan.
*3 Department of Transfusion Medicine and Cell Therapy, Saitama Medical Center, Saitama Medical University, 1981 Kamoda, Kawagoe 350-8550, Japan.
*4 Laboratory section of Japanese Red Cross Hokkaido Block Blood Center, Sapporo, Japan.
*5 Department of Clinical Laboratory Medicine, Faculty of Medicine, Saga University, 5-1-1 Nabeshima, Saga 849-8501, Japan.

ABSTRACT

Partial E is a qualitative mutation of the E antigen that lacks one or more components of the E antigen, and several variants have been reported. We report a 72-year-old man having partial E (allele name: *RHCE*cEFM*) who expressed alloanti-E antibody after platelet concentrates transfusions. The patient was diagnosed with relapsed non-Hodgkin's lymphoma and received salvage chemotherapy. One platelet transfusion was from a donor with the R1R2 phenotype when he received three rounds of transfusions of 10 units platelet concentrate from February to April 2009 for myelosuppression by chemotherapy. The patient, who had no history of transfusion prior to 2009, was sensitized by small amounts of allogeneic red blood cells contaminating platelet concentrates and developed alloanti-E antibodies. The anti-E antibody was detected in the patient's serum, and Rh phenotype determination revealed relatively weak reactivity (2+) for a monoclonal anti-E reagent but negative for another one. According to these results, an E variant phenotype was suspected. Direct sequencing of exon 5 on the *RHCE* gene revealed mutations of C to G at nucleotide c.697 and A to G at nucleotide c.712 in the *E* allele, resulting in amino acid substitutions phenylalanine to alanine and methionine to valine, respectively. Combining this result with reactivity based on an antigen screening test for E antigen using monoclonal antibodies, we classified the patient's RBC phenotype as partial E due to *RHCE* alterations. To our knowledge, this is the first case report of the *RHCE* rare variant patient with alloanti-E antibody produced by platelet concentrates transfusions.

〔Lab Med Int 2024; 3(3): 66-69〕

Key Words
Rh blood type, E antigen, Partial E blood type, *RHD* gene

I. Introduction

Partial E blood type is a rare E variant that lacks some of the Rh system antigens[1)-5)]. There are at least 5 types of partial E in the genetic background. These include a single nucleotide exchange T to A at codon 500 in the *RHCE* gene, resulting in amino acid substitution of methionine to lysine at codon 167 (allele name: *RHCE**-

cEEW) ; replacement of exons 1, 2, and 3 in the *RHCE* gene with the *RHD* gene, resulting in a hybrid *RHD-CE* gene (allele name: *RHCE*cEKK*) ; a rearrangement of exon 5 in the *RHCE* gene with the *RHD* gene; and amino acid substitutions glutamic acid to glutamine at codon 233 and methionine to valine at codon 238, resulting in the *RHCE-D-CE* variant hybrid gene (allele name: *RHCE*cEFM*) ; amino acid substitution arginine to threonine at codon 201, which locates in transmembrane domain 6, resulting in the *RHCE-D-CE* rearranged gene (allele name: *RHCE*cIV*) ; and a one-base mutation G to A at codon 461 with amino acid substitution arginine to threonine at codon 154 in the *RHCE* gene (allele name: *RHCE*cEKH*)[3),4)].

Here we report the unique clinical course of a non-Hodgkin's lymphoma (NHL) patient who expressed alloanti-E antibodies after platelet transfusion, and the results of genetic and serological analysis for RhE phenotype.

II. Case and clinical course

In 2009, a seventy-two-year-old man was admitted to our hospital because of recurrence of NHL. His blood type was A and RhD positive based on serological tests. His medical history showed no blood transfusions before 2009, and in 2006 he tested negative for irregular antibodies as determined by the low ionic strength solution-enhanced indirect anti-globulin test (LISS-IAT) and the polyethylene glycol-enhanced indirect anti-globulin test (PEG-IAT).

The patient received three rounds of transfusions of 10 units platelet concentrate between February and April 2009 due to myelosuppression caused by chemotherapy; after these transfusions, he also received red blood cell (RBC) concentrates because of severe anemia. Screening for irregular antibodies before RBC transfusion was conducted and returned a result of positive for anti-E antibody. Precise examination for Rh phenotypes showed positive agglutination of RBCs to the following monoclonal antibodies: anti-C (4+), anti-c (3+), anti-E (w+), and anti-e (3+), as well as weak activity for monoclonal anti-E reagent. Reactivity for human type A anti-E sera was positive (1+) by PEG-IAT, and no reactivity between the patient's own RBC and patient serum with anti-E antibody was observed by PEG-IAT.

In 2013 the patient was readmitted to our hospital due to a second relapse of NHL, at which time he received salvage chemotherapy. Severe anemia (hemoglobin 5.4 g/dL) was observed so he was given RBC transfusions. Antibody screening before RBC transfusion showed no irregular antibodies. Rh phenotype determination revealed relatively weak activity (2+) for monoclonal anti-E reagent (Ortho Bioclone®) and negative activity for another monoclonal anti-E reagent (Gamma-clone®). According to these results, an E variant was suspected and we requested further, more precise, evaluation of RhE phenotype and genotyping by the Japanese Red Cross Hokkaido Block Blood Center.

III. Methods

1. Serological tests

Twenty-three monoclonal anti-E antibodies, which are approved by the 4th International Workshop on Monoclonal Antibodies Against Human Red Blood Cells and Related Antigens, were used for evaluation of RhE phenotype. R1R2 RBC and rr RBC were used for positive and negative controls, respectively. Four types of unclassified partial E RBCs were also analyzed in these assays.

2. Genotyping

Genomic DNA was extracted from whole blood. Specific primers for exons 3, 4, and 5 of the *RHCE* gene were designed and genomes amplified by PCR were sequenced. Primer sets used for the *RHCE* gene are as follows: exon 3 sense 5'-ATCCTGGCTCTCCTTCTCA-3', anti-sense 5'-CAAGTGATCTTCCCTCCTCAA-3'; exon 4 sense 5'-TGAACTTTCTCCAAGGACCAT-3', anti-sense 5'-AATTTAGCAAACACTACTCAAAGAAG-3'; exon 5 sense 5'-GCAACAGAGCAAGAGTCCA-3', anti-sense 5'-GTGACCACCCAGCATTCTT-3'.

3. Ethics

This study was approved by the Institutional Review Board of Saga University Hospital (2020-02-R-11).

IV. Results

1. Serological examinations

The patient's RBCs showed no reactivity against 13 of the 23 monoclonal anti-E antibodies examined (**Table 1**). They showed reactive patterns that resembled one of the unclassified partial E RBCs against monoclonal anti-E antibodies (**Table 1**).

2. Genotyping

Exons 3 and 4 of the *RHCE* gene had no mutation. Heterozygous mutation peaks were observed at nucleotides c.676 (C to G), c.697 (C to G), and c.712 (A to G) in the *E* allele. Among them, the c.676C>G (p.Pro226Ala) mutation is responsible for the expression of e antigen, which was positive in the patient's RBCs. In addition, the c.697C>G and c.712A>G sequences are identical with the sequences in exon 5 of the *RHD* gene. These results suggest that a partial region in exon 5 of the *RHCE* gene was substituted into a homologous region in exon 5

of the *RHD* gene, resulting in an *RHCE-D-CE* gene containing amino acid substitutions p.Gln233Glu and p.Met238Val, producing a partial E phenotype (allele name: *RHCE*cEFM*) (**Fig. 1**).

V. Discussion

In the literature, five types of partial E have been evaluated genetically[3),4)]. In addition to the partial E phenotype, E^{w} (RH11) phenotype—a rare variant form of E

Table 1 Reactive patterns of the patient's RBCs against various monoclonal anti-E antibodies

			Patient	PC	NC	partial E			
	Laboratory	Clone		R1R2	rr	EVH2	EVH3	EVH6	EVH7
1	Diagast Laboratoires	907	2+	3+	0	3+	0	0	3+
2	JRC Kanto-Koshinetsu Block Blood Center	HIRO-91	0	3+	0	0	0	w+	w+
3	JRC Kinki Block Center	OSK20-1	0	3+	0	0	0	3+	3+
4	EFS - Pays de la Loire	NaTH110-1D6	w+	4+	0	0	0	w+	1+
5	EFS - Pays de la Loire	NaTH110-1H4	w+	4+	0	0	0	w+	1+
6	Diagast Laboratoires	906	w+	4+	0	2+	0	1+	4+
7	JRC Hokkaido Block Blood Center	HMR37	0	3+	0	0	0	0	1+
8	Serologicals	MS-12	4+	4+	0	4+	0	w+	3+
9	Biotest AG	BS 270	0	4+	0	0	0	0	2+
10	Biotest AG	BS 271	0	4+	0	0	0	0	0
11	Dominion Biologicals Limited	F561 1B11	0	4+	0	0	0	4+	2+
12	Dominion Biologicals Limited	F5601E9	0	3+	0	0	0	0	2+
13	JRC Kinki Block Blood Center	OSK20	0	3+	0	0	0	3+	0
14	Diagast Laboratoires	P3x234	0	3+	0	0	0	0	3+
15	JRC Kanto-Koshinetsu Block Blood Center	HIRO-22	4+	3+	0	4+	0	1+	1+
16	JRC Kanto-Koshinetsu Block Blood Center	HIRO-23	0	3+	0	0	0	0	1+
17	JRC Kanto-Koshinetsu Block Blood Center	HIRO-24	w+	4+	0	w+	0	w+	3+
18	JRC Kanto-Koshinetsu Block Blood Center	HIRO-25	4+	4+	0	4+	w+	4+	4+
19	JRC Kanto-Koshinetsu Block Blood Center	HIRO-78	0	4+	0	0	w+	0	3+
20	JRC Kinki Block Blood Center	OSK20-2	3+	3+	0	2+	0	0	1+
21	Australian Red Cross Blood Service-NSW	3F10	0	4+	0	0	0	3+	2+
22	Australian Red Cross Blood Service-NSW	4C8	0	3+	0	0	0	3+	2+
23	Biotest AG	BS 272	2+	4+	0	3+	2+	3+	3+

PC: positive control NC: negative control

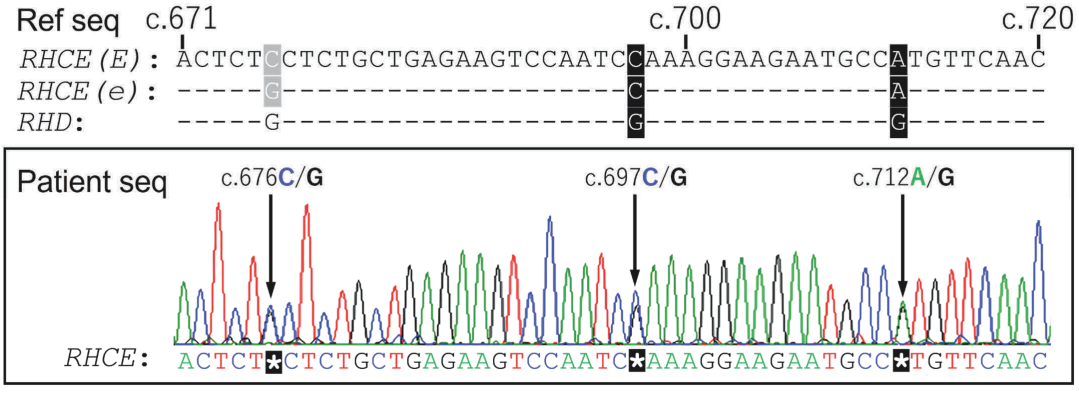

Figure 1 Three heterozygous peaks were observed in the patient *RHCE* exon5. The upper panel indicates a part of reference sequence of *RHCE* (NM_020485.5) and *RHD* (NM_016124.4) exon5. Gray background at c.676 in *RHCE* is responsible for the expression of e or E antigen. Black background at c.697 and c.712 means different nucleotide between *RHCE* and *RHD*. Hyphen in the *RHD* sequence and the *RHCE* (e) sequence indicates homology with the *RHCE* (E) sequence. We analyzed the patient sequence of *RHCE* exon3, 4 and 5 by using genomic DNA from whole blood and specific primers. The lower panel indicates a part of the direct sequence data of *RHCE* (from c.671 to c.720) of the patient. White asterisks in black background (c.676, c.697 and c.712) represents the heterozygous peak of patient *RHCE* exon5.

antigen showing unique reactivity against anti-E antibodies—has been reported, and an individual carrying the E^w (RH11) produced alloanti-E antibodies[6)-8)].

Our patient expressed alloanti-E antibody in his sera after being given platelet transfusions. The appearance of irregular antibodies to allo-RBCs after transfusions with platelet concentrates has been reported in several cases[9),10)]. Our patient received platelets from a donor who was carrying the R1R2 phenotype, suggesting that the patient was sensitized by small amounts of allo-RBCs contaminating the platelet concentrates. The subtype of detected anti-E antibody in the patient could not be determined conclusively, but was probably IgG because the antibody was negative for assay with saline and positive (1+) for PEG-IAT. Furthermore, no reactivity between the patient's own RBCs and patient serum with anti-E antibodies was observed by PEG-IAT, suggesting that the anti-E antibody was induced by allo-RBCs. In the present case, since anti-E has been detected, the appropriate response is to transfuse E antigen-negative red blood cell products.

In summary, we report a rare variant of Rh E antigen, partial E (allele name: *RHCE*cEFM*). This is the first case report of partial E (*RHCE*cEFM*) genetically confirmed in a Japanese patient with alloanti-E antibody. Our case possesses alloanti-E antibodies to the deficient part of the E antigen, possibly due to exposure from allo-RBCs expressing the E antigen in platelet concentrates. Testing with multiple monoclonal anti-E reagents or *RHCE* gene analysis is important if the reaction with the monoclonal anti-E reagent is weak because of the possibility of partial E.

Acknowledgments

This work was supported in part by the following Grants-in Aid for Cancer Research: Special Cancer Research, from the Ministry of Education, Science, Sports and Culture, Japan, and for the Research on Hematopoietic Stem Cell Preservation Study from Saga Prefecture, Japan, and Saitama Medical University Research Grant (No. 23-B-1-04).

Authorship

Contributions: M.Y., N.Y., and Y.K. performed the analyses, interpreted the data and wrote the paper. E.T., T.M., and S.S. performed serological tests and genotyping for RhE phenotype. M.N., H.N., and S.K. interpreted the data. E.S. designed the research, interpreted the data, and wrote the paper. In addition, all authors provided their final approval of the manuscript.

Conflicts of Interest

The authors declare that they have no conflict of interest.

References

1) Avent ND, Reid ME. The Rh blood group system: a review. Blood 2000; 95 (2): 375-87.
2) Avent ND, Finning KM, Liu W, et al. Molecular biology of partial D phenotypes. Transfus Clin Biol 1996; 3 (6): 511-6. doi: 10.1016/s1246-7820 (96) 80073-5.
3) Noizat-Pirenne F, Mouro I, Gane P, et al. Heterogeneity of blood group RhE variants revealed by serological analysis and molecular alteration of the RHCE gene and transcript. Br J Haematol 1998; 103 (2): 429-36. doi: 10.1046/j.1365-2141.1998.01004.x.
4) Kashiwase K, Ishikawa Y, Hyodo H, et al. E variants found in Japanese and c antigenicity alteration without substitution in the second extracellular loop. Transfusion 2001; 41 (11): 1408-12. doi: 10.1046/j.1537-2995.2001.41111408.x.
5) Chérif-Zahar B, Raynal V, D'Ambrosio AM, et al. Molecular analysis of the structure and expression of the RH locus in individuals with D--, Dc-, and DCw- gene complexes. Blood 1994; 84 (12): 4354-60.
6) Strobel E, Noizat-Pirenne F, Hofmann S, et al. The molecular basis of the Rhesus antigen Ew. Transfusion 2004; 44 (3): 407-9. doi: 10.1111/j.1537-2995.2004.00655.x.
7) Lubenko A, Burslem SJ, Fairclough LM, et al. A new qualitative variant of the RhE antigen revealed by heterogeneity among anti-E sera. Vox Sang 1991; 60 (4): 235-40. doi: 10.1111/j.1423-0410.1991.tb00912.x.
8) Henke J, Kasulke D. The first example of the Rh antigen Ew in Western Europe. Vox Sang 1976; 30 (4): 305-7. doi: 10.1111/j.1423-0410.1976.tb02832.x.
9) Bartley AN, Carpenter JB, Berg MP. D^+ Platelet trans-fusion in D^-patients: cause for concern? Immunohematology 2009; 25 (1): 5-8.
10) Kitazawa J, Nollet K, Morioka H. Non-D Rh anti-bodies appearing after apheresis platelet transfusion: stimulation by red cells or microparticles? Vox Sang 2011; 100 (4): 395-400. doi: 10.1111/j.1423-0410.2010.01435.x.

Original

Evaluation of the Loopamp SARS-CoV-2 detection kit using saliva for the detection of SARS-CoV-2 Omicron

Satoshi Oguri[*1], Sumio Iwasaki*[*1], Tasuku Inao*[*2],*
Isao Yokota[*2], Kaoru Murakami*[*3], Kumiko Tanaka*[*3],*
Kasumi Hayasaka[*1], Shinichi Fujisawa*[*1], Chiaki Watanabe*[*1],*
Satoshi Konno[*4], Masaaki Murakami*[*3], †Takanori Teshima*[*1,5]*

†Correspondence: Department of Hematology, Hokkaido University Faculty of Medicine. N15, W7, Kita-ku, Sapporo, Hokkaido, Japan.
E-mail: teshima@med.hokudai.ac.jp
Received January 25, 2023; accepted June 8, 2024
*1 Division of Laboratory and Transfusion Medicine, Hokkaido University Hospital, N15 W7, Kita-Ku, Sapporo 060-8638, Japan
*2 Department of Biostatistics, Hokkaido University Faculty of Medicine, N15 W7, Kita-Ku, Sapporo 060-8638, Japan
*3 Division of Molecular Psychoimmunology, Institute for Genetic Medicine, Graduate School of Medicine, Hokkaido University, N15 W7, Kita-Ku, Sapporo 060-8638, Japan
*4 Department of Respiratory Medicine, Hokkaido University Faculty of Medicine, N15 W7, Kita-Ku, Sapporo 060-8638, Japan
*5 Department of Hematology, Hokkaido University Faculty of Medicine, N15 W7, Kita-Ku, Sapporo 060-8638, Japan

ABSTRACT

Aims: The Omicron variant of SARS-CoV-2 spreads more rapidly than ancestral lineages. Reverse-transcription loop-mediated isothermal amplification (RT-LAMP) provides results more rapidly than reverse-transcription polymerase chain reaction (RT-PCR). However, the reliability in detecting omicrons variant is still unclear due to possible differences in target sequences.
Methods: Fifty-one saliva specimens, which were positive for the Omicron variant SARS-CoV-2 by real-time RT-PCR and sequencing of the S region, were subjects for this study. The RT-LAMP assay was performed using the Loopamp SARS-CoV-2 detection kit with (n=51) or without it (n=50).
Results: The RT-LAMP assay following RNA extraction from saliva specimens had a sensitivity of 100% (95%CI: 93.0–100.0%) with 0.969 Kendall's coefficient of concordance between LAMP threshold time and PCR cycle threshold value. Forty-five of fifty (90.0%, 95%CI: 78.2–96.7%) specimens positive were also positive by RT-LAMP without RNA extraction.
Conclusions: The Omicron variant was effectively detected in saliva by RT-LAMP using saliva specimens and RNA extraction could improve its efficacy.

〔Lab Med Int 2024; 3(3): 70-73〕

Key Words
SARS-CoV-2, Omicron, loop-mediated isothermal amplification, saliva

I. Introduction

Omicron is the variant of concern (VOC) with multiple S-gene mutations conferring high transmissibility in the population and is now the predominant SARS-CoV-2 variant worldwide[1) 2)]. Because incubation period of this VOC is only two to three days compared to four to five days for Alpha and Delta variants[3)], detection methods were demanded in a short reaction time for rapid decision making and quantitative reverse transcription-polymerase chain reaction (RT-PCR), the "gold standard" of viral detection, may be too long[4)-6)].

Reverse transcription-loop-mediated isothermal amplification (RT-LAMP) tests offer results in thirty minutes, with additional benefits of lower economic burden and laboratory independent point-of-care diagnosis. However, most studies using RT-LAMP for detection of SARS-CoV-2 were performed prior to the emergence of Omicron, and its utility in detecting this VOC remains to be scrutinized.

This study was designed prospectively to evaluate the detection of Omicron using the Loopamp 2019-SARS-CoV-2 Detection Kit (Eiken Chemical, Tokyo, Japan), which is a RT-LAMP targeting the N and RdRp genes of SARS-CoV-2 RNA. According to the database of Stanford University, Alpha, Beta, Gamma, Delta, and Omicron all have the P323L mutation in the RdRP gene, while the G671S mutation is only found in Delta and Omicron. Mutations in the N gene are highly variable among the five VOCs. Considering further variation in the sublineages of Omicron, these and other mutations question the utility of current detection methods.

Self-collected saliva is as effective as nasopharyngeal swabs, making major strides in any type of screening with expedited specimen collection with less cost and effort [7)-11)]. Rapid detection of the virus by RT-LAMP using self-collected saliva may help reduce the spread of the Omicron.

II. Materials and methods

We used self-collected saliva as test specimens since numerous reports have demonstrated equivalent results compared with nasopharyngeal swabs, with expedited specimen collection more suitable for real world implementation [7)-11)]. Saliva specimens are consecutively collected from hospitalized patients with COVID-19, symptomatic persons, and asymptomatic persons that have been in close contact with COVID-19 patients at Hokkaido University Hospital. This study was approved by the Institutional Ethics Board (Hokkaido University Hospital Division of Clinical Research Administration Number: 020-0116) and informed consent was obtained from all individuals orally to avoid spreading of the virus. This study was conducted in accordance with the Declaration of Helsinki and Ethical Guidelines for Medical and Biological Research Involving Human Subjects.

Saliva specimens were self-collected as described previously [12)]. 200 μL of saliva was added to 600 μL PBS and stored at -20℃. Frozen specimens were thawed and centrifuged at 20,000 × g for 5 minutes at 4℃ to remove debris. Total RNA was extracted from 140 μL of the supernatant by adding 50 μL of elution buffer with QIAamp Viral RNA Mini Kit (Qiagen, Hilden, Germany). TRexGeneTM SARS-CoV-2 detection kit (Toyobo, Osaka, Japan) was used; 10 μL of extracted specimens were mixed with 40 μL of reaction reagent containing polymerase, dNTP, primers, and probes. Multiplex RT-PCR was performed with LightCycler 96 system (Roche, Basel, Switzerland) at 42℃ for 5 minutes for reverse transcription, at 95℃ for 10 seconds for the initial denaturation, and 45 cycles of PCR at 95℃ for 5 seconds for the denature and 60℃ for 30 seconds for the annealing and extension. Primers of 2019-nCoV-N1-F (5'-GACCCCAAAATCAGCGAAAT-3'), 2019-nCoV-N1-R (5'-TCTGGTTACTGCCAGTTGAATCTG-3'), NIID-2019-nCoV-N-F2 (5'-AAATTTTGGGGACCAGGAAC-3'), and 2019-nCoV-N2-R (5'-GCGCGACATTCCGAAGAA-3') and probes of 2019-nCoV-N1-P (5'-Cy5-ACCCCGCATTACGTTTGGTGGACC-BHQ2-3') and 2019-nCoV_N2-P (5'-ROX-ACAATTTGCCCCCAGCGCTTCAG-BHQ2-3') were described in the US CDC's "2019-Novel Coronavirus Real-time RT-PCR Panel Primers and Probes" and the National Institute of Infectious Diseases's "pathogen detection manual 2019-nCoV ver.2.9.1" [13)]. Positivity was defined as N1 and/or N2 Ct values less than 40, with the smaller value adopted as the result.

SARS-CoV-2 variants were screened by Sanger sequencing method. Briefly, 100 μL of saliva specimens were homogenized in 300 μL of Isogen-LS (NIPPON GENE, Tokyo) and 80 μL of chloroform was added, then centrifuged. Following isopropanol precipitation of aqueous phase, the final pellet was dissolved in 40 μL of RNase free water, and cDNA was made using the QuantiTect Reverse Transcription Kit (Qiagen) according to the manufacturer's instructions. To amplify a DNA fragment of the spike gene, a high-efficiency and fidelity DNA Polymerase KOD FX Neo PCR enzyme (Toyobo) was used with primer sets; CS_1F (5'-TTGTTTTTCTTGTTTTATTGCCACT-3') and CS_1R (5'-CCCTGTTTTCCTTCAAGGTCC-3'), or N1S_4F (5'-TGGTGGACAGCCTTTGTTACT-3') and N1S_4R (5'-TCAAGTGCACAGTCTACAGCAT-3'), resulting a 547 and a 1221 base pair (bp) fragments respectively. PCR was performed using a T100 Thermal Cycler (BIO-RAD) with a temperature profile of 2 minutes at 94℃ followed by 45 cycles of 10 seconds at 98℃, 10 seconds at 58℃, and 30 seconds at 72℃. The amplified fragments were purified using Wizard SV Gel and PCR Clean-Up System (Promega, Madison, WI, USA), then sequenced with Big Dye Terminator kit v3.1 (Applied Biosystems, Foster City, CA, USA) with primer G_1R (TAAGTAGGGACTGGGTCTTCG), which was on the conserved sequences for all variants. The resulting sequence was analyzed for genotypes.

RT-LAMP with RNA extraction was carried out to detect SARS-CoV-2 RNA using Loopamp 2019-SARS-CoV-2 Detection Kit (Eiken Chemical). 10 μL of the RNA specimen extracted with QIAamp Viral RNA Mini Kit (Qiagen) and 15 μL of Primer Mix containing SARS-CoV-2 specific primers was dispensed into a reaction tube with dried amplification reagents including Bst DNA polymerase and AMV reverse transcriptase. This tube was incubated at 62.5℃ with turbidity readings at 650 nm and monitored for 35 minutes using the Loopamp Real-time Turbidimeter (Eiken Chemical). When turbidity was increased within the reaction time, specimen was interpreted as a positive. We defined RT-PCR diagnosis as the gold standard test. Sensitivity was calculated for RT-LAMP with 95% Clopper-Pearson exact confidence interval. All statistical analyses were conducted by R 4.1.1 (R Core Team, Vienna, Austria).

III. Results

Sixty saliva specimens showing RT-PCR positivity for SARS-CoV-2 collected from Jan 21 to Mar 7, 2022, were subjects of this research. Among them, SARS-CoV-2 was identified as Omicron BA.1 by Sanger sequencing method in 51 specimens. The remaining nine specimens were unable to be sequenced due to the small amount of RNA recovery. Fifty-one RT-PCR positive specimens that were detected both N1 and N2 PCR amplification were obtained from 37 symptomatic individuals and 14 asymptomatic individuals. There were 24 male and 27 female patients, with a median age of 41 (range, 15-77). In symptomatic individuals, the median time of sampling was 2 days (range, 1-22 days) after symptom onset. In the controls, we also analyzed 60 RT-PCR negative specimens, detected neither N1 nor N2 PCR amplification, by RT-LAMP.

The utility of RT-PCR and RT-LAMP following RNA extraction (extracted RT-LAMP) were compared using the freeze-thaw specimens (**Figure 1A**). The sensitivity of the extracted RT-LAMP was 100.0% (95%CI: 93.0–100.0%). Kendall's coefficient of concordance *W* between cycle threshold (Ct) values of RT-PCR and the RT-LAMP threshold time values was 0.969, indicating high correlation (**Figure 1A**). The median RT-LAMP threshold time was 774 sec (range: 618-1086 sec). All sixty RT-PCR negative specimens were negative by RT-LAMP.

We also compared the utility of RT-LAMP in specimens with and without RNA extraction (direct RT-LAMP) using twice freeze-thaw specimens (**Figure 1B**). For direct RT-LAMP, 100 μL of saliva was mixed with 4 mL of Loopamp Viral RNA Extraction Reagent (Eiken Chemical). 15 μL of Primer Mix (Eiken Chemical) was added to 10 μL of the mixture before performing RT-LAMP as described above.

In 51 specimens, one specimen could not be examined due to lack of saliva volume. Forty-five of fifty (90.0%, 95%CI: 78.2–96.7%) direct RT-LAMP were positively detected by extracted RT-LAMP. The LAMP threshold times showed excellent correlation with Kendall's *W* as

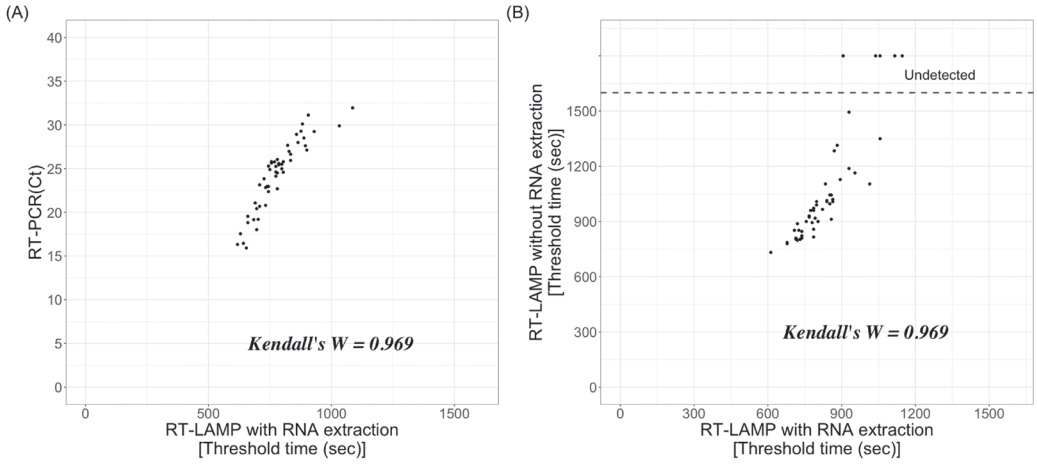

Figure 1 Performance of RT-LAMP using RT-PCR positive saliva specimens with Omicron.

(A) The correlation between the Ct values of RT-PCR and the threshold time values (sec) of RT-LAMP using RNA extracted from the saliva specimens is shown by a scatter plot and Kendall's coefficient of concordance *W* for RT-PCR positive specimens.

(B) The correlation of the threshold time values (sec) between RT-LAMP with and without RNA extraction from saliva specimens is shown by a scatter plot and Kendall's coefficient of concordance *W* for RT-PCR positive specimens. Twice freeze-thaw specimens were used. SARS-CoV-2 was undetectable in 5 specimens by RT-LAMP without RNA extraction.

0.969 (**Figure 1B**). Although the specimens underwent freeze-thaw once (**Figure 1A**) or twice (**Figure 1B**), all specimens were found to be positive by the extracted RT-LAMP.

IV. Discussion

We recently demonstrated RT-LAMP to be a reliable alternative to RT-PCR albeit in a study conducted prior to the emergence of Omicron[6]. In addition, sensitivity of RT-LAMP with target N and E genes was high and specific for Omicron[14]. In this study, we chose the RT-PCR and RT-LAMP detection kits that have been used before Omicron without primer changes. First of all, we proved the RT-PCR efficiency to detect Omicron with 51 specimens that were certified Omicron by Sanger sequencing method. Then, we confirmed that all 51 specimens were determined as positive by the RT-LAMP detection kit. Comparing direct and extracted RT-LAMP, the latter method showed a slightly lower detection rate, most likely due to higher concentrations of viral RNA resulting from the extraction method. RT-LAMP has already been implemented in combination with chemiluminescent enzyme immunoassay at Japanese airport quarantines using self-collected saliva specimens, facilitating expeditious processing of international travelers with all tests performed at points of care. Our results demonstrate that Omicron can be effectively detected in saliva using RT-LAMP.

Conflict of interest

Loopamp Real-time Turbidimeter were supplied by Eiken Chemical (Tokyo, Japan).

Funding sources

This study was supported by Japan Agency for Medical Research and Development (AMED) under Grant Number JP 20fk0108471 and 21fk0108489.

ICMJE statement: S. Oguri, S. Iwasaki, K. Murakami, K. Tanaka, K. Hayasaka, S. Fujisawa, S. C. Watanabe, Konno, M. Murakami: Acquisition, analysis, and interpretation of data: T. Inao, I. Yokota: Statistical analysis, writing of the manuscript: T. Teshima: Chief investigator, Conceptualization, writing of the manuscript. All the authors contributed to the writing of the final manuscript and meet the ICMJE authorship criteria.

References

1) Karim SSA, Karim QA. Omicron SARS-CoV-2 variant: a new chapter in the COVID-19 pandemic. Lancet 2021; 398 (10317): 2126-28.
2) Volz E, Mishra S, Chand M, et al. Assessing transmissibility of SARS-CoV-2 lineage B.1.1.7 in England. Nature 2021; 593 (7858): 266-9.
3) Brandal LT, MacDonald E, Veneti L, et al. Outbreak caused by the SARS-CoV-2 Omicron variant in Norway, November to December 2021. Euro Surveill 2021; 26 (50): 2101147.
4) Nagura-Ikeda M, Imai K, Tabata S, et al. Clinical evaluation of self-collected saliva by Quantitative Reverse Transcription-PCR (RT-qPCR), direct RT-qPCR, Reverse Transcription-Loop-Mediated Isothermal Amplification, and a rapid antigen test to diagnose COVID-19. J Clin Microbiol 2020; 58 (9): e01438-20.
5) Hirotsu Y, Maejima M, Shibusawa M, et al. Comparison of automated SARS-CoV-2 antigen test for COVID-19 infection with quantitative RT-PCR using 313 nasopharyngeal swabs, including from seven serially followed patients. Int J Infect Dis 2020; 99: 397-402.
6) Yokota I, Shane PY, Okada K, et al. A novel strategy for SARS-CoV-2 mass screening with quantitative antigen testing of saliva: a diagnostic accuracy study. Lancet Microbe 2021; 2 (8): e397-e404.
7) Wyllie AL, Fournier J, Casanovas-Massana A, et al. Saliva or Nasopharyngeal Swab Specimens for Detection of SARS-CoV-2. N Engl J Med 2020; 383 (13): 1283-6.
8) Yokota I, Shane PY, Okada K, et al. Mass Screening of Asymptomatic Persons for Severe Acute Respiratory Syndrome Coronavirus 2 Using Saliva. Clin Infect Dis 2021; 73 (3): e559-65.
9) Bastos ML, Perlman-Arrow S, Menzies D, et al. The Sensitivity and Costs of Testing for SARS-CoV-2 Infection With Saliva Versus Nasopharyngeal Swabs : A Systematic Review and Meta-analysis. Ann Intern Med 2021; 174 (4): 501-10.
10) Yokota I, Hattori T, Shane PY, et al. Equivalent SARS-CoV-2 viral loads by PCR between nasopharyngeal swab and saliva in symptomatic patients. Sci Rep 2021; 11 (1): 4500.
11) Butler-Laporte G, Lawandi A, Schiller I, et al. Comparison of Saliva and Nasopharyngeal Swab Nucleic Acid Amplification Testing for Detection of SARS-CoV-2: A Systematic Review and Meta-analysis. JAMA Intern Med 2021; 181 (3): 353-60.
12) Iwasaki S, Fujisawa S, Nakakubo S, et al. Comparison of SARS-CoV-2 detection in nasopharyngeal swab and saliva. J Infect 2020; 81 (2): e145-7.
13) Shirato K, Nao N, Katano H, et al. Development of Genetic Diagnostic Methods for Detection for Novel Coronavirus 2019 (nCoV-2019) in Japan. Jpn J Infect Dis 2020; 73 (4): 304-7.
14) Almeida LT, Gonçalves AB, Franco-Luiz APM, et al. Molecular detection of omicron SARS-CoV-2 variant is achieved by RT-LAMP despite genomic mutations. Mem Inst Oswaldo Cruz 2022; 117: e220050.

Original

Sonographic findings of malignant peripheral nerve sheath tumors – case series –

Maiko Osaka[*1], †Tomonori Kishino,*[*1,2,3], Naoko Shimamori*[*1], Satsuki Matsushima*[*2], Satoko Yamasaki*[*1,2], Kouki Ohtsuka*[*1,2], Hiroki Yasudo*[*1,2], Takeshi Morii*[*4], Junji Shibahara*[*5], Takashi Watanabe*[*6], Hiroaki Ohnishi*[*1,2]

†Correspondence: Kyorin University Faculty of Health Sciences, 5-4-1 Shimorenjaku, Mitaka, Tokyo 181-8612, Japan
E-mail: kishino@ks.kyorin-u.ac.jp
Received April 28, 2023; accepted June 8, 2024
*1 Department of Clinical Laboratory, Kyorin University Hospital, Tokyo, Japan
*2 Department of Laboratory Medicine, Kyorin University School of Medicine, Tokyo, Japan
*3 Department of Clinical Engineering, Kyorin University Faculty of Health Sciences, Tokyo, Japan
*4 Department of Orthopaedic Surgery, Kyorin University School of Medicine, Tokyo, Japan
*5 Department of Pathology, Kyorin University School of Medicine, Tokyo, Japan
*6 President, Kyorin University, Tokyo, Japan

ABSTRACT

Purpose: Malignant peripheral nerve sheath tumor (MPNST) is a sarcoma deriving from peripheral nerves, accounting for 3–10% of all malignant soft tissue tumors. Around half of cases develop secondary to neurofibromatosis type 1 (NF1). While magnetic resonance imaging has been considered the best imaging modality for diagnosing MPNST, the efficacy of sonography has not been precisely investigated. The present study therefore aimed to clarify the sonographic findings for this rare entity in a case series.
Methods: Sonographic findings of four cases with MPNST that had been diagnosed by histopathological studies of specimens obtained via biopsy or surgical resection in our hospital between 2013 and 2023 were evaluated. Age range was 51–56 years and three of the four patients were male. MPNST developed secondary to NF1 in three cases, and the tumors had developed in the thigh and retroperitoneum in two cases each. All cases showed rapid tumor growth within 1 year.
Results: The MPNSTs were large masses appearing hypervascular on Doppler images. Although shapes and contours varied, MPNSTs were depicted as heterogeneously hypoechoic masses with well-defined margins. The well-defined margin is distinct from findings observed in most malignant soft-tissue tumors.
Conclusion: Development of MPNST should be considered when a well-defined margin is observed on sonography of rapidly growing masses in soft tissues, particularly in patients with NF1. 〔Lab Med Int 2024; 3(3): 74-83〕

Key Words
malignant peripheral nerve sheath tumor (MPNST), soft-tissue tumor, sonography, well-defined margin

I. Introduction

Malignant peripheral nerve sheath tumor (MPNST) is a sarcoma deriving from peripheral nerves, accounting for 3–10% of all malignant soft-tissue tumors[1)-3)]. Around 50% of MPNSTs occur as transformation from neurofibroma in patients with neurofibromatosis type 1 (NF1), also known as von Recklinghausen's disease, an autosomal dominant disorder[4) 5)]. Conversely, around 5-15% of patients with NF1 develop MPNST. About 10% of MPNSTs arise in the setting of prior radiation therapy, and the remaining up to 50% of MPNST arise de novo from the peripheral nerve sheath[6)]. Common sites of development are the extremities and trunk, followed by the head and neck, with poor prognosis due to the high malignancy in terms of local recurrence and hematogenous metastasis.

Imaging examinations are therefore essential for differentiation from benign tumors and other soft-tissue malignancies. Magnetic resonance imaging (MRI) in combination with 18F-fluorodeoxyglucose positron emission tomography (PET) has been a gold standard imaging modality to distinguish MPNST from benign peripheral nerve sheath tumors (PNSTs) such as neurofibroma [1)7)8)]. Meanwhile, sonography has been utilized as an initial imaging modality for screening examinations, taking advantage of its ready accessibility, non-invasiveness and inexpensiveness. We have reported that malignant soft tissue tumors generally appear as a large mass with ill-defined margins and hypervascularity on sonography [9)]. However, the appearance of the MPNST margin on imaging has reportedly varied among studies. A cohort study utilizing sonography found that MPNST presented with an ill-defined margin [10)]. In contrast, MPNST exhibits well-defined or partially ill-defined margins on MRI when compared with non-neurogenic malignant soft tissue tumors [11)]. The present study therefore aimed to clarify the features of MPNST on sonography using findings from a case series.

II. MATERIALS AND METHODS

Institutional case series

MPNST cases pathologically diagnosed in our hospital from October 2013 to December 2023 were included in the present study. Only cases in which sonographic examinations had been performed before surgery or biopsy were included. Cases in which chemotherapy and/or radiation therapy were performed before imaging examinations were excluded. In this period, four cases with MPNST meeting these requirements were identified. This study was approved by the ethics committee at our institute (approval no. 1956) and performed in accordance with the ethical standards formulated in the Declaration of Helsinki and its revisions. The aim, significance, and protocol of the study were disclosed on the website of our hospital and made available to the public (https://www.kyorin-u.ac.jp/hospital/clinic/support02/pdf/support02_optout202209.pdf). Patients were assured of the right to opt out of the use of their data at any time if they declared to the institution their decision not to be integrated into the study. All study procedures met the requirements of the Ethical Guidelines for Medical and Health Research Involving Human Subjects of the Japanese government.

Sonographic examination

Sonographic examinations were performed using an Aplio500 ultrasound system (Canon Medical Systems Corporation, Tochigi, Japan), with the combination of a 3.5-MHz convex-array transducer and an 8.0- or 10.0-MHz linear-array transducer. Examinations were performed by one of the sonographers with more than 10 years of experience and specializing in sonographic examination in our hospital. Tumor location, shape, size, margin, echogenicity, and texture were evaluated on gray-scale images, and vascularity was evaluated on images from Doppler sonography [9)12)-14)]. All sonographic findings other than tumor size were evaluated independently on the basis of preserved images in the sonographic machine by two sonographers certified as experts on soft-tissue sonography by The Japan Society of Ultrasonics in Medicine. Both sonographers were blinded to histology, then a consensus was reached [9)13)14)].

III. RESULTS

Case 1

A 51-year-old man had been diagnosed with NF1 based on the development of multiple neurofibromas on his body at another clinic. He complained of rapid growth of a lesion in the left thigh from 3 cm to 20 cm in the last 6 months, accompanied by neurological symptoms of lumbago. Sonographic examination in our hospital revealed a hypoechoic oval mass with a maximum diameter of 210 mm in the muscle layer of the left thigh (**Figure 1a, b**). Although the margin was well-defined and the contour was regular, textures in the tumor were heterogeneous intermingled with anechoic areas. Doppler sonography showed moderate vascularity at the tumor periphery. MRI also showed a relatively well-demarcated mass measuring 200 × 85 × 70 mm across the left rectus femoris and sartorius muscles. The mass exhibited signal hypointensity compared with surrounding muscle on T1-weighted imaging, and heterogeneous signal hyperintensity on T2-weighted imaging (**Figure 2a, b**). Contrast-enhanced MRI demonstrated heterogeneous enhancement at the tumor periphery, but no enhancement at the center of the tumor suggestive of liquid components was observed. Macroscopic examination of the resected tumor revealed a nodular lesion with necrosis and hemorrhage. Microscopically, the lesion showed fascicular growth of atypical spindle tumor cells with alternating hyper- and hypocellular areas (**Figure 3a**). Tumor cells were focally immunoreactive to S-100 and exhibited partial skeletal muscle differentiation [5)]. Mitotic figures were present at a rate of 20–25 per 10 high-power fields. These findings led to a diagnosis of MPNST with skeletal muscle differentiation (malignant triton tumor).

Case 2

A 56-year-old man with no history of NF1 presented with a 10-year history of a mass in the right thigh. The mass had increased in size over the last 6 months, causing right leg pain. Sonographic examination revealed a hypoechoic, lobular mass measuring 97 mm in diameter, with partial hyperechoic areas in the muscle layer of the right thigh (**Figure 1c, d**). Although the margin was well-defined, the internal texture was heterogeneous. Doppler sonography showed hypervascularity mainly in the center of the mass. MRI also showed a mass measuring 90 × 70 × 60 mm in the adductor longus muscle (**Figure 2c, d**). The mass exhibited signal isointensity as compared with surrounding muscle on T1-weighted imaging, and heterogeneous signal hyperintensity on T2-weighted imaging. The mass was biopsied, revealing a lesion comprising fascicular growth of atypical spindle cells (**Figure 3b**). Mitotic figures were present at a rate of 20–25 per 10 high-power fields. On im-

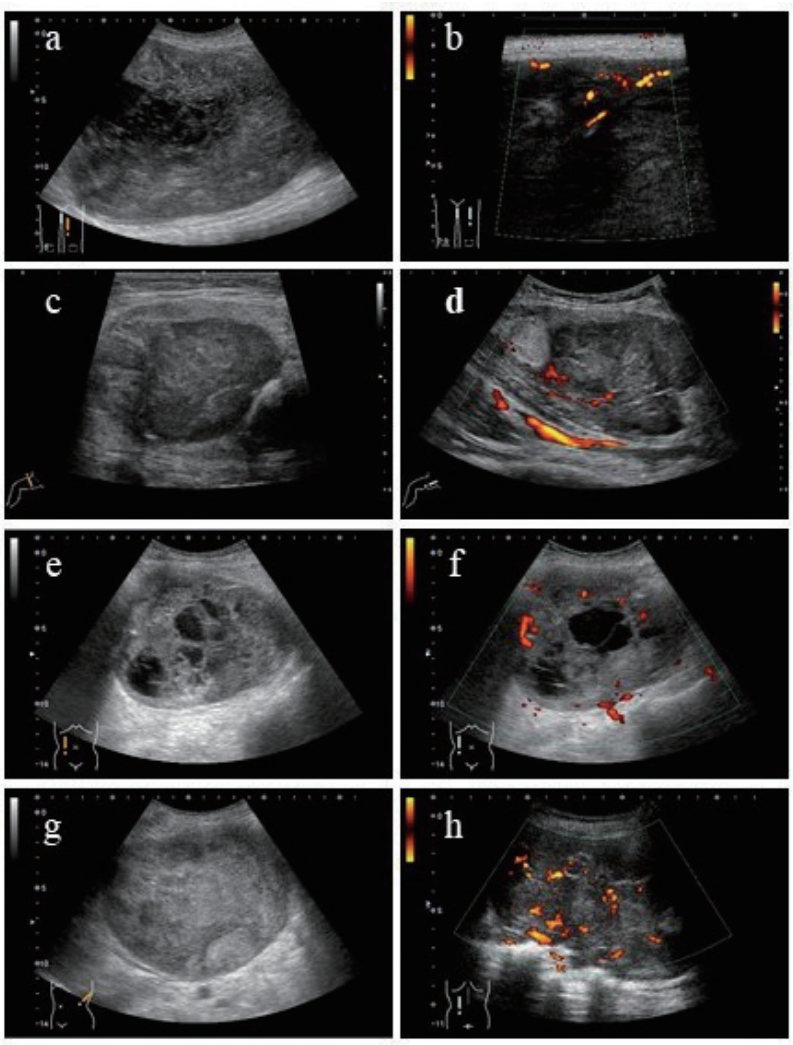

Figure 1

a, b) The tumor presents as an oval mass, 210 mm in maximal diameter on sonography. The mass exhibits heterogeneous hypoechoic intermingled with anechoic areas. The margin is well-defined. Doppler sonography shows moderate vascularity at the tumor periphery.

c, d) The tumor presents as a lobulated mass, 97 mm in size on sonography. The mass appears heterogeneously hypoechoic. The margin of the mass, however, is well-defined. Doppler sonography shows hypervascularity, mainly in the center of the mass.

e, f) The tumor presents as a rounded mass, 119 mm in diameter on sonography. The mass exhibits intermingled heterogeneous hypoechoic and anechoic areas. The margin of the mass is well-defined. Doppler sonography shows hypervascularity with internal vessels.

g, h) The tumor presents as two irregular masses measuring 144 mm and 128 mm on sonography, which thereafter turned out to be one connected lesion. The mass appears heterogeneously hypoechoic. The margin of the mass is, however, well-defined. Doppler sonography shows hypervascularity with internal vessels.

munohistochemistry, the tumor exhibited focal reactivity to S-100 and loss of H3K27me3 [5) 15)]. These findings led to a diagnosis of MPNST.

Case 3

A 56-year-old man had a history of lower limb amputation due to NF1. He recognized a rapidly growing abdominal mass within the preceding year. Sonographic examination at our hospital revealed three hypoechoic, rounded masses with diameters of 119 mm, 60 mm and 48 mm. The rapidly growing mass was considered to correspond to the 119-mm lesion (**Figure 1e, f**). Although the margin was well-defined and the contour was regular, textures in the tumor were intermingled with heterogeneous and anechoic areas. Doppler sonography showed hypervascularity with internal vessels. MRI showed a fusiform mass suggestive of neurogenic tumor in the retroperitoneum,

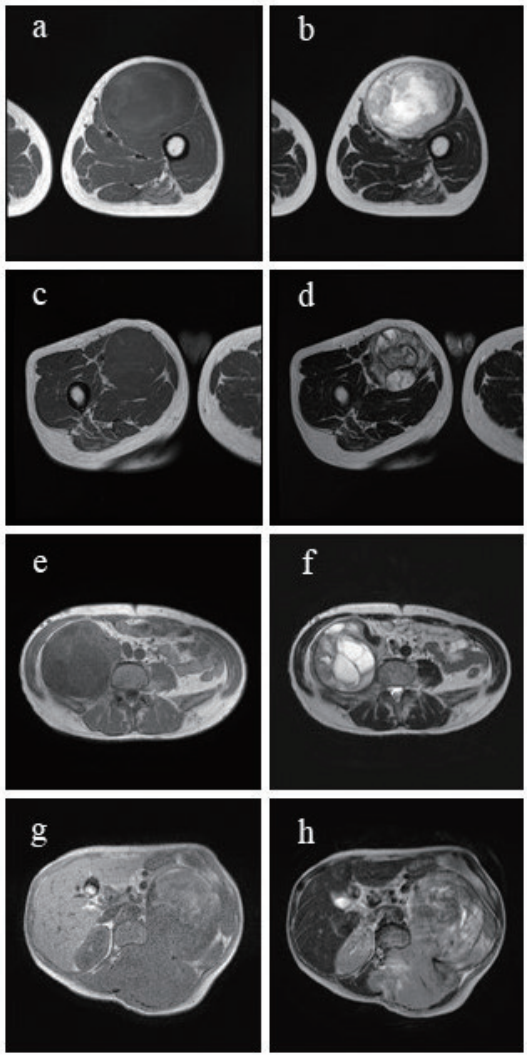

Figure 2

a, b) MRI shows a relatively well-demarcated mass measuring 200 × 85 × 70 mm across the left rectus femoris and sartorius muscles. The mass exhibits signal hypointensity as compared with surrounding muscle on T1-weighted imaging, and heterogeneous signal hyperintensity on T2-weighted imaging.

c, d) MRI shows a mass measuring 90 × 70 × 60 mm in the adductor longus muscle. The mass exhibits signal isointensity as compared with the surrounding muscle on T1-weighted imaging, and heterogeneous signal hyperintensity on T2-weighted imaging.

e, f) MRI shows a fusiform mass suggesting a neurogenic tumor, 115 × 95 × 85 mm, in the retroperitoneum and ventral to the right iliopsoas muscle. The mass exhibits signal hypo- and isointensity as compared with surrounding muscle on T1-weighted imaging, and heterogeneous signal hyperintensity intermingled with signal hypointense septa on T2-weighted imaging.

g, h) MRI shows a mass, 160 × 110 mm, in the left retroperitoneum, including erector spinae muscles. The mass exhibits heterogeneous hypo- to isointensity as compared with abdominal fat or muscle on T1-weighted imaging, and heterogeneous isointensity intermingled by signal hyperintensity on T2-weighted imaging.

measuring 115 × 95 × 85 mm and ventral to the right iliopsoas muscle (**Figure 2e, f**). The mass exhibited signal hypo- to isointensity compared with surrounding muscle on T1-weighted imaging, and heterogeneous signal hyperintensity intermingled with signal hypointense septa on T2-weighted imaging. Contrast-enhanced MRI showed increased enhancement at the tumor periphery in the early phase of enhancement and much more enhancement in the late phase of enhancement. A biopsy specimen obtained from the largest mass revealed mitotic figures at a rate of over 50 per 10 high-power fields and intermingled necrotic regions, leading to a final diagnosis of MPNST composing highly atypical tumor cells (anaplastic MPNST) (**Figure 3c**).

Case 4

A 55-year-old woman with NF1 had been suffering from lumbago for 1 year. A mass was identified from the back to retroperitoneum. Sonographic examination in our hospital revealed two irregular, hypoechoic masses with maximum diameters of 144 mm and 128 mm (**Figure 1g, h**). Al-

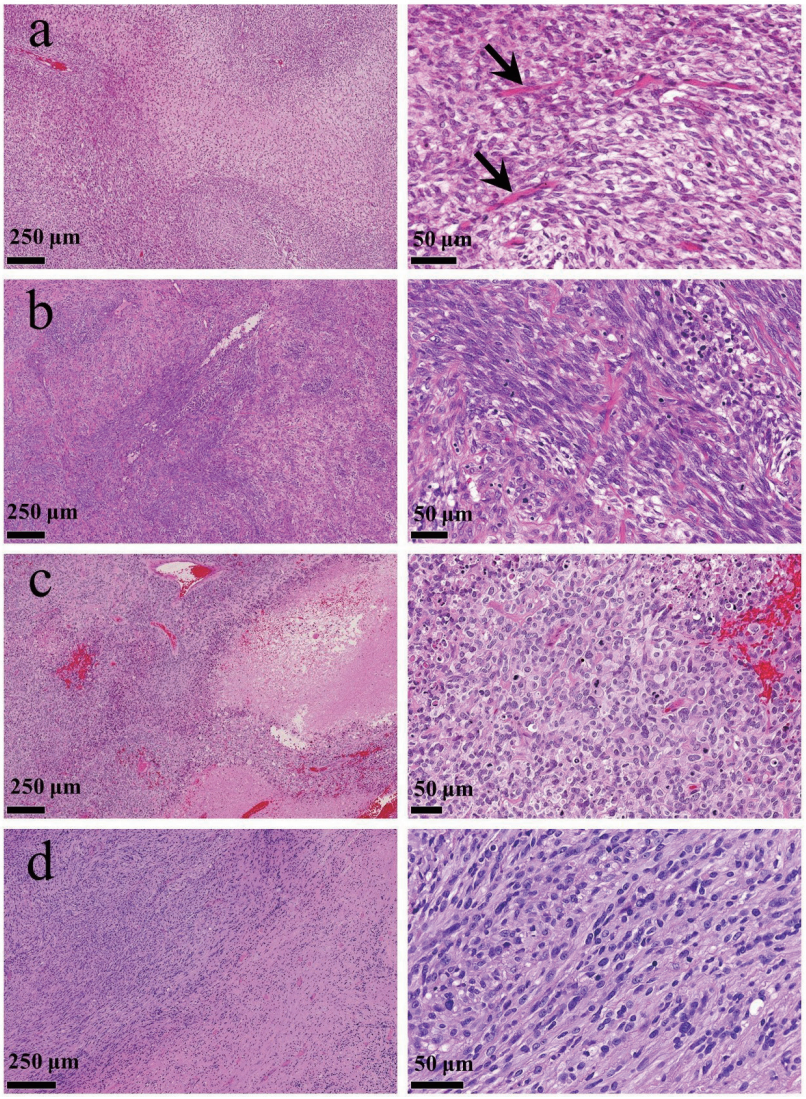

Figure 3

a) Spindle tumor cells show fascicular growth with focal skeletal muscle differentiation (arrows) (hematoxylin and eosin (HE) stain).

b) Atypical spindle cells proliferate in a fascicular pattern (HE stain).

c) The cellular tumor exhibits high-grade nuclear atypia (HE stain).

d) Spindle-shaped tumor cells show fascicular growth (HE stain).

Spindle cell sarcomas with alternating cellularity and brisk mitotic activity, typical of the pathology in MPNST, are present in all cases. No differences are apparent between **a**) and **b**) or **d**) other than the focal skeletal muscle differentiation in **a**). Although **c**) represents a so-called 'anaplastic MPNST', all four cases correspond to high-grade MPNST comprising sarcoma with high cellularity.

Table 1 Sonographic findings of malignant and benign neurogenic tumors, including the present 4 cases of MPNST

	Malignant soft tissue tumors in general	MPNST: 4 cases in the present study	MPNST: cases reported with sonographic findings	Neurofibroma	Schwannoma (=Neurilemoma)
Maximal diameter	≥ 46 mm; >50 mm	210 mm; 97 mm; 119 mm; >144 mm	mean 56 mm (42–110 mm) large (but not described); 50 mm	mean 22 mm (2–49 mm)	≤ 50 mm
Location		thigh; thigh; retroperitoneum; retroperitoneum	thigh; retroperitoneum		
Shape	irregular or lobulated	oval; lobulated; round; irregular	elongated; fusiform; irregular	oval; extensive lobulated; serpentine and partly oval in plexiform tumors	oval > lobulated; peripheral nerve entering and exiting
Margin	ill-defined	well-defined	ill-defined; well-defined; range from well-defined to infiltrating	well-defined; ill-defined	well-defined
Echogenicity	hypo, iso or hyper	hypo	hypo	hypo	hypo
Texture	heterogeneous	heterogeneous	heterogeneous (with necrosis, hemorrhage and/or calcification)	homogeneous; more heterogeneous than schwannomas	homogeneous but heterogenous due to degeneration in 'ancient' (larger) tumors
Vascularity	hyper	hyper	hyper; intrinsic anarchic vascular pattern with spectral waveform; flow within cystic area; stenosis, occlusion, trifurcation and archaic vascular pattern	hypo	hyper
Posterior enhancement	(not described)	not detected	present	present	present
Target sign (hyperechoic central area with hypoechoic periphery)	(not described)	absent	rarely present	present	present; rarely present

Abbreviation: MPNST, malignant peripheral nerve sheath tumor.

though the margins were well-defined, the contours were irregular and textures in the tumors were heterogeneous. Doppler sonography showed hyper-vascularity with internal vessels. MRI showed a mass measuring 160 × 110 mm in the left retroperitoneum that had invaded both the erector spinae muscles and the spinal canal (**Figure 2g, h**). The mass exhibited heterogeneous hypo- to isointensity as compared with abdominal fat or muscle on T1-weighted imaging, and heterogeneous isointensity intermingled by signal hyperintensity suggesting hemorrhagic necrosis on T2-weghted imaging. While sonographic examination depicted the mass as two lesions, MRI showed that these lesions were connected. A biopsy specimen from the mass revealed mitotic figures present at a rate of 15 per 10 high-power fields, and diagnosed as a MPNST (**Figure 3d**).

III. DISCUSSION

MPNSTs are histologically classified into four subtypes: conventional, malignant triton tumor, glandular, and epithelioid types [3) 6) 15) -17)]. Conventional MPNST is the most common, accounting for 80–85% of MPNSTs. The remaining 15% comprise the other three subtypes with various differentiations. Malignant triton tumor defined as MPNST with rhabdomyoblastic differentiation as seen in Case 1 of the present study accounts for 5% of MPNSTs and exhibits aggressive behavior with poor outcomes as compared with conventional MPNST [18)]. Cases 1 and 2 finally underwent surgical resection. Although the contour was regular or lobular in each tumor, the margins were well-defined on sonography (**Figure 1a-c; Table 1**), which represented nodular lesions macroscopically. Cases 3 and 4 were pathologically diagnosed from the biopsied specimens. Although the contours of Cases 3 and 4 tumors were regular and irregular, respectively,

Table 2 MRI findings of MPNST and representative benign neurogenic tumors

	MPNST	Neurofibroma	Schwannoma (Neurilemoma)
Age	20–50 years	20–30 years	20–40 years
Size	large, >5 cm		
Shape		fusiform (with tapered ends); multilobulated	fusiform (with tapered ends)
Margin	poorly defined; well-defined	well-defined	well-defined
Texture	heterogeneous, including intratumoral cystic areas suggesting hemorrhage or necrosis	homogeneous on T1; heterogeneous on T2	heterogeneous
MRI: T1 / T2	low or intermediate; iso to adjacent muscle (high representing hemorrhage)/ heterogeneous high	low or intermediate; iso to skeletal muscle / heterogeneously high	low or intermediate / heterogeneously high
Enhanced MRI (contrast-enhanced T1)	heterogeneous peripheral enhancement with non-enhancing areas representing cystic changes or necrosis	hyper homogeneous and patchy mild reversed target sign	hyper with or without internal cystic areas
Target sign	absent; rarely present	present (hyperintense ring and hypointense center on T2WI)	present (peripheral high and central low on T2WI)
Split fat sign	absent	present	present
Perilesional edema	present	absent	absent

Abbreviations: MPNST, malignant peripheral nerve sheath tumor; MRI, magnetic resonance imaging; WI, weighted imaging.

the margins were well-defined in both (**Figure 1e-h; Table 1**). However, contrast with the macroscopic pathology could not be performed because the diagnoses were made from of biopsied specimens. The heterogeneous internal texture observed in all four cases (**Figure 1; Table 1**) could have been due to spindle cell sarcomas with alternating cellularity and brisk mitotic activity, typical for the pathology of MPNST (**Figure 3**). No differences were noted between Case 1 and Cases 2 and 4 other than focal skeletal muscle differentiation in Case 1. Although Case 3 was a so-called 'anaplastic MPNST', all four cases corresponded to high-grade MPNST comprising sarcoma with high cellularity. Intermingled anechoic areas in Cases 1 and 3 (**Figure 1a, e**) may have corresponded to necrotic and hemorrhagic areas in malignant triton tumor type and anaplastic MPNST (**Figure 3c**).

When compared with benign soft-tissue tumors, malignant soft-tissue tumors generally exhibit large size, ill-defined margins and hypervascularity on sonography, as described in our previous study [9) 19)]. In contrast, no differences are found concerning echogenicity or internal texture between benign and malignant soft-tissue tumors (**Table 1**). The present four cases suggest that MPNST forms a large, well-defined, heterogeneously hypoechoic mass with hypervascularity. The features of large size and hypervascularity are consistent with those of malignant soft-tissue tumors in general. In contrast, the well-defined margin could serve as a distinct feature of MPNST, differing from the general finding of malignant soft-tissue tumors. Actually, three case reports of MPNST have demonstrated well-defined margins on sonographic imaging [18) 20) 21)]. This supports our hypothesis that MPNST is likely to show well-defined margins on sonography.

The most recent study utilizing sonography in a large group of patients with PNSTs concluded that MPNST shows an ill-defined margin [10)]. That study settled on the strict numerical criteria for evaluations of tumor margin, as follows: well-defined, > 90% of whole margin is well demarcated; and ill-defined, ≤ 90% of the whole margin is well demarcated. However, tumor margins have been evaluated qualitatively by trained sonographers on sonography in most studies, including our own [9) 13) 14)]. Since tracing the whole margin of these mostly large MPNSTs could be difficult within the restricted field of vision on sonography, the criterion of whether over or less than 90% of the tumor margin is well- or poorly demarcated on sonography [10)] may not be practical. Because our criteria for evaluating the tumor margin have been concordant in most previous studies applying non-numerical criteria [22)-25)], the margin for MPNST should be 16 considered well-defined in clinical practice.

Among the current imaging examination modalities,

MRI has been the most advantageous to diagnose soft-tissue tumors, including MPNST, because of its ability to evaluate tumor properties. Representative findings on MRI for MPNST are shown in **Table 2**. MPNST has been reported to exhibit well-defined or partially ill-defined margins on MRI as compared with non-neurogenic malignant soft-tissue tumors [11) 18)]. A large series investigating differential features on MRI between MPNST and neurofibroma identified that both tumors exhibit well-defined margin with no significant differences [7)]. Meanwhile, that study also concluded that two or more among the four features of tumor size, peripheral enhancement, perilesional edema and intratumoral cystic change could augment discrimination of MPNST from neurofibroma. Another study demonstrated that a recent advance in MRI using diffusion-weighted imaging values combined with conventional MRI findings could discriminate MPNST from benign tumors [26)]. However, ill-defined margins were included among the conventional MRI findings suggesting MPNST in that study. Thus, the use of well- or poorly defined margins for the diagnosis of MPNST on MRI has varied between studies. MRI has actually been serving as the most reliable imaging modality to diagnose soft-tissue tumors, including MPNST, because several sequences provide tumor features. However, MRI remains challenging in terms of accessibility due to cost, low procedural throughput, and invasiveness for some patients, such as those with pacemakers. Further, not all institutions can equip themselves with MRI machines.

In contrast, sonography could solve these problems, particularly as an initial imaging examination. When encountering tumors originating from soft tissues on sonography, a large mass with ill-defined margin and hypervascularity on Doppler imaging could be suggestive of malignant tumors in general [9)]. Homogeneous masses with well-defined margins may well be benign tumors, but even if well-defined margins are present, heterogeneous masses may be malignant. Examiners should therefore be cautious in reporting. The probability of MPNST should increase considerably, especially for large, rapidly growing masses with well-defined margins, although the hypoechogenicity, heterogeneous internal texture and hypervascularity seen in MPNST could not be definitively discriminated from the features in benign tumors (**Table 1**) [18)-21)27)-29)].

Basically, half of MPNSTs arise from preexisting neurofibromas in patients with NF1, as in Cases 1, 3 and 4. Development of MPNST should thus always be considered in patients with NF1 [4) 5)]. MPNST can also develop sporadically in otherwise normal tissues [6)]. When a rapidly growing mass exhibits sonographic findings similar to those in the present cases in the soft-tissues of patients, especially those with a history of NF1, MPNST should be considered among the differential diagnoses.

As a limitation of sonographic examinations as compared with MRI in the diagnosis of MPNST, tracing the entire margin of a tumor could be difficult in the restricted field of vision because of the large size of most MPNSTs, as described above. Further, tumor invading bones or bone marrow may not be depicted. MPNSTs arising from areas in the trunk such as the pleural cavity or retroperitoneal cavity might be difficult to observe, depending on conditions such as gas in the body. The internal texture of MPNSTs could be heterogeneous on sonography, while several sequences on MRI can evaluate the detailed context of tumor textures. Contrast-enhanced sonography is better than Doppler sonography for evaluating tumor vascularity, as contrast-enhanced MRI uses gadolinium in addition to several sequences of MRI [30)]. Histopathological differences might thus be partly responsible for the differences in sonographic images of MPNSTs. The possible contribution of histological differences in MPNST subtypes to sonographic image differences remains to be clarified by accumulating more cases of this rare pathology.

IV. CONCLUSION

The present study clarified several sonographic findings characteristic of MPNST that are similar to those observed in malignant soft-tissue tumors, such as heterogeneity and hypervascularity. A well-defined margin could represent a point of distinction from malignant soft-tissue tumors in general. Sonography alone may not warrant a definitive diagnosis of MPNST, but seems useful as an initial imaging modality. When a large, hypervascular tumor with features of malignant soft-tissue tumor exhibits a well-defined margin on sonography, MPNST should be considered as a differentiated diagnosis.

Acknowledgements:

This work was supported by a research fund from the Kyorin University Faculty of Health Sciences (Grant Number: R401010001).

Authorship contributions:

MO and NS performed the sonographic examinations and evaluated the imaging findings. TK contributed to the conception and design of the study, and wrote the manuscript. SM created figures. SY, KO and HY provided suggestions during the study. TM performed the sur-

geries in Cases 1 and 2. JS pathologically diagnosed the cases. TW gave comprehensive advice on the study and manuscript. HO revised the manuscript. All authors read and approved the final version of the manuscript.

Conflict of interest:

Maiko Osaka, Tomonori Kishino, Naoko Shimamori, Satsuki Matsushima, Satoko Yamasaki, Kouki Ohtsuka, Hiroki Yasudo, Takeshi Morii, Junji Shibahara, Takashi Watanabe, and Hiroaki Ohnishi declare that they have no conflict of interest.

REFERENCES

1) Lin J, Martel W. Cross-sectional imaging of peripheral nerve sheath tumors: characteristic signs on CT, MR imaging, and sonography. AJR Am J Roentgenol 2001; 176 (1) : 75-82. doi: 10.2214/ajr.176.1.1760075.
2) Durbin AD, Ki DH, He S, et al. Malignant peripheral nerve sheath tumors. Adv Exp Med Biol 2016; 916: 495-530. doi: 10.1007/978-3-319-30654-4_22.
3) Nielsen GP, Chi P. Malignant peripheral nerve sheath tumour. In: WHO Classification of Tumours Editorial Board, editor. WHO Classification of Tumours, 5th ed., Vol.3, Soft Tissue & Bone Tumours, WORLD HEALTH ORGANIZATION; 2020, p.254-7.
4) James AW, Shurell E, Singh A, et al. Malignant peripheral nerve sheath tumor. Surg Oncol Clin N Am 2016; 25 (4) : 789-802. doi: 10.1016/j.soc.2016.05.009.
5) Miettinen MM, Antonescu CR, Fletcher CDM, et al. Histopathologic evaluation of atypical neurofibromatous tumors and their transformation into malignant peripheral nerve sheath tumor in patients with neurofibromatosis 1 - a consensus overview. Hum Pathol 2017; 67: 1-10. doi: 10.1016/j.humpath.2017.05.010.
6) Abdel Razek AAK, Gamaleldin OA, Elsebaie NA. Peripheral nerve sheath tumors of head and neck: imaging-based review of World Health Organization classification. J Comput Assist Tomogr 2020; 44 (6) : 928-40. doi: 10.1097/RCT.0000000000001109.
7) Wasa J, Nishida Y, Tsukushi S, et al. MRI features in the differentiation of malignant peripheral nerve sheath tumors and neurofibromas. AJR Am J Roentgenol 2010; 194 (6) : 1568-74. doi: 10.2214/AJR.09.2724.
8) Koike H, Nishida Y, Ito S, et al. Diffusion-weighted magnetic resonance imaging improves the accuracy of differentiation of benign from malignant peripheral nerve sheath tumors. World Neurosurg 2022; 157: e207-14. doi: 10.1016/j.wneu.2021.09.130.
9) Morii T, Kishino T, Shimamori N, et al. Differential diagnosis between benign and malignant soft tissue tumors utilizing ultrasound parameters. J Med Ultrason (2001) 2018; 45 (1) : 113-9. doi: 10.1007/s10396-017-0796-3.
10) Jin Z, Zhao K, Guo W, et al. Investigation of ultrasound parameters for the differential diagnosis of malignant and benign peripheral nerve sheath tumors. J Ultrasound Med 2022; 41 (12) : 3091-101. doi: 10.1002/jum.16089.
11) Van Herendael BH, Heyman SRG, Vanhoenacker FM, et al. The value of magnetic resonance imaging in the differentiation between malignant peripheral nerve-sheath tumors and non-neurogenic malignant soft-tissue tumors. Skeletal Radiol 2006; 35 (10) : 745-53. doi: 10.1007/s00256-006-0160-y.
12) Giovagnorio F, Andreoli C, De Cicco ML. Color Doppler sonography of focal lesions of the skin and subcutaneous tissue. J Ultrasound Med 1999; 18 (2) : 89-93. doi: 10.7863/jum.1999.18.2.89.
13) Shimamori N, Kishino T, Morii T, et al. Sonographic appearances of liposarcoma: correlations with pathologic subtypes. Ultrasound Med Biol 2019; 45 (9) : 2568-74. doi: 10.1016/j.ultrasmedbio.2019.05.020.
14) Shimamori N, Kishino T, Okabe N, et al. Discrimination of well-differentiated liposarcoma from benign lipoma on sonography: an uncontrolled retrospective study. J Med Ultrason (2001) 2020; 47 (4) : 617-23. doi: 10.1007/s10396-020-01051-5.
15) Otsuka H, Kohashi K, Yoshimoto M, et al. Immunohistochemical evaluation of H3K27 trimethylation in malignant peripheral nerve sheath tumors. Pathol Res Pract 2018; 214 (3) : 417-25. doi: 10.1016/j.prp.2017.12.015.
16) Meyer A, Billings SD. What' s new in nerve sheath tumors. Virchows Arch 2020; 476 (1) : 65-80. doi: 10.1007/s00428-019-02671-0.
17) Berner EA, Hung YP, Nielsen GP, et al. Malignant peripheral nerve sheath tumors arising from schwannomas: case series and literature review. APMIS 2021; 129 (8) : 524-32. doi: 10.1111/apm.13139.
18) Kamran SC, Shinagare AB, Howard SA, et al. A-Z of malignant peripheral nerve sheath tumors. Cancer Imaging 2012; 12 (3) : 475-83. doi: 10.1102/1470-7330.2012.0043.
19) Chiou HJ, Chou YH, Chiu SY, et al. Differentiation of benign and malignant superficial soft-tissue masses using grayscale and color Doppler ultrasonography. J Chin Med Assoc 2009; 72 (6) : 307-15. doi: 10.1016/S1726-4901 (09) 70377-6.
20) Chatzistefanou A, Mantatzis M, Deftereos S, et al. Peripheral nerve sheath tumors. Benign or malignant? The role of MRI and ultrasonography in a case report. J Neuroimaging 2014; 24 (3) : 308-10. doi: 10.1111/j.1552-6569.2012.00731.x.
21) Jha A, Gupta P, Wahab S, et al. Role of ultrasonography in detection of renal artery pseudoaneurysm caused by retroperitoneal malignant peripheral nerve sheath tumor in a patient with neurofibromatosis type 1. J Med Ultrason (2001) 2014;

41 (1): 87-91. doi: 10.1007/s10396-013-0467-y.

22) Cheng JW, Tang SF, Yu TY, et al. Sonographic features of soft tissue tumors in the hand and forearm. Chang Gung Med J 2007; 30 (6): 547-54.

23) Chen W, Jia JW, Wang JR. Soft tissue diffuse neurofibromas: sonographic findings. J Ultrasound Med 2007; 26 (4): 513-8. doi: 10.7863/jum.2007.26.4.513.

24) Wang Y, Tang J, Luo Y. Sonographic diagnosis of fibromatosis. J Clin Ultrasound 2008; 36 (6): 330-4. doi: 10.1002/jcu.20483.

25) Gong X, Ying H, Zhang Z, et al. Ultrasonography and magnetic resonance imaging features of kaposiform hemangioendothelioma and tufted angioma. J Dermatol 2019; 46 (10): 835-42. doi: 10.1111/1346-8138.15025.

26) Yun JS, Lee MH, Lee SM, et al. Peripheral nerve sheath tumor: differentiation of malignant from benign tumors with conventional and diffusion-weighted MRI. Eur Radiol 2021; 31 (3): 1548-57. doi: 10.1007/s00330-020-07234-5.

27) Lin J, Jacobson JA, Hayes CW. Sonographic target sign in neurofibromas. J Ultrasound Med 1999; 18 (7): 513-7. doi: 10.7863/jum.1999.18.7.513.

28) Grover DSB, Kundra DR, Grover DH, et al. Imaging diagnosis of plexiform neurofibroma- unravelling the confounding features: a report of two cases. Radiol Case Rep. 2021; 16 (9): 2824-33. doi: 10.1016/j.radcr.2021.06.025.

29) Winter N, Dohrn MF, Wittlinger J, et al. Role of high-resolution ultrasound in detection and monitoring of peripheral nerve tumor burden in neurofibromatosis in children. Childs Nerv Syst 2020; 36 (10): 2427-32. doi: 10.1007/s00381-020-04718-z.

30) Costelloe CM, Amini B, Madewell JE. Risks and benefits of gadolinium-based contrast-enhanced MRI. Semin Ultrasound CT MR 2020; 41 (2): 170-82. doi: 10.1053/j.sult.2019.12.005.

Original

Retrospective study of the prognosis, viral load estimated by RT-PCR cycle threshold values, and monocyte distribution width (MDW) in COVID-19

†Kentaro Wakamatsu, MD, PhD[1], Zenzo Nagasawa, MT, PhD*[2], Kouta Katsuki, MT*[3], Hiroyuki Kumazoe, MD*[1], Masayo Yasuda, MT*[3], Sae Kawamoto, MT*[3], Ayano Kawamura, MT*[3], Junji Otsuka, M.D, PhD*[1], Ruriko Kiyotani*[1], Izumi Fukui*[1], Sanae Maki, MD, PhD*[1], Nobuhiko Nagata, MD, PhD*[4], Masayuki Kawasaki, MD, PhD*[1], Satomi Asai, MD, PhD*[5], Hozumi Yamada, MD, PhD*[6]*

†Correspondence: Department of Respiratory Medicine, National Hospital Organization Omuta National Hospital
1044-1 Oaza, Tachibana, Omuta City, Fukuoka 837-0911, Japan
E-mail: wakamatsu.kentaro.fe@mail.hosp.go.jp
Received October 3, 2023; accepted May 14, 2024
*1 Department of Respiratory Medicine, National Hospital Organization Omuta National Hospital
*2 Department of Medical Technology and Science, Faculty of Fukuoka Health Care, International University of Health and Welfare
*3 Department of Clinical Laboratory, National Hospital Organization Omuta National Hospital
*4 Department of Respiratory Medicine, Fukuoka Sanno Hospital
*5 Department of Laboratory Medicine, Tokai University School of Medicine
*6 Department of Respiratory Medicine, Keitendo Koga Hospital

ABSTRACT

Objectives: There are reports on prognostic factors including viral load, the presence/absence of pneumonia and MDW at the time of hospital admission, however there are several challenges.

Methods:

Cohort 1: A total of 235 patients diagnosed with COVID-19 admitted to our hospital between July 2020 and July 2021 were investigated for prognostic factors including the presence/absence of concurrent pneumonia and viral load.

Cohort 2: This investigation planned to investigate the prognostic significance of MDW included 80 patients diagnosed with COVID-19 who were admitted to our hospital between April 2021 when automatic blood cell counter measuring MDW was introduced in our hospital and September 2021.

Results:

Cohort 1: Based on the results of multivariate analysis, advanced age, high body mass index (BMI), diabetes mellitus, and concurrent pneumonia were considered to be independent poor prognostic factors.

Cohort 2: The mean age and MDW on admission were significantly higher in the poor prognosis group (n=38) than in the good prognosis group (n=42) ($p<0.01$), while high BMI, diabetes mellitus, and concurrent pneumonia showed no significant difference between the two groups.

Conclusions: MDW may be used as a biomarker of aggravation of COVID-19 on admission.

〔Lab Med Int 2024; 3(3): 84-94〕

Key Words

COVID-19, SARS-CoV-2, MDW, Ct, Prognosis

List of abbreviations

Alb = albumin; ALT = alanine aminotransferase; APTT = activated partial thromboplastin time; AUC = area under the curve; AST = aspartate aminotransferase; BMI = body mass index; BUN = blood urea nitrogen; CBC = complete blood count; CDC = Center for Disease Control and Prevention; CK = Creatine Kinase; COPD = chronic obstructive pulmonary disease; COVID-19 = coronavirus disease 2019; Cre = creatinine; CRP = C-reactive protein; Ct = cycle threshold; CT = Computed Tomography; EDTA = ethylenediaminetetraacetic acid; Glu = glucose; Hb = hemoglobin; HbA1c = Hemoglobin A1c; KL-6 = krebs von den lungen-6; LD = lactate dehydrogenase; Ly = lymphocyte count; MDW = monocyte distribution width; Neu = Neutrophil count; NLR = neutrophil-to-lymphocyte ratio; NPV = negative predictive value; PCR = polymerase chain reaction; PCT = procalcitonin; Plt = platelet count; PPV = positive predictive value; PT = prothrombin time; RBC = red blood cell; RNA = ribo nucleic acid; ROC = receiver operating characteristic; RT-PCR = Reverse Transcription-PCR; SARS-CoV-2 = severe acute respiratory syndrome coronavirus 2; SIRS = systemic inflammatory response syndrome; SP-A = surfactant protein A; SP-D = surfactant protein D; SpO2 = oxygen saturation of peripheral artery; T-bil = total bilirubin; US = United States; WBC = white blood cell; WHO = World Health Organization

I. Introduction

Coronavirus disease 2019 (COVID-19) is an acute respiratory infection caused by severe acute respiratory syndrome coronavirus 2 (SARS-CoV-2) which was originally reported in December 2019 as "pneumonia of unknown cause" in Wuhan, Hubei, China. It was officially pronounced a new type of coronavirus by the Chinese Center for Disease Control and Prevention (CDC) on January 7, 2020.[1)]

We often experience patients with COVID-19 not having any serious respiratory symptoms on admission, however rapid aggravation of respiratory status during follow-up. Therefore, for the treatment of COVID-19, it is important to diagnose the disease early, predict its aggravation, and provide therapeutic intervention early. The 6.2th edition of the Clinical Practice Guidelines for Novel Coronavirus Infections (COVID-19) lists the following risk factors for aggravation: (1) elderly persons aged 65 years or older, (2) malignant tumor, (3) chronic obstructive pulmonary disease (COPD), (4) chronic kidney disease, (5) type 2 diabetes mellitus, (6) hypertension, (7) dyslipidemia, (8) obesity (BMI of 30 kg/m^2 or higher), (9) smoking, (10) immunodeficiency after solid organ transplant, (11) late pregnancy. Multiple factors have also been listed as markers of aggravation, including (1) elevated D-dimer, (2) elevated CRP, (3) elevated LD, (4) elevated ferritin, (5) lymphopenia, (6) elevated creatinine, (7) elevated troponin, and (8) elevated KL-6. 2

Computed Tomography (CT) scans can be performed relatively easily, since our hospital has a dedicated CT examination device for COVID-19 patients. It is also possible to estimate the viral RNA amount using the number of positive Ct value of the Smart Gene®, a PCR reagent for SARS-CoV-2 detection (MIZUHO MEDY Co., Ltd.)[3)]. There are reports on prognostic factors including viral load and the presence/absence of pneumonia at the time of hospital admission, however there are several challenges.

As previously reported, in recent years, devices that can analyze detailed white blood cell information with automated hematology analyzers have appeared, and it has been reported that Monocyte Distribution Width (MDW) is useful for diagnosing sepsis and assessing the severity of COVID-19[4)-23)].

In this study we examined prognostic factors in COVID-19, including the presence/absence of concurrent pneumonia and viral load, and also examined MDW.

II. Methods

1. Study subjects

Cohort 1: The study included 235 patients (severity: mild: 74 patients, moderate I: 116 patients, and moderate II: 45 patients) admitted to the National Hospital Organization Omuta Hospital and confirmed to have COVID-19 by SARS-CoV-2 PCR test between July 2020 and July 2021. In the evaluation, a comparative evaluation was performed retrospectively using blood samples collected at the initial visit. Severity was classified according to the 6.2th edition of the Clinical Practice Guidelines[2)]. The details of patient background are shown in **Table 1**.

In the diagnosis of COVID-19, nasopharyngeal swabs were collected from patients and the samples are analyzed by a fully automated genetic analyzer, Smart Gene® (Mizuho Medy, Co., Ltd.).

Pneumonia was diagnosed based on chest CT findings by 2 radiologists and 1 pulmonologist. The presence/absence of pneumonia was evaluated based on the chest CT image at the initial visit to the hospital.

Cohort 2: The 88 patients with COVID-19 confirmed by SARS-CoV-2 PCR test who visited the National Hospital Organization Omuta National Hospital between April and

September 2021 when the automatic blood cell counter UniCel DxH 900 series Coulter Cellular Analysis System (Beckman Coulter, hereafter referred to as DxH 900) was introduced, included 80 patients (severity: mild in 18 patients, moderate I in 46 patients, and moderate II in 16 patients) whose MDW was measured on admission.

MDW in EDTA 2K-added whole blood venous sample was measured by DxH 900 (Beckman Coulter, K.K.).

This study was conducted after being approved by the ethics committee of the National Hospital Organization Omuta Hospital (Approval No.: 3-19).

2. Detection method of SARS-CoV-2 with Smart Gene® (nasopharyngeal swab samples)

RT-PCR was performed using the previously reported method[3),20)].

3. Evaluated items at the initial hospital visit

At the initial visit, the following data were obtained: age, gender, smoking history, drinking history, time from onset to the initial visit, hospitalization period, BMI, underlying medical conditions, presence/absence of pneumonia, symptoms at the initial visit, white blood cell count, neutrophil count, lymphocyte count, hemoglobin, platelet count, APTT, PT, D-dimer, albumin, total bilirubin, ALT, AST, LD, CK, BUN, creatinine, glucose, CRP, procalcitonin, ferritin, KL-6, SP-D, SP-A, HbA1c, SpO_2, and Ct value (number of cycles).

4. Method to evaluate the prognostic factors of COVID-19 in Cohort 1

The statistical analysis to evaluate the prognostic factors of COVID-19 in Cohort 1 was based on comparing good prognosis and poor prognosis. Prognosis should essentially be evaluated based on survival/death. However, since no deaths were observed in this study, poor prognosis was defined as patients who were hospitalized for 14 days or longer or who were transferred to other facilities due to exacerbation of symptoms after hospitalization, while good prognosis was defined as patients who were hospitalized for shorter than 14 days. A multivariate analysis of prognostic factors was performed, considering the results of univariate analysis and previously reported prognostic factors.

5. Relationship between the number of cycle threshold (Ct value) for positive samples and severity

The relationship between Ct value and severity was evaluated in 204 patients (severity: mild: 64 patients, moderate I: 99 patients, and moderate II: 41 patients) whose Ct value was measured among 235 patients admitted to the National Hospital Organization Omuta Hospital and confirmed to have COVID-19 by SARS-CoV-2 PCR test between July 2020 and July 2021.

6. Evaluation of MDW to predict prognosis of COVID-19 in Cohort 2

MDW analysis was started from April 2021 when DxH 900 was installed. In Cohort 2, MDW in 80 patients was evaluated to predict prognosis of COVID-19 in reference to the results of the multivariate analysis in Cohort 1.

7. Statistical analysis

Since the data did not show a normal distribution, the data were presented in medians and quartiles, and the analysis was performed in a nonparametric manner. The Mann-Whitney U and χ^2 tests were performed as the test between 2 groups, and the Kruskal-Wallis test was performed as the test between 3 groups. Considering the results of univariate analysis and previously reported prognostic factors, multivariate analysis was performed using the method of binomial logistic regression analysis to evaluate the good and poor prognosis groups. Factors associated with MDW were analyzed by binomial logistic regression analysis. $p<0.05$ was regarded as statistically significant. All the statistical analyses were performed using Bellcurve for Excel (version 3.21, Social Survey Research Information Co., Ltd.).

III. Results

Cohort 1

1. The background of patients with COVID-19

The background of patients with COVID-19 (Cohort 1) is shown in **Table 1**. The median age was 56 years of age (42 years in the good prognosis group and 65 years in the poor prognosis group), and age was significantly higher in the poor prognosis group ($p<0.001$). In addition to this, BMI ($p=0.02$), frequency of concurrent pneumonia ($p<0.001$), and severity on admission were also significantly higher ($p<0.001$).

Treatment was performed significantly more frequently in the poor prognosis group ($p<0.001$), partly because patients with severe disease were treated more actively ($p<0.001$) (**Table 1**). Regarding underlying disease, diabetes mellitus ($p<0.01$) and hypertension ($p<0.01$) were statistically higher in the poor prognosis group (**Table 1**).

2. Symptoms of patients with COVID-19

Pharyngitis, headache, taste disturbance, and olfactory disturbance were statistically different in the good prognosis group, while there were no significant differences in fever between the 2 groups (**Table 1**).

3. Laboratory findings in patients with COVID-19 (Cohort 1)

Laboratory findings at the initial visit in the poor prognosis group showed significant increases in neutrophil count ($p=0.03$), D-dimer ($p<0.01$), total bilirubin

Table 1 Background of patients with COVID-19 (Cohort 1)

		Total (n=235)	The group with good prognosis (n=117)	The group with poor prognosis** (n=118)	P-value
Age (years)		56 (39～69)	43.521 (25～61)	63.992 (54～74)	<0.001
sex (male / female)		129 / 106	63 / 54	66 /52	0.7480
Smoking history (presence / absence)		115 / 120	53 / 64	62 / 56	0.2947
Alcohol history (presence / absence)		121 / 114	59 / 58	62 / 56	0.9104
Period from onset* to hospital admission (days)		5 (1～19)	5 (1～14)	5 (1～19)	0.6880
Hospital stay (days)		13 (11～20)	11 (9～12)	20 (15～25.75)	
BMI (kg/m^2)		23.03 (20.67～25.945)	22.27 (15.7～24.91)	23.77 (21.45～26/893)	0.0246
Blood pressure	Systolic pressure	127 (114.25～136.75)	124 (114～135)	129 (117～138)	0.0851
	Diastolic pressure	79.5 (71～88)	78 (72～87)	85 (70～89)	0.5959
Pneumonia (presence / absence)		159 / 76	58 / 59	101 / 17	<0.001
Severity at admission (mild/moderate I/moderate II)		74/116/45	58/50/9	16/66/36	<0.001
Therapy (presence / absence)		157***/78	51/66	106/12	<0.001
continued					
Underlying disease:					
Cardiovascular disease		19 (8.1%)	6 (5.1%)	13 (11.0%)	0.1055
diabetes mellitus		32 (13.6%)	7 (6.0%)	25 (21.2%)	0.0014
Cerebrovascular disorder		8 (3.4%)	2 (1.7%)	6 (5.1%)	0.1738
Pulmonary disease		28 (11.9%)	12 (10.3%)	16 (13.6%)	0.4359
Malignant disease		18 (7.7%)	6 (5.1%)	12 (10.2%)	0.1536
Neuromuscular disease		0 (0%)	0 (0%)	0 (%)	
Hypertension		62 (26.4%)	22 (13.7%)	40 (39.0%)	<0.001
presence		139 (59.1%)	48 (41.0%)	91 (77.1%)	<0.001
continued					
Symptoms					
Fever (≥ 37.5°C)		101 (43.0%)	48 (41.0%)	53 (44.9%)	0.5471
Cough		114 (48.5%)	58 (49.6%)	56 (47.5%)	0.7451
Pharyngitis		37 (15.7%)	25 (21.4%)	12 (10.2%)	0.0209
General malaise		69 (29.4%)	34 (29.1%)	35 (29.7%)	0.9194
Nasal discharge		21 (8.9%)	13 (11.1%)	8 (6.8%)	0.2489
Headache		52 (22.1%)	36 (30.8%)	16 (13.6%)	0.0019
Diarrhea		22 (9.4%)	11 (9.4%)	11 (9.3%)	0.9833
Joint pain・Myalgia		12 (5.1%)	9 (7.7%)	3 (2.5%)	0.0876
Dyspnea		39 (16.6%)	17 (14.5%)	22 (18.6%)	0.3977
Taste disturbance		40 (17.0%)	26 (22.2%)	14 (11.9%)	0.0372
Olfactory disturbance		30 (12.8%)	22 (18.8%)	8 (6.8%)	0.0079
Others		45 (19.1%)	19 (16.2%)	26 (22.0%)	0.2605
None		32 (13.6%)	12 (10.3%)	20 (16.9%)	0.1383

Data are expressed as the median (range)

*If no symptoms were observed, the date of positive confirmation was regarded as the date of onset.
**Among the patients with poor prognosis, 4 patients were transferred to other facilities.
***Antiviral drug alone in 1 patient, antiviral drug + steroid in 152 patients, antiviral drug + steroid + baricitinib in 4 patients
Abbreviation: BMI: Body mass index

(p<0.01), ALT (p<0.01), AST (p<0.01), LD (p<0.01), CK (p<0.01), BUN (p<0.01), creatinine (p<0.01), glucose (p<0.01), CRP (p<0.01), procalcitonin (p<0.01), ferritin (p<0.01), KL-6 (p<0.01), SP-A (p=0.03), and HbA1c (p<0.01), and significant decreases in lymphocyte count (p<0.01), albumin (p<0.01) and SpO_2 (p<0.01). The Ct value did not show statistical difference between the good and poor prognosis groups. Furthermore, the relationship between the Ct value and severity was evaluated. The Ct showed higher values as the severity increased (**Table 2**). In particular, Ct values were not statistically different between patients with moderate I and moderate II, however were statistically higher in patients with moderate I and moderate II than in those with mild in severity (**Fig.1**).

4. Factors related to poor prognosis in patients with COVID-19

Multivariate analysis of prognostic factors considering the results of univariate analysis and previously reported prognostic factors showed that age (p<0.01), BMI (p=0.01), diabetes mellitus (p=0.04), and concurrent pneumonia (p=0.02) were independent prognostic factors (**Table 3**).

Cohort 2

Background and prognostic factors of patients with COVID-19

Since age, BMI, diabetes mellitus, and concurrent pneumonia were found to be independent prognostic factors of COVID-19 in Cohort 1, we also evaluated MDW as a prognostic factor in addition to age, BMI, diabetes mellitus, and concurrent pneumonia. The results showed significantly higher values for age and MDW (**Table 4, Fig. 2**).

Table 2 COVID-19 laboratory findings at the initial visit to the hospital in patients with COVID-19

Laboratory findings	Total (n=235)	The group with good prognosis (n=117)	The group with poor prognosis** (n=118)	P-value
WBC	4800 (3700～6100)	4600 (3500～6100)	4950 (3825～6100)	0.2217
Neu	3189.8 (2185.4～4354.4)	2916 (1907.5～4127.2)	3348.4 (2386.9～4478.6)	0.0283
Ly	1056.1 (809.7～1356.4)	1142.4 (874.0～1415.7)	988.6 (752.6～1232.2)	0.0037
Hb	14.5 (13.5～15.4)	14.6 (13.5～15.5)	14.45 (13.4～15.3)	0.4654
Plt	19.0 (15.8～23.6)	191 (16.5～23.3)	186 (14.6～23.6)	0.7405
APTT	34.7 (32.0～38.2)	34.65 (31.9～37.3)	34.8 (32.3～38.9)	0.1449
PT	10.9 (10.4～11.4)	10.9 (10.3～11.4)	10.9 (10.5～11.5)	0.2027
D-dimer	0.5 (0.2～0.9)	0.4 (0.2～0.7)	0.7 (0.3～1.1)	<0.001
Alb	4.1 (3.8～4.4)	4.3 (4.0～4.6)	4.0 (3.6～4.3)	<0.001
T-bil	0.6 (0.5～0.8)	0.6 (0.5～0.7)	0.6 (05～0.8)	0.0062
ALT	23 (16.0～38.0)	20 (16.0～29.0)	25 (19.0～45.5)	0.0019
AST	27 (21.0～37.0)	22 (19.0～30.0)	32 (23.3～44.5)	<0.001
LD	213 (181.0～274.0)	196 (165～238.0)	244 (197.5～316.5)	<0.001
CK	82 (55.0～121.5)	74 (52.0～100.3)	91 (61.0～143.5)	0.0086
BUN	13 (10.0～15.5)	12 (10.0～15.0)	14 (11.0～17.0)	<0.001
Cre	0.79 (0.63～0.93)	0.75 (0.60～0.91)	0.81 (0.67～0.94)	0.0016
Glu	108.5 (97.0～131.0)	101.5 (93.0～117.0)	115 (104.0～138.8)	<0.001
CRP	0.7 (0.23～3.07)	0.36 (0.11～1.44)	1.19 (0.40～5.50)	<0.001
PCT	0.03 (0.02～0.05)	0.02 (0.02～0.04)	0.03 (0.02～0.06)	0.0011
Ferritin	161 (84.0～279.0)	113 (46.8～183.5)	240 (116.3～433.8)	<0.001
KL-6	230 (166.5～344.0)	188 (146.0～281.0)	267.5 (202.5～440.5)	<0.001
SP-D	34.5 (23.5～53.6)	32.2 (21.8～47.0)	37.7 (24.3～60.1)	0.1226
SP-A	27.5 (19.9～39.9)	25.8 (18.1～34.9)	30.45 (22.3～45.5)	0.0338
HbA1c	5.6 (5.3～5.9)	5.5 (5.2～5.7)	5.7 (5.5～6.3)	<0.001
SpO2	97 (96～98)	98 (97～98)	97 (95～98)	<0.001
Ct value	29.5 (25.0～34.0)	29 (25.0～33.0)	30 (26.0～35.0)	0.2035

Data are expressed as the median (range)

Abbreviation: WBC: white blood cell, Neu: Neutrophil count, Ly: lymphocyte count, Hb: hemoglobin, Plt: platelet count, APTT: activated partial thromboplastin time, PT: prothrombin time, Alb: albumin, T-bil: Total bilirubin, ALT: alanine aminotransferase, AST: aspartate aminotransferase, LD: lactate dehydrogenase, CK: creatine kinase, BUN: blood urea nitrogen, Cre: creatinine, Glu: glucose, CRP: C-reactive protein, PCT: procalcitonin, KL-6=krebs von den lungen-6, SP-D: surfactant protein D, SP-A= surfactant protein A, HbA1c: Hemoglobin A1c, SpO2: oxygen saturation of peripheral artery, Ct: cycle threshold

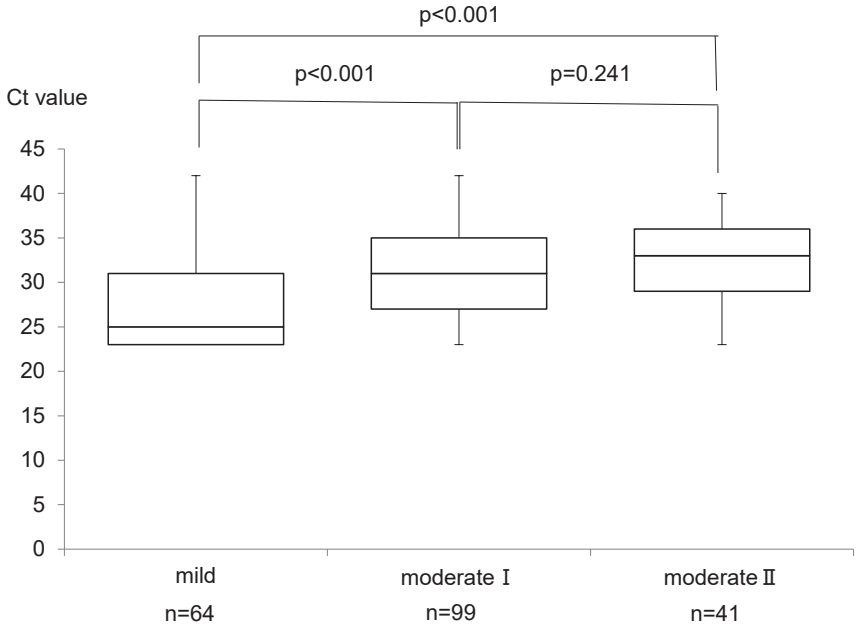

Figure 1 Relationship between the number of positive test cycles (Ct value) and severity in 204 patients who tested positive with the Smart Gene®, a reagent for new coronavirus detection (Cohort 1)

Table 3 Factors related to poor prognosis of patients with COVID-19: Multivariate analysis by binomial logistic regression analysis

Parameters	95% Confidence interval		P-value
	Lower limit	Upper limit	
Age	0.0355	0.088	<0.001
BMI	0.0227	0.1885	0.0125
Diabetes mellitus	0.0343	2.2610	0.0433
Hypertention	-0.7975	0.8607	0.9404
Ly	-0.0011	0.0005	0.4542
T-bil	-0.8892	1.9267	0.4702
BUN	-0.1640	0.0172	0.1124
CRP	-0.1752	0.0904	0.5314
PCT	-5.8445	14.0572	0.4186
Ferritin	-0.0001	0.0036	0.0654
D-dimer	-0.3010	0.5311	0.5877
Pneumonia	0.1734	1.8432	0.0179

Data are expressed as the median (range)

Abbreviation: BMI: Body mass index, Ly: lymphocyte count, T-bil: Total bilirubin, BUN: blood urea nitrogen, CRP: C-reactive protein, PCT: procalcitonin

Table 4 Factors related to poor prognosis of patients with COVID-19: Analysis by binomial logistic regression analysis (univariate analysis)

Parameters	Total (n=80)	The group with good prognosis (n=42)	The group with poor prognosis** (n=38)	95% Confidence interval		P-value
				Lower limit	Upper limit	
Age	49.5 (15.0～65.5)	36.0 (26.0～53.0)	62.5 (49.8～74.8)	0.0228	0.0732	<0.001
BMI	23.5 (20.8-26.7)	23.5 (20.9-27.0)	23.8 (20.8-26.4)	-0.0975	0.0991	0.9879
Diabetes mellitus	7 (8.8%)	2 (4.8%)	5 (13.2%)	-0.5947	2.8120	0.2021
Pneumonia	62 (77.5%)	30 (71.4%)	32 (84.2%)	-0.3416	1.8570	0.1767
MDW	23.3 (22.2-26.5)	22.4 (21.0-24.3)	24.5 (22.6-27.0)	0.0539	0.3450	0.0072

Data are expressed as the median (range)

Abbreviation: BMI: Body mass index, MDW: monocyte distribution width

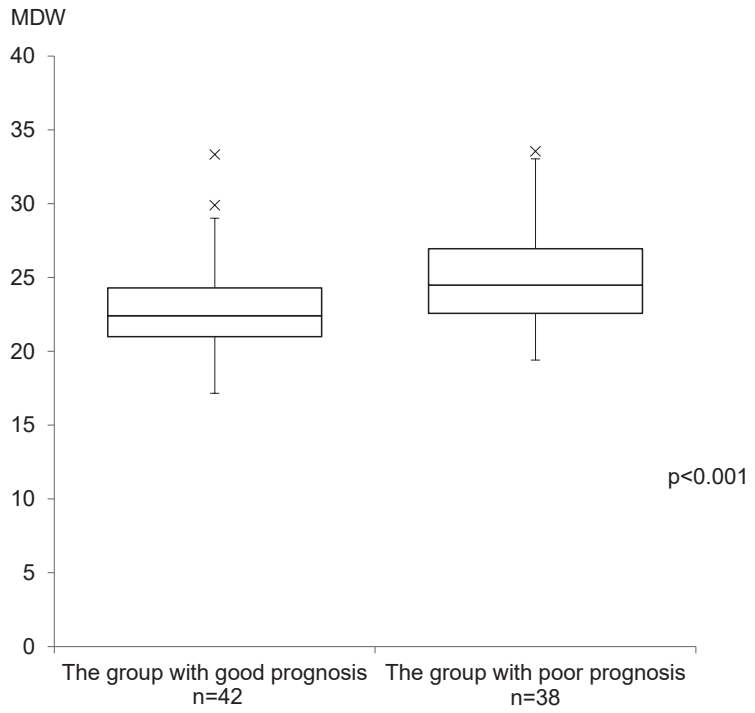

Figure 2 Relationship between prognosis and MDW in COVID-19 (Cohort 2) MDW at the time of hospital admission was significantly higher in the poor prognosis group.

IV. Discussion

Prognostic factors and markers of aggravation of COVID-19 have been investigated in many studies [24)-34)]. However, there have been no reports on studies of the presence/absence of pneumonia based on chest CT images or studies including viral load at the initial visit to the hospital. There are not many studies of MDW related to COVID-19.

Prognosis should essentially be evaluated based on survival/death. However, since no deaths were observed in this study, poor prognosis was defined as patients who were hospitalized for 14 days or longer or who were transferred to other facilities due to exacerbation of symptoms after hospitalization, while good prognosis was defined as patients who were hospitalized for shorter than 14 days. As a result of multivariate analysis, age, BMI, diabetes mellitus, and concurrent pneumonia are found as independent prognostic factors in our study.

Advanced age was consistently found to be a prognostic factor in most of the previously reported studies in COVID-19 [24), 28), 30), 33)]. High BMI [25), 28)] and diabetes mellitus [24)] are also often reported to be poor prognostic factors.

Malik P et al. investigated biomarkers of COVID-19 aggravation and reported that lymphopenia, thrombocytopenia, elevated D-dimer, elevated CRP, elevated procalcitonin, elevated AST, elevated ALT, elevated creatinine, and elevated LD were significantly associated with mechanical ventilation and death [34)]. This report is almost consistent with the results of univariate analysis in our study. Therefore, it was considered that the definitions of the poor and the good prognosis groups might be reasonable in view of the analysis of prognostic factors.

The severity of concurrent pneumonia is assessed as moderate or higher according to the 6.2th version of the Clinical Practice Guidelines [2)], however it is unknown whether concurrent pneumonia on admission is related to subsequent aggravation. In some cases, pneumonia will be observed after hospitalization and become severe. COVID-19 pneumonia is considered to appear a few days after the onset of COVID-19. However, since the median time from the onset of COVID-19 infection to hospitalization in the patients investigated in this study was 5 days, the patients in whom COVID-19 infection became severe may have had pneumonia at the time of hospital admission.

According to a systematic review by Shah VP. et al., hospitalized patients with lower Ct value (i.e., higher levels of viral RNA) have higher disease severity and mortality, however it is also noted that the results of this analysis should be interpreted with caution, given the limitations and lack of assay standardization [35)].

Our results showed that the viral load (Ct value) on admission was not associated with prognosis, and was

statistically lower in patients with higher severity. It has already been reported that the viral load is the highest immediately after onset, and that there becomes no isolation of the virus from the 7th day after onset [36]. The results of the Ct value in this study may suggest that the immune response plays a stronger role in the aggravation of COVID-19 than the virus itself, and that COVID-19 pneumonia is caused by the immune response. The Ct value does not only provide useful information for infection control since the viral concentration in specimens and the estimation of time of onset, but also might be used actively for the selection of antiviral and anti-inflammatory drugs.

Although many studies have been conducted on markers of aggravation, it is desirable to predict the prognosis of COVID-19 easily within the scope of routine clinical examinations.

MDW generated by DxH 900 which was evaluated in this study, is a new cytometric parameter that reflects monocyte changes in cell volume caused by the activation of monocytes. The result is obtained in around 1 minute with routine CBC and WBC differential testing without the need for ordering additional tests. Therefore, MDW values can be easily confirmed as a routine clinical examination. MDW may be considered a promising screening test parameter for COVID-19, if it's prognostic prediction for COVID-19 is superior.

Originally, monocytes play an important role in the innate immune system against infection, and are believed to be involved in phagocytosis, antigen presentation, cytokine production, and activation of acquired immune system. Additionally, activation of monocytes is considered to result in the expression of various functions and the diversity of morphology [37)-42)]. Similarly, neutrophil volume and distribution width are changed, however, Crouser et al.[43)-46)] evaluated MDW in patients in the emergency department and reported that MDW was superior in detecting sepsis patients and effective as the initial biomarker to aid in diagnosis and severity assessment of infection.

It is also reported that MDW may be effective as a diagnostic aid and a severity assessment biomarker for COVID-19. Ognibene et al.[47)] reported an observational study analyzing 147 patients suspected of having COVID-19 who visited the emergency room. The mean MDW was 27.3 ± 4.9 in the SARS-CoV-2 -positive patients (n=41) and 20.3 ± 3.3 (p<0.005) in the SARS-CoV-2 -negative patients (n=106). In addition, when the MDW of 23 patients admitted to the ICU and 18 patients not admitted to the ICU were compared among SARS-CoV-2 positive patients, the mean values were 28.8 ± 5.3 and 25.4 ± 3.6 (P<0.05), respectively, and was significantly higher in the patients admitted to the ICU, suggesting that MDW is useful for the diagnosis and severity evaluation of COVID-19. However, it was not evaluated as a biomarker of aggravation in that study. Investigations as biomarkers of severe disease have been reported by Riva G, et al.[48)] and Frugoli A, et al.[49)]

Riva G, et al. studied 71 good prognosis cases (81.6%) and 16 poor prognosis cases (deaths) (18.4%) and reported that the last MDW value detected during the follow-up after diagnosis in each patient (n=87) was significantly higher in the poor prognosis group with a median value of 26.1 than in the good prognosis group. Frugeli et al. also studied 284 good prognosis cases (85.54%) and 47 poor prognosis cases (deaths) (14.16%) and reported that the median value at the first visit in the poor prognosis group was 24.9, significantly higher than in the good prognosis group. In our study, MDW was evaluated as a biomarker of aggravation, and MDW was significantly higher in the poor prognosis group. Riva G, et al. showed higher values than our results because they looked at the last value of MDW detected during the follow-up after diagnosis, but were in close agreement with the results of Frugeli et al.

Frugoli A, et al. also showed the usefulness of MDW as a predictive marker of sepsis in COVID-19 patients. In the present study, PCT was significantly higher in the poor prognosis group in cohort 1, suggesting that poor prognosis cases may have concurrent sepsis. This point may need further investigation with a larger number of cases.

These results suggest that MDW may be used as a biomarker of aggravation at the time of hospital admission.

This study has some limitations. First, prognosis should essentially be evaluated based on survival/death. However, since no deaths were observed in this study, poor prognosis was defined as patients who were hospitalized for 14 days or longer or who were transferred to other facilities due to exacerbation of symptoms after hospitalization, while good prognosis was defined as patients who were hospitalized for shorter than 14 days. Second, in this study, the prognostic factors were analyzed from July 2020, however since DxH 900 was installed in April 2021, the number of patients in whom MDW was analyzed was small and it was hard to examine in the same cohort. Third, the study was retrospective in design, used data obtained from a single center study. Finally, it did not include severe patients.

V. Conclusions

Viral load (Ct value) at the initial visit to the hospital may be not related to prognosis. However, it does not only provide useful information for infection control since viral concentration in the specimens and the time of onset may be estimated, but also might be used actively for the selection of antiviral and anti-inflammatory drugs.

MDW is a test that can be performed quickly and easily in peripheral blood testing, which is collected in a routine clinical examination and it is not necessary to use nasopharyngeal swab samples, etc. MDW is expected to be widely used clinically as a supplementary test to predict the prognosis of COVID-19 in various medical institutions such as small and medium-sized hospitals and clinics.

Declarations

Ethics approval and consent to participate

This study was conducted after being approved by the ethics committee of National Hospital Organization Omuta National Hospital (Approval No.: 3-19).

Competing interests

The authors declare that they have no conflicts of interest and no competing interests.

Funding

No funding was received for conducting this study.

Authors' contributions

K. W. assisted with study design and interpretation of the data, had full access to the study data, assumes responsibility for the integrity of the data and the accuracy of the analysis, and drafted the manuscript. Z. N., K. K., M. Y., S. K., A. K., J. O., S. M., N. N., M. K., S.A. and H. Y. assisted with study design and interpretation of the data and edited the initial draft of the manuscript. I. F. and R. K. contributed to data collection and management. H. K. contributed to the categorization of patients with COVID-19.

Acknowledgements

None.

References

1) Li Q, Guan X, Wu P, et al. Early Transmission Dynamics in Wuhan, China, of Novel Coronavirus-Infected Pneumonia. N Engl J Med 2020; 382 (13): 1199-207.
2) Novel coronavirus infection (COVID-19) medical practice guidelines version 6.2. 2022. https://www.mhlw.go.jp/content/000888608.pdf. Accessed 27 Jan 2022.
3) Wakamatsu K, Katsuki K, Ikeda T, et al. Study of threshold cycle (Ct Value) in SARS-CoV-2 RT-PCR test with smart gene. Jpn J Med Pharm Sci. 2021; 78: 643-51.
4) Crouser ED, Parrillo JE, Seymour C, et al. Improved early detection of sepsis in the ED with a novel monocyte distribution width biomarker. Chest 2017; 152 (3): 518-26.
5) Crouser ED, Parrillo JE, Seymour CW, et al. Monocyte distribution width: a novel indicator of sepsis-2 and sepsis-3 in high-risk emergency department patients. Crit Care Med 2019; 47 (8): 1018-25.
6) Crouser ED, Parrillo JE, Martin GS, et al. Monocyte distribution width enhances early sepsis detection in the emergency department beyond SIRS and qSOFA. J Intensive Care 2020; 8: 33.
7) Woo A, Oh DK, Park CJ, et al. Monocyte distribution width compared with C-reactive protein and procalcitonin for early sepsis detection in the emergency department. PLoS One 2021; 16 (4): e0250101.
8) Hausfater P, Boter NR, Indiano CM, et al. Monocyte distribution width (MDW) performance as an early sepsis indicator in the emergency department: comparison with CRP and procalcitonin in a multicenter international European prospective study. Crit Care 2021; 25 (1): 227.
9) Agnello L, Bivona G, Vidali M, et al. Monocyte distribution width (MDW) as a screening tool for sepsis in the emergency department. Clin Chem Lab Med 2020; 58 (11): 1951-7.
10) Agnello L, Sasso BL, Giglio RV, et al. Monocyte distribution width as a biomarker of sepsis in the intensive care unit: a pilot study. Ann Clin Biochem 2021; 58 (1): 70-3.
11) Piva E, Zuin J, Pelloso M, et al. Monocyte distribution width (MDW) parameter as a sepsis indicator in intensive care units. Clin Chem Lab Med 2021; 59 (7): 1307-14.
12) Guo C, Li B, Ma H, et al. Single-cell analysis of two severe COVID-19 patients reveals a monocyte-associated and tocilizumab-responding cytokine storm. Nat Commun 2020; 11 (1): 3924.
13) Chousterman BG, Swirski FK, Weber GF. Cytokine storm and sepsis disease pathogenesis. Semin Immunopathol. 2017; 39 (5): 517-28.
14) Mukherjee R, Barman PK, Thatoi PK, et al. Non-classical monocytes display inflammatory features: validation in sepsis and systemic lupus erythematous. Sci Rep. 2015; 5: 13886.
15) Sprangers S, De Vries TJ, Everts V. Monocyte heterogeneity: consequences for monocyte-derived immune cells. J Immunol Res 2016; 2016: 1475435.
16) Cormican S, Griffin MD. Human monocyte subset distinctions and function: insights from gene expression analysis.

Front Immunol 2020; 11: 1070.
17) Kaur G, Sandeep F, Olayinka O, et al. Morphologic changes in circulating blood cells of COVID-19 patients. Cureus 2021; 13 (2): e13416.
18) Mehta P, McAuley DF, Brown M, et al. COVID-19: consider cytokine storm syndromes and immunosuppression. Lancet 2020; 395 (10229): 1033-4.
19) Huang C, Wang Y, Li X, et al. Clinical features of patients infected with 2019 novel coronavirus in Wuhan, China. Lancet 2020; 395 (10223): 497-506.
20) Wakamatsu K, Nagasawa Z, Katsuki K, et al. Retrospective study on the efficacy of monocyte distribution width (MDW) as a screening test for COVID-19. European Journal of Medical Research 2023; 28 (1): 136. doi: 10.1186/s40001-023-01086-7.
21) Ognibene A, Lorubbio M, Magliocca P, et al. Elevated monocyte distribution width in COVID-19 patients: the contribution of the novel sepsis indicator. Clin Chim Acta 2020; 509: 22-4.
22) Lin HA, Lin SF, Chang HW, et al. Clinical impact of monocyte distribution width and neutrophil-to-lymphocyte ratio for distinguishing COVID-19 and influenza from other upper respiratory tract infections: a pilot study. PLoS One 2020; 15 (11): e0241262.
23) Riva G, Castellano S, Nasillo V, et al. Monocyte distribution width (MDW) as novel inflammatory marker with prognostic significance in COVID-19 patients. Sci Rep 2021; 11 (1): 12716.
24) Terada M, Ohtsu H, Saito S, et al. Risk factors for severity on admission and the disease progression during hospitalization in a large cohort of patients with COVID-19 in Japan. BMJ Open 2021; 11 (6): e047007. doi:10.1136/bmjopen-2020-047007.
25) de Siqueira JVV, Almeida LG, Zica BO, et al. Impact of obesity on hospitalizations and mortality, due to COVID-19: A systematic review. Obes Res Clin Pract 2020; 14 (5): 398-403. doi:10.1016/j.orcp.2020.07.005.
26) Pranata R, Lim MA, Huang I, et al. Hypertension is associated with increased mortality and severity of disease in COVID-19 pneumonia: A systematic review, meta-analysis and meta-regression. J Renin Angiotensin Aldosterone Syst 2020; 21 (2):1470320320926899. doi:10.1177/1470320320926899.
27) Lippi G, Wong J, Henry BM. Hypertension in patients with coronavirus disease 2019 (COVID-19): a pooled analysis. Pol Arch Intern Med 2020; 130 (4): 304-9. doi:10.20452/pamw.15272.
28) Fried MW, Crawford JM, Mospan AR, et al. Patient Characteristics and Outcomes of 11,721 Patients with Coronavirus Disease 2019 (COVID-19) Hospitalized Across the United States. Clin Infect Dis 2021; 72 (10): e558-65. doi:10.1093/cid/ciaa1268.
29) Wang B, Li R, Lu Z, et al. Does comorbidity increase the risk of patients with COVID-19: evidence from meta-analysis. Aging (Albany NY) 2020; 12 (7): 6049-57. doi:10.18632/aging.103000.
30) Fang X, Li S, Yu H, et al. Epidemiological, comorbidity factors with severity and prognosis of COVID-19: a systematic review and meta-analysis. Aging (Albany NY) 2020; 12 (13): 12493-503. doi:10.18632/aging.103579.
31) Zhou Y, He Y, Yang H, et al. Development and validation a nomogram for predicting the risk of severe COVID-19: A multi-center study in Sichuan, China. PLoS One 2020; 15 (5): e0233328. doi:10.1371/journal.pone.0233328.
32) Patel U, Malik P, Usman MS, et al. Age-Adjusted Risk Factors Associated with Mortality and Mechanical Ventilation Utilization Amongst COVID-19 Hospitalizations-a Systematic Review and Meta-Analysis. SN Compr Clin Med 2020; 2 (10): 1740-9. doi:10.1007/s42399-020-00476-w.
33) Harrison SL, Fazio-Eynullayeva E, Lane DA, et al. Comorbidities associated with mortality in 31,461 adults with COVID-19 in the United States: A federated electronic medical record analysis. PLoS Med 2020; 17 (9): e1003321. doi:10.1371/journal.pmed.1003321.
34) Malik P, Patel U, Mehta D, et al. Biomarkers and outcomes of COVID-19 hospitalisations: systematic review and meta analysis. BMJ Evi Based Med 2021; 26 (3): 107-8. doi: 10.1136/bmjebm-2020-111536. Epub 2020 Sep 15.
35) Shah VP, Farah WH, Hill JC, et. al. Association Between SARS-CoV-2 Cycle Threshold Values and Clinical Outcomes in Patients With COVID-19: A Systematic Review and Meta-analysis. Open Forum Infect Dis 2021; 8 (9): ofab453.
36) Sethuraman N, Jeremiah SS, Ryo A. Interpreting Diagnostic Tests for SARS-CoV-2. JAMA 2020; 323 (22): 2249-51.
37) Guo C, Li B, Ma H, et al. Single-cell analysis of two severe COVID-19 patients reveals a monocyte-associated and tocilizumab-responding cytokine storm. Nat Commun 2020; 11 (1): 3924.
38) Chousterman BG, Swirski FK, Weber GF. Cytokine storm and sepsis disease pathogenesis. Semin Immunopathol 2017; 39 (5): 517-28.
39) Mukherjee R, Barman PK, Thatoi PK, et al. Non-classical monocytes display inflammatory features: validation in sepsis and systemic lupus erythematous. Sci Rep 2015; 5: 13886.
40) Sprangers S, De Vries TJ, Everts V. Monocyte heterogeneity: consequences for monocyte-derived immune cells. J Immunol Res 2016; 2016: 1475435.
41) Cormican S, Griffin MD. Human monocyte subset distinctions and function: insights from gene expression analysis. Front Immunol 2020; 11: 1070.
42) Kaur G, Sandeep F, Olayinka O, et al. Morphologic changes

in circulating blood cells of COVID-19 patients. Cureus 2021; 13 (2): e13416.

43) Crouser ED, Parrillo JE, Seymour C, et al. Improved early detection of sepsis in the ED with a novel monocyte distribution width biomarker. Chest 2017; 152 (3): 518-26.

44) Crouser ED, Parrillo JE, Seymour C, et al. Improved early detection of sepsis in the ED with a novel monocyte distribution width biomarker. Chest 2017; 152 (3): 518-26.

45) Crouser ED, Parrillo JE, Seymour CW, et al. Monocyte distribution width: a novel indicator of sepsis-2 and sepsis-3 in high-risk emergency department patients. Crit Care Med 2019; 47 (8): 1018-25.

46) Crouser ED, Parrillo JE, Martin GS, et al. Monocyte distribution width enhances early sepsis detection in the emergency department beyond SIRS and qSOFA. J Intensive Care 2020; 8: 33.

47) Ognibene A, Lorubbio M, Magliocca P, et al. Elevated monocyte distribution width in COVID-19 patients: the contribution of the novel sepsis indicator. Clin Chim Acta. 2020; 509: 22–4.

48) Riva G, Castellano S, Nasillo V, et al. Monocyte Distribution Width (MDW) as novel inflammatory marker with prognostic significance in COVID-19 patients. Sci Rep 2021; 11 (1): 12716. doi: 10.1038/s41598-021-92236-6

49) Frugoli A, Ong J, Meyer B, et al. Monocyte Distribution Width Predicts Sepsis, Respiratory Failure, and Death in COVID-19. Cureus 2023; 15 (12): e50525. doi:10.7759/cureus.50525.

Original

miR-4485-5p in large extracellular vesicles as a new potent biomarker for diagnosis of deep vein thrombosis

†Hiromichi Shiotsu[*1], Daisuke Sueta*[*2], Satoru Shinriki*[*3],*
Mikuri Ryu[*1], Hiroki Usuku*[*2,4], Megumi Nakata*[*2],*
Takeshi Uchiumi[*1], Kenichi Tsujita*[*2], Hirotaka Matsui*[*5,6]*

†Correspondence: Department of Health Sciences, Graduate School of Medical Sciences, Kyushu University, 3-1-1 Maidashi Higashi-ku, Fukuoka, 812-8582, Japan E-mail: shiotsu.hiromichi.566@m.kyushu-u.ac.jp
Received February 5, 2024; accepted August 22, 2024
*1 Department of Health Science, Graduate School of Medical Sciences, Kyushu University
*2 Department of Cardiovascular Medicine, Graduate School of Medical Sciences, Kumamoto University, Kumamoto, Japan
*3 Department of Molecular Laboratory Medicine, Faculty of Life Sciences, Kumamoto University, Kumamoto, Japan
*4 Department of Laboratory Medicine, Kumamoto University Hospital, Kumamoto, Japan
*5 Department of Laboratory Medicine, National Cancer Center Hospital, Tokyo, Japan
*6 Department of Medical Oncology and Translational Research, Graduate School of Medical Sciences, Kumamoto University, Kumamoto, Japan

ABSTRACT

Deep vein thrombosis (DVT) is a pathological condition where blood clots form in the veins deeper than the fascia, sometimes leading to serious complications such as pulmonary embolism. DVT is a significant complication of cancer; given the situation where the frequency of cancer is predicted to increase, early diagnosis and intervention of DVT are crucial. Current diagnostic methods, such as blood D-dimer test and ultrasonography of the lower limbs, have limitations in terms of specificity and sensitivity.

In this study, we focused on large extracellular vesicles (LEVs) in the plasma of DVT patients and investigated whether microRNAs (miRNAs) enriched in these LEVs could serve as new biomarkers. While the total number of LEVs in patients with DVT was comparable to the control group, there was an increase in platelet-derived LEVs. Specifically, 13 miRNAs were decreased while 4 miRNAs were increased in LEVs in DVT patients (DVT LEVs), among which miR-4485-5p showed a significant 10.9-fold increase, demonstrating a good diagnostic performance for DVT with an area under the curve of 0.81.

Overexpression of miR-4485-5p in human umbilical vein endothelial cells (HUVEC) led to the suppression of tissue plasminogen activator, a predicted target of miR-4485p and a key component of the fibrinolytic system. Additionally, co-culture of HUVEC with DVT LEVs resulted in increased intracellular miR-4485-5p. These findings suggest that miR-4485-5p in platelet-derived LEVs could serve as a valuable biomarker for DVT and may contribute to thrombus formation by suppressing the fibrinolytic system.

〔Lab Med Int 2024; 3(3): 95-107〕

Key Words
microRNA, Deep vein thrombosis, Extracellular vesicles, Biomarker

I. Introduction

Deep vein thrombosis (DVT) is a condition characterized by the formation of thrombosis in the deep veins of the lower limbs and pelvis [1]. The development of a thrombus in more central veins, such as the vena cava, can lead to a life-threatening condition known as pulmonary thromboembolism (PE). DVT and PE are collectively referred to as venous thromboembolism (VTE) [1]. Virchow's triad, comprising venous stasis, endothelial injury, and hypercoagulability, is a well-established risk factor for VTE [2]. Cancer patients, in particular, are at an increased risk of developing DVT due to the elevated blood coagulopathy, a phenomenon known as cancer-as-

sociated thrombosis [3), 4)]. Indeed, an analysis of patients with acute VTE has revealed that active cancer or a history of cancer is a predominant risk factor, accounting for 31% of all cases [5)]. Furthermore, cancer patients with metastases face a significantly higher risk of VTE, up to 19.8 times higher than those without metastases, due to increased hypercoagulability of the blood [6), 7)]. As the global population continues to age, the prevalence of cancer is predicted to rise, leading to an anticipated increase in the number of patients experiencing VTE in the near future [1), 8)].

DVT is typically diagnosed through venous ultrasonography of the lower limbs, following the exclusion of obviously negative cases using a blood D-dimer test [9)]. While the blood D-dimer test exhibits high sensitivity for DVT diagnosis, its specificity is relatively low [9)]. One possible contributing factor to this limitation is the age-related increase in blood D-dimer levels, with extremely low specificity observed in patients aged 70 and 80 years or older at 22% and 9%, respectively [10)]. Additionally, reduced specificity is noted in cancer cases, where 46% of patients with abdominal malignancies but without DVT display values exceeding the conventional cutoff of 0.5 ng/mL [11)]. In addition, the blood D-dimer test is not ideal for screening purposes for DVT diagnosis, as it can be elevated in conditions such as inflammation, infection, trauma, and surgery [9)]. Although venous ultrasonography demonstrates high diagnostic performance, challenges include unstable delineation of deep veins and reliance on operator expertise and equipment performance for accurate diagnosis [9)]. Therefore, the identification of a novel biomarker for DVT diagnosis, characterized by significant specificity and consistent diagnostic accuracy, is of paramount importance.

To enhance the diagnostic accuracy of DVT, the study focused on large extracellular vesicles (LEVs) released from vascular endothelium, monocytes, and activated platelets [12), 13)]. Elevated levels of LEVs are observed in patients with DVT, cancer, and inflammation [14)-18)]. The increase in LEV levels is presumed to contribute to blood coagulation by exposing tissue factor (TF) on their surface [19)]. However, the diagnostic accuracy of DVT based on TF concentration and activity on the LEV surface varies across studies [20)], suggesting that measuring TF alone is insufficient for improving diagnostic accuracy.

LEVs also serve as carriers of microRNAs (miRNAs) involved in gene expression suppression [21)]. Moreover, extracellular vesicles from tumor cells and damaged organs exhibit a unique miRNA profile distinct from that in normal tissues [21), 22)]. This phenomenon has been observed in various malignancies and diseases, such as prostate cancer, lung cancer, Alzheimer's disease, and myocardial infarction [21)-23)]. Consequently, miRNAs in LEVs hold promise as novel clinical biomarkers [21)-23)]. miRNAs may migrate to other cells, modify gene expression, and regulate the pathogenesis of diverse diseases [23)]. While some miRNAs have shown utility in the diagnosis of DVT, the mechanisms related to pathogenesis and their association with LEVs have not been thoroughly investigated [24)]. In line with these observations, the study hypothesized that identifying clinically useful miRNAs in LEVs and elucidating their involvement in DVT pathogenesis could lead to the establishment of new biomarkers.

In this study, we analyzed the number of LEVs collected from DVT patients (referred to as DVT LEVs) and characterized the associated miRNAs. LEVs derived from platelets were found to be significantly increased in the DVT group. A comprehensive analysis of miRNAs extracted from DVT LEVs revealed changes in 17 miRNAs, among which miR-4485-5p showed a significant increase and demonstrated good diagnostic performance in the receiver operating characteristic (ROC) analysis. Functional analysis indicated that overexpression of miR-4485-5p suppressed tissue plasminogen activator (tPA), which is a candidate target of the miRNA, in human umbilical vein endothelial cells (HUVEC). Lastly, co-culture of HUVEC with LEVs recovered from clinical specimens significantly increased intracellular miR-4485-5p.

II. Materials and methods

2.1 Sample Collection

Plasma specimens were collected from 28 DVT patients (10 males and 18 females) (**Table 1, 2**). The diagnosis of DVT was conducted by well-trained cardiologists according to its diagnostic criteria and confirmed through enhanced computed tomography or lower extremity ultrasound sonography [25)]. Only new-onset DVT cases were included; cases with initiated treatment or recurrent DVT were excluded from the study. miRNAs were extracted from plasma of 24 out of 28 cases, excluding two instances with severe hemolysis occurred during plasma separation and two cases where the volume of specimens for nucleic acid extraction was insufficient. As a control group, the same analysis was performed on 14 age-matched healthy volunteers (4 males and 10 females).

2.2 Isolation of plasma LEVs and miRNA extraction

Seven mL of peripheral blood was collected in blood collection tubes supplemented with EDTA-Na (Venoject II; Terumo, Tokyo, Japan) and centrifuged for 10 minutes at 1,900g. The collected plasma was stored at −80℃ until

RNA extraction. Since this study focused on LEVs with a diameter less than 1,000 nm, previously referred to as 'microvesicles' or 'microparticles' [26], 1,000 μL of plasma was filtered through a membrane filter with a pore size of 1,000 nm (Membrane Solutions, Texas, USA) and centrifuged for 20 minutes at 17,000g [26]. Total RNA was extracted from the LEV pellets using the miRNeasy Plasma/Serum Kit (Qiagen, Hilden, Germany) following the manufacturer's protocol. As a spike-in control for quantitative analysis, 1 fmol of cel-miR-39, a *C. elegans*-derived miRNA, was added. The extracted total RNA was stored at −80℃ until further usage.

2.3 Flow cytometry (FCM) analysis

LEVs in the plasma samples (n=5 for the DVT group and n=6 for the control group) were counted by FCM. Isolated LEVs were washed three times with calcium- and magnesium-free Dulbecco's phosphate-buffered saline (Nacalai Tesque, Kyoto, Japan). LEVs hold identical surface markers to the original cell because the outer layer consists of the cell membrane [26]. We stained platelet-derived LEVs with CD31-APC-Cy5 (Biolegend, San Diego, USA) and CD61-FITC (Biolegend) antibodies for identification. Control beads (Spherotech, Lake Forest, USA) were added for size control. Stained LEVs were measured by FACS Verse (BD Biosciences, New Jersey, USA). Particles smaller than the size control beads with a diameter of 1,000 nm were counted as LEVs.

2.4 Microarray analysis

A 3D-gene miRNA Oligo Chip (Toray, Tokyo, Japan) was employed to generate a comprehensive miRNA profile in DVT LEVs. The signal intensities obtained for each well were corrected using the 75th percentile signal intensities, which were further normalized by conversion to $\log_2$ values. A heat map and a volcano plot were generated with a cut-off of at least a 2-fold change in miRNA expression and a p-value of less than 0.05 by Welch's t-test. R (4.2.0) and gplots package (3.1.3) were utilized to generate the heat map and volcano plot [27].

2.5 Real-time quantitative PCR (RT-qPCR) analysis of miRNAs

Candidate miRNAs for DVT biomarkers were analyzed by RT-qPCR. Equal amounts of total RNA were reverse transcribed using the TaqMan microRNA Reverse Transcription kit (Thermo Fisher Scientific, Massachusetts, USA). Synthesized complementary DNA (cDNA) was then amplified on a DICE TP800BE thermal cycler (Takara, Shiga, Japan) using the Luna Universal Probe qPCR Master Mix (New England Biolabs, Massachusetts, USA) and TaqMan MicroRNA Assay (Thermo Fisher Scientific). The PCR reaction conditions were set as follows: enzyme activation at 95℃ for 10 minutes, followed by 40 cycles of 95℃ for 15 seconds and 60℃ for 1 minute. During RNA extraction, 1 fmol of cel-miR-39 was spiked in and used as an exogenous control. The expression levels were calculated from the obtained amplification curves using the comparative threshold cycle (Ct) method, and the values were presented relative to the average of the control group.

2.6 Cell culture

HUVEC, an endothelial cell-derived cell line, was obtained from the JCRB Cell Bank (Osaka, Japan) and cultured in DMEM/HAM's F12K medium (FUJIFILM Wako Pure Chemical, Osaka, Japan) supplemented with 10% fetal bovine serum, 50 μg/mL endothelial cell growth supplement (FUJIFILM Wako Pure Chemical), and 100 μg /mL heparin (FUJIFILM Wako Pure Chemical) at 37℃ with 5% CO_2.

2.7 Transfection of miRNA mimic and inhibitor into HUVEC

HUVEC was transfected with mirVana miR-4485-5p inhibitor and mimic (each from Thermo Fisher Scientific) using Lipofectamine RNAiMAX (Thermo Fisher Scientific). The concentrations of the inhibitor and mimic were set at 10, 30, and 50 nM per well. Cells were collected 24 hours after transfection, and protein and RNA were extracted from the cells.

2.8 RT-qPCR analysis of candidate miRNA target genes

mRNA expression in HUVEC was measured by RT-qPCR. An equal amount of RNA was first reverse transcribed with the PrimeScript RT-PCR kit (Takara). The cDNA was amplified using TB Green Premix Ex Taq (Takara) under the following conditions: enzyme activation: 95℃, 30 sec; PCR reaction: 40 cycles of 95℃ for 5 sec, and 60℃ for 30 sec. The expression of *PLAT* (encoding tPA) was measured using the following primers: forward primer: CATATTTCGTGTGCCAGTGC and reverse primer: GACCCATTCCCAAAGTAGCA. *IPO8* was used as an internal control with the following primers: forward primer: GGCATACAGTTTAACCTGCCAC and reverse primer: CAGGAGAGGCATCATGTCTGTAA [28]. The expression levels were calculated from the obtained amplification curves using the Ct method, and the values were presented relative to the mean of the control group.

2.9 Immunoblotting

HUVEC was harvested, and radio-immunoprecipitation assay (RIPA) buffer was added to the cells, followed by sonication to lyse the cells. The lysed sample was mixed with an equal volume of sample buffer (FUJIFILM Wako Pure Chemical). The mixture was separated on a 10%

SDS-PAGE gel and transferred to a polyvinylidene difluoride membrane. The transferred membrane was blocked with Blocking One (Nacalai Tesque) and incubated with an anti-tPA antibody (ab227069, Abcam, Cambridge, UK) or anti-GAPDH antibody (2118, Cell Signaling, Danvers, USA) overnight at 4℃. After incubation, the membrane was washed three times with phosphate-buffered saline (PBS) with 0.1% Tween 20. Subsequently, the membrane was incubated for 2 hours at room temperature with horse radish peroxidase (HRP) -labeled anti-rabbit antibody (1:1,000) (7074, Cell Signaling). Signals were visualized with Western blot hyper HRP substrate (Takara) and analyzed by LAS-2000 (GE Healthcare, Fairfield, USA).

2.10 Co-culture of HUVEC with LEVs isolated from plasma

HUVEC (3.0×10^4) was adhered to 24-well plates (Corning, New York, USA) and cultured for 24 hours. One hundred thousand FCM-counted LEVs from DVT and control samples were dissolved in 200 μL Opti-MEM (Thermo Fisher Scientific) and added to the culture medium. After 24 hours, the LEVs in the culture medium were removed. HUVEC was collected after washing with PBS and lysed for RNA extraction.

2.11 Statistical analysis

Welch's t-test was employed to compare the two groups [29), 30)]. A p-value less than 0.05 was considered significant. The diagnostic performance of miR-4485-5p was determined by the area under the curve (AUC) calculated by ROC analysis. Optimal sensitivity and specificity were determined by the Youden index. R (4.2.0) and pROC package (1.18.0) were used for the analysis [31)].

2.12 Ethical Consideration

This study was conducted following approval from the ethics committees of Kumamoto University (Approval No. 2016) and Kyushu University (Approval No. 2020-250). Samples were exclusively collected from individuals who provided written informed consent, and all procedures adhered to the principles of the Declaration of Helsinki. Samples were obtained from adult participants between August 13, 2020, and February 31, 2022.

III. Results

3.1 Characteristics of DVT patients included in the study

Table 1 and 2 present the characteristics of the DVT and control groups. The mean age of the DVT patients was 69.1 years (range: 39-86 years). Coagulation and hematological tests revealed significantly higher blood D-dimer levels in the DVT group ($p < 0.001$) (**Table 1**), whereas the red blood cell count ($p = 0.005$), hemoglobin ($p < 0.001$), and hematocrit ($p < 0.001$) were significantly lower in the DVT group.

Among the 28 DVT patients, cancer (n=20, 71.4%) was the most common primary disease in the cohort; two patients (7.1%) had collagen disease, and one patient (3.6%) had varicose veins (**Table 2**). Collectively, the cases in this study included typical patients with underlying conditions associated with a high risk of developing DVT, thus the selection of subjects was considered appropriate.

3.2 Increased platelet-derived LEVs in DVT patients

The number of plasma LEVs was counted by FCM (n=5 in the DVT group, n=6 in the control group). The total number of LEVs per mL was comparable between the DVT and control groups (**Figure 1a**). Previous studies have shown that LEVs formed by the platelet (referred to as platelet-derived LEVs) are increased in DVT [32)-34)]. Indeed, when we labeled platelet-derived LEVs with their respective surface markers, CD31 and CD61, they were significantly increased in the DVT cases (**Figure 1b, 1c**). This result suggests that the increase in LEVs in DVT was primarily due to release from platelets, although the specificity of CD31 for the marker of platelet-derived LEVs needs further study [34)]. While, the absolute number of LEVs did not increase, and the degree of increase in CD31- and CD61-positive LEVs was almost equal. This indicates that the increase in LEVs in DVT is more likely to be derived from platelets.

3.3 Increased miR-4485-5p in LEV fraction as a diagnostic marker for DVT

Given the increased platelet-derived LEVs in DVT cases, we hypothesized that their miRNA expression levels might be altered. We conducted a comprehensive analysis of miRNA profiles within LEVs obtained from the plasma of both DVT and control subjects.

Firstly, we performed microarray analysis on samples from five age- and sex-matched subjects each from the DVT and control groups after extracting miRNAs within LEVs. Four out of five DVT patients in this subset also had concomitant cancer. The generated heat map shows clustering based on signal intensity (**Figure 2a**), and the volcano plot illustrated significant alterations in 4 miRNAs with an increase and 13 miRNAs with a decrease in the DVT group (**Figure 2b**). These miRNAs that were significantly altered by microarray analysis are shown in **Table 3**. Given the specific increase of CD31- and CD61-positive LEVs (**Figure 1b, 1c**), the changes in miRNA level were suggested to be influenced by an increase in platelet-derived LEVs.

Table 1

	DVT	Control	*p* value
n	28	14	
Sex, male: n (%)	8 (28.6)	4 (28.6)	
Age (years)	69.1 ± 2.2	67.8 ± 2.9	0.71
WBC ($\times 10^3/\mu L$)	6.8 ± 0.5	5.7 ± 0.3	0.08
RBC ($\times 10^6/\mu L$)	3.7 ± 0.2	4.3 ± 0.1	<0.01
Hgb (g/dL)	11.1 ± 0.4	13.7 ± 0.3	<0.001
Hct (%)	33.8 ± 1.3	40.4 ± 0.9	<0.001
MCV (fL)	93.3 ± 1.6	95.4 ± 2.1	0.41
MCH (pg)	30.8 ± 0.7	32.5 ± 1.2	0.26
MCHC (g/dL)	32.9 ± 0.3	33.9 ± 0.4	0.11
PLT ($\times 10^3/\mu L$)	232.0 ± 22.6	211.7 ± 2.9	0.85
PT (sec)	12.4 ± 0.2	11.9 ± 0.2	0.11
APTT (sec)	31.9 ± 3.2	30.2 ± 1.0	0.74
D-dimer (μg/mL)	9.6 ± 1.5	0.7 ± 0.1	<0.001

All values are expressed as means ± SEMs.

Table 2

Comorbidities		n (%)
Cancer		20 (71.4)
	Head and neck	6 (21.4)
	Uterine	5 (17.8)
	Hematological	2 (7.1)
	Esophageal	2 (7.1)
	Ovarian	2 (7.1)
	Pancreatic	1 (3.6)
	Breast	1 (3.6)
	Bladder	1 (3.6)
Collagen disease		2 (7.1)
Varicose vein		1 (3.6)
Fixation		1 (3.6)
Not applicable		4 (14.3)

Table 3

Up-regulated miRNA			Down-regulated miRNA		
miRNA ID	Log_2 (Fold change)	*p* value	miRNA ID	Log_2 (Fold change)	*p* value
miR-4485-5p	4.3	<0.01	miR-451a	-4.3	<0.01
miR-1973	4.8	<0.05	miR-92b-3p	-3.2	<0.05
miR-12136	2.8	<0.05	miR-122-3p	-3.1	<0.05
miR-361-3p	1.7	<0.05	miR-1343-3p	-2.7	<0.05
			miR-4317	-2.6	<0.05
			miR-12115	-2.6	<0.05
			miR-100-5p	-2.5	<0.05
			miR-128-1-5p	-2.5	<0.05
			miR-99a-5p	-2.3	<0.05
			miR-6887-5p	-2.1	<0.05
			miR-8052	-2.1	<0.05
			miR-6880-5p	-1.9	<0.05
			miR-23a-3p	-1.3	<0.05

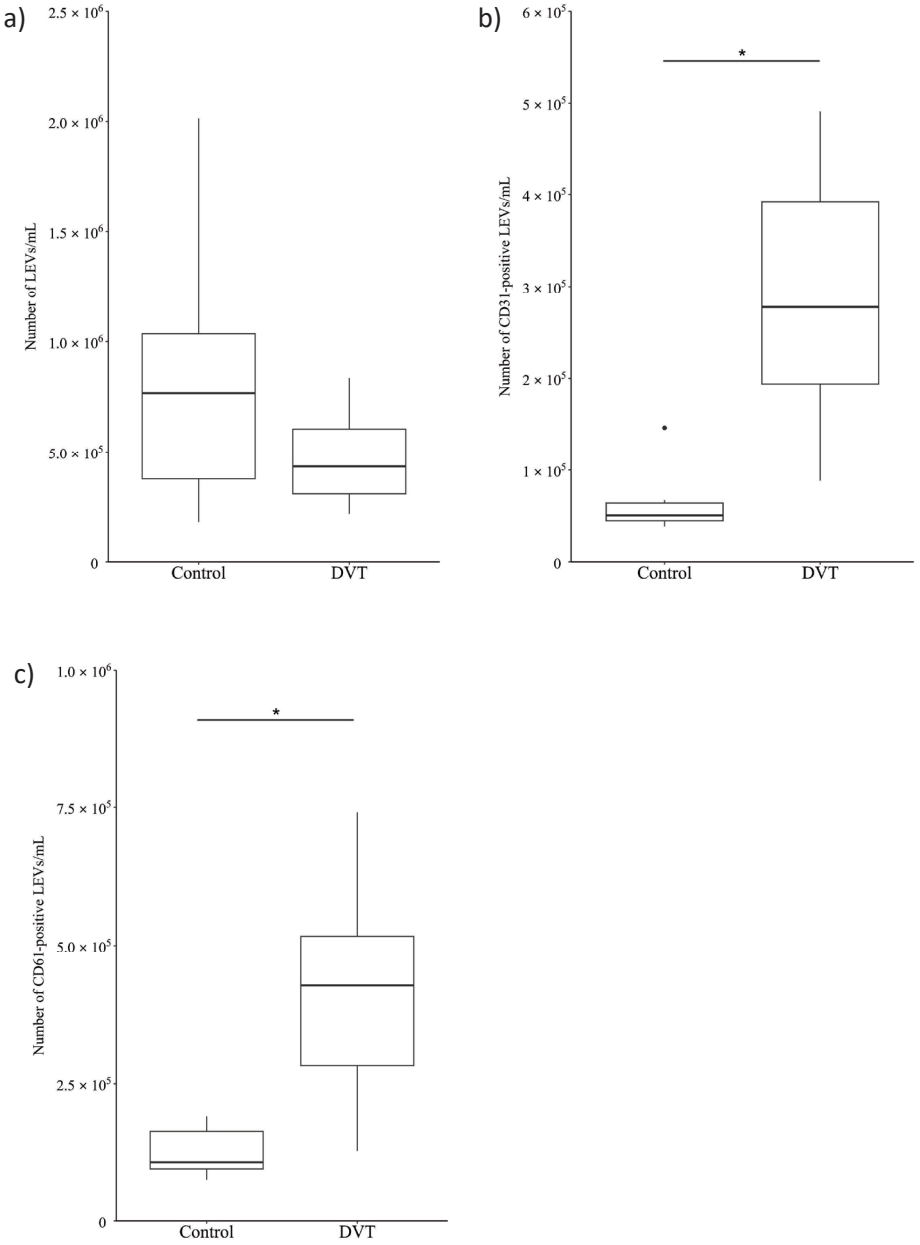

Figure 1 Increased platelet-derived LEVs in plasma of DVT patients
(a) Number of total LEVs. (b and c) CD31- and CD61-positive LEVs in plasma analyzed by FCM. Each value in the graph shows the number of LEVs per mL. (n = 6 for control group and n=5 for DVT group) (* $p < 0.05$).

We next quantified miR-4485-5p, the miRNA with the most significant increase in the microarray. Nineteen DVT and fourteen control samples, different from those used for microarray analysis, were employed. As expected, the expression level of miR-4485-5p was significantly elevated in the DVT group (10.9-fold higher than in the control group, $p = 0.008$) (**Figure 2c**). Thus, it was confirmed that miR-4485-5p was markedly elevated by increased platelet-derived LEVs in DVT patients.

Finally, the diagnostic efficacy of increased miR-4485-5p within LEVs for DVT was evaluated using ROC analysis. The AUC of miR-4485-5p in LEVs was 0.81 (95% confidence interval 0.65-0.97), with a diagnostic sensitivity of 0.74 and specificity of 0.94 when the optimal cut-off value was set at 1.825, as determined by the Youden index (**Figure 2d**). Collectively, increased miR-4485-5p in LEVs was deemed a valuable marker for DVT diagnosis.

3.4 Reduced tPA expression by miR-4485-5p in HUVEC

We then explored the impact of miR-4485-5p on target cells, specifically investigating its effects on candidate target genes. Using miRwalk [35], a target mining tool, we identified 36,713 genes as potential targets; we selected genes highly expressed in venous tissue and involved

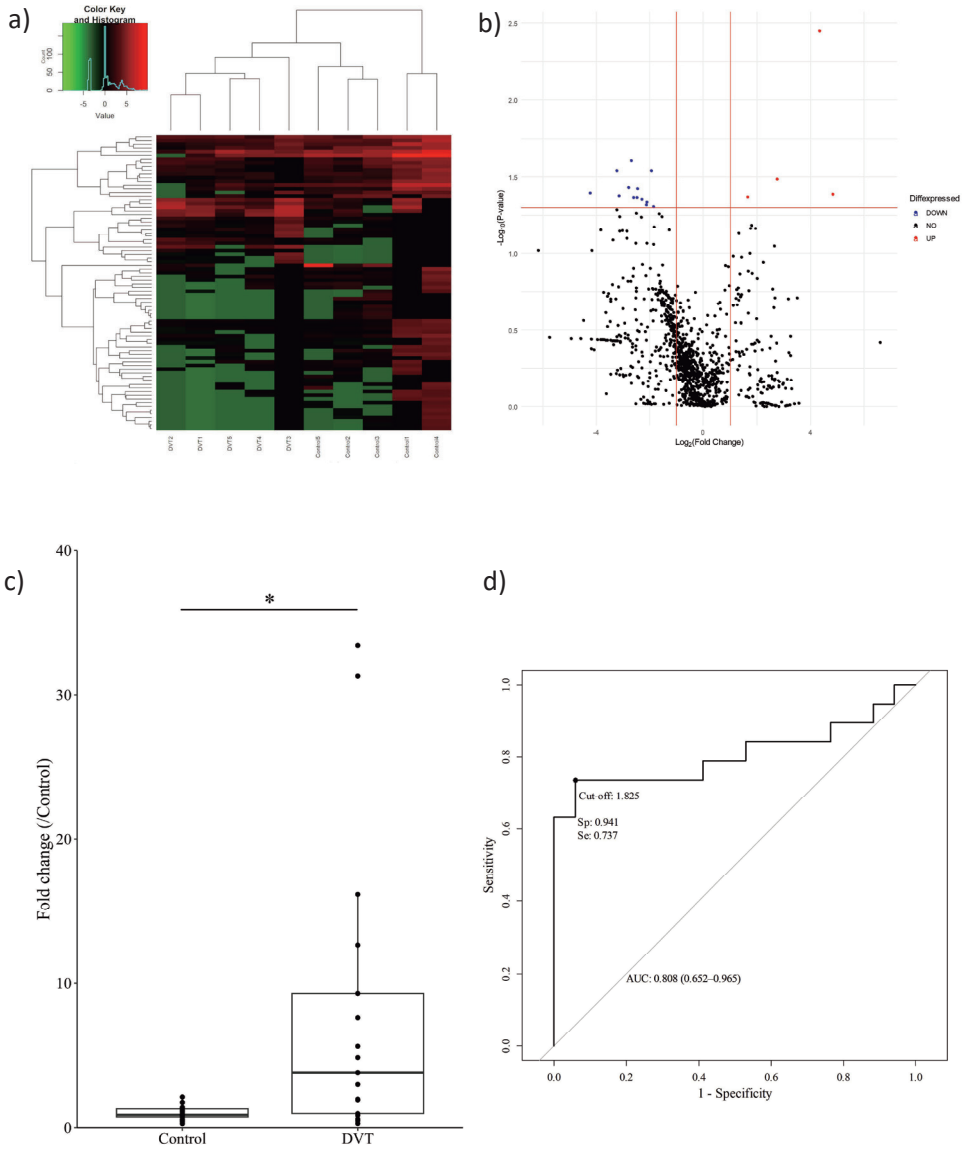

Figure 2 Increased miR-4485-5p LEVs from DVT patients

(a) Heat map of differentially expressed miRNAs in DVT versus control LEVs. Expression levels are shown as color, where red represents high expression level and green represents low in each sample. (b) Volcano plot of microarray analysis. Red lines indicate cut-offs of 1 on the X-axis (fold change > 2.0) and 1.3 on the Y-axis ($p < 0.05$). (c) RT-qPCR analysis of miR-4485-5p in LEVs (control n=14, DVT n=19). As a control, 1 fmol of cel-miR-39 was used. The top and bottom edges of the box indicate the first and third quartiles, respectively. The upper and lower whiskers indicate the maximum and minimum values, excluding outliers. (d) Receiver operating characteristic (ROC) analysis of miR-4485-5p for DVT. Sp: specificity, Se: sensitivity (* $p < 0.05$).

in the complement and coagulation cascade (KEGG pathway: hsa04610) as promising candidates [36]. Among these, *PLAT*, a gene encoding tPA, emerged as a functional target with sequences complementary to miR-4485-5p in both the 3'UTR and coding region (**Figure 3a**).

Subsequently, we investigated the expression of *PLAT* in HUVEC when miR-4485-5p expression was modulated using the miR-4485-5p mimic and inhibitor. Introduction of the miRNA mimic led to a 38.0-fold increase in miR-4485-5p expression in HUVEC, resulting in a 0.68-fold decrease in *PLAT* expression compared to the control (p =0.02) (**Figure 3b, 3d**). Conversely, the miRNA inhibitor decreased miR-4485-5p expression in HUVEC by 0.35-fold and increased *PLAT* expression by 1.46-fold (p =0.03) (**Figure 3c, 3e**). Additionally, tPA expression, assessed by Western blotting, was significantly reduced by 0.29-fold in HUVEC transfected with the miR-4485-5p mimic (p =0.014) (**Figure 3f**), although no significant change in tPA protein was observed in HUVEC treated

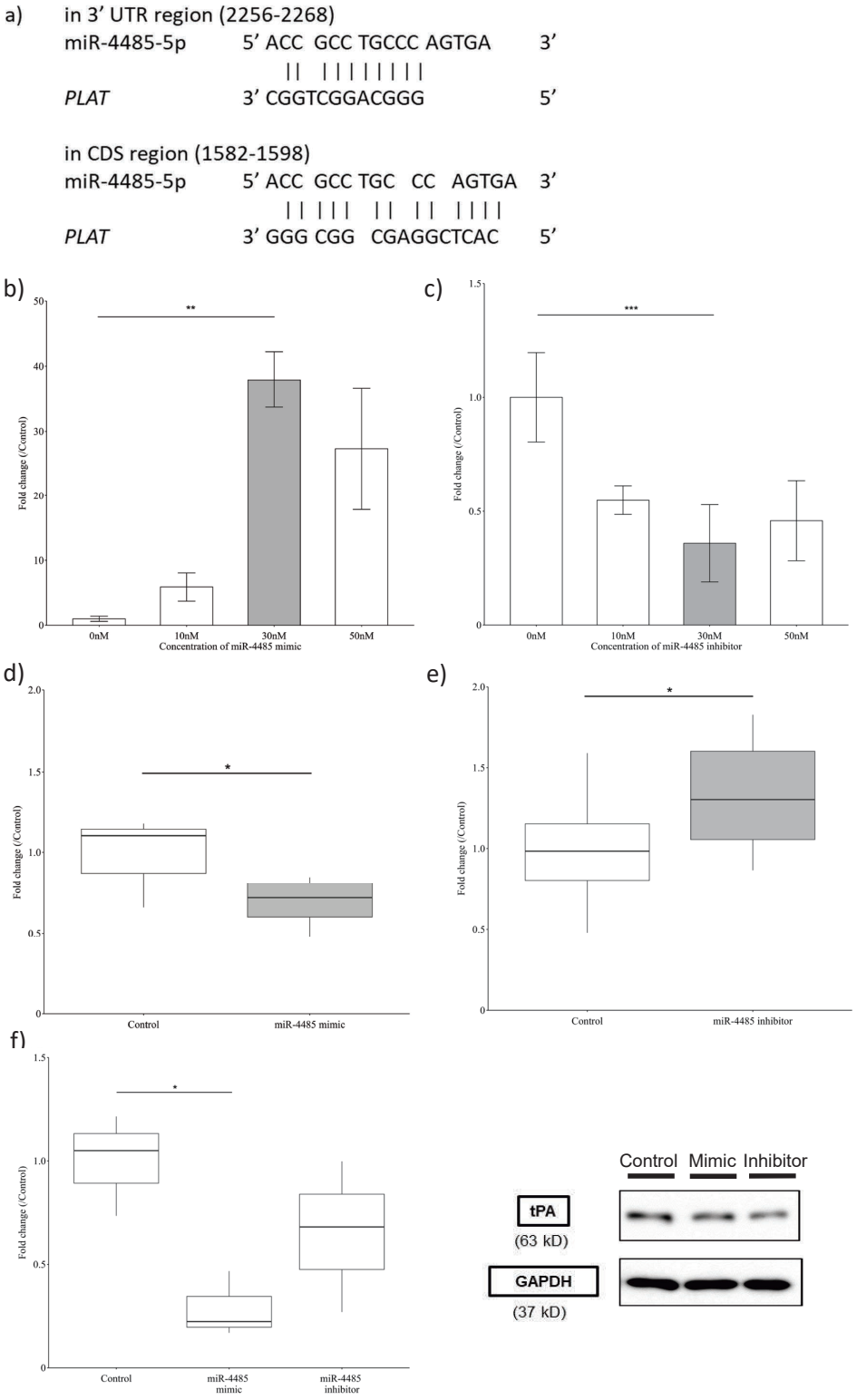

Figure 3 Suppression of tPA by miR-4485-5p in HUVEC.
(a) Binding sites of miR-4485-5p with *PLAT*, as predicted by miRwalk. (b) miR-4485-5p expression in HUVEC with each concentration of miR-4485-5p mimic (n=3) and (**c**) inhibitor (n=3). (d) *PLAT* expression in HUVEC exposed with 30nM miR-4485-5p mimic (n=6) and (**e**) inhibitor (n=10). (f) Western blot analysis of tPA protein treated with miR-4485-5p mimic and inhibitor (n=3). tPA protein in HUVEC treated with miR-4485-5p mimic and inhibitor are corrected for GAPDH to compare with control (* $p < 0.05$, ** $p < 0.01$, *** $p < 0.001$).

with the miR-4485-5p inhibitor (p =0.24). Previous studies showed that over 90% of the tPA protein produced by HUVECs is secreted extracellularly, with only a minor fraction remaining intracellular[37),38)]. Therefore, it is possible that miRNA inhibitor did not contribute to the increase in tPA protein in HUVEC when measured by Western blot analysis. Overall, these findings suggest that an increase in miR-4485-5p exerts an inhibitory effect on tPA expression in vascular endothelial cells.

3.5 Increased miR-4485-5p in HUVEC exposed to LEVs from DVT patients

Finally, we investigated the impact of DVT LEVs on intracellular miR-4485-5p levels in HUVEC. LEVs from three DVT and control samples, with similar particle size distributions as determined by FCM, were selected for the experiment. Two of the three DVT samples were associated with cancer, while the remaining one was linked to collagen disease. We confirmed that miR-4485-5p levels in LEVs from all three DVT cases were more than 2-fold higher than the mean level in the control group (**Figure 2c**).

Comparing HUVEC co-cultured with LEVs from DVT patients or non-DVT donors to those cultured without LEVs, both groups exhibited a significant increase in intracellular miR-4485-5p levels (by 1.16-fold or 1.23-fold, respectively), but there was no significant difference between the DVT and non-DVT groups (p =0.29) (**Figure 4a**). These findings suggest that LEVs can elevate miR-4485-5p levels in target cells. Furthermore, the *PLAT* expression in HUVECs co-cultured with non-DVT LEVs compared to HUVECs cultured without LEVs was 1.51 and 0.97 in those co-cultured with DVT LEVs. The results indicated that DVT LEVs reduced the *PLAT* expression in HUVECs compared to non-DVT LEVs. However, the difference was not statistically significant (p = 0.099) (**Figure 4b**). The lack of distinction between the DVT and control groups in this experiment may be attributed to the use of unsorted LEVs instead of purified platelet-derived LEVs due to technical constraints. Western blot analysis of tPA protein could not be performed due to the insufficient recovery of protein extract required for the assay.

IV. Discussion

In this study, the analysis of miRNAs in DVT LEVs aimed to elucidate their significance in the pathogenesis and potential as biomarkers. Among the 17 significantly altered miRNAs in DVT LEVs, miR-4485-5p exhibited notable diagnostic performance for DVT. This miRNA was found to suppress tPA in HUVEC, suggesting its involvement in thrombus formation through the inhibition of the fibrinolytic system.

Notably, the increase in miR-4485-5p levels is suggested to link to impaired mitochondrial function, as evidenced by reduced ATP production and increased reactive oxygen species (ROS) in cells[39)-43)]. Despite the precise mechanisms connecting increased miR-4485-5p to mitochondrial dysfunction remain unknown, the study showing that vascular tissue in mice with mitochondrial dysfunction exhibited increased levels of both ASncmtRNA-2, a precursor antisense non-coding mitochondrial RNA of miR-4485-5p[40)-43)], and miR-4485-5p imply a connection between these and mitochondria regulation[40),42)]. In addition, previous study suggests a potential connection between mitochondrial dysfunction and increased LEVs; Burger et al. reported that cells with reduced mitochondrial function produced more LEVs, and conversely, an increase in

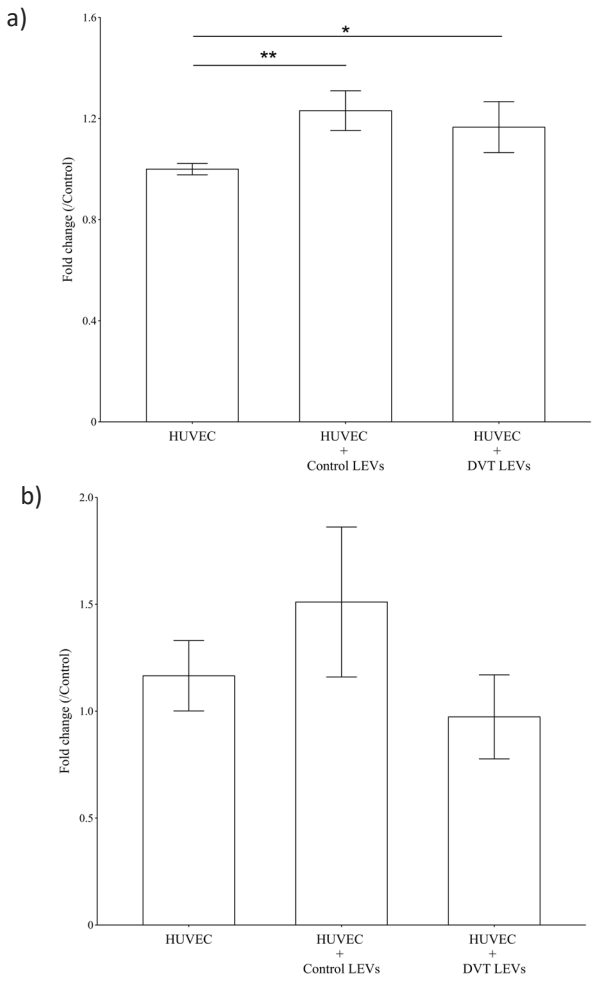

Figure 4 Increase of miR-4485-5p induced by LEVs. (a) Expression level of miR-4485-5p and (b) *PLAT* in HUVEC with 100,000 control and DVT LEVs after 24 hours, as analyzed by RT-qPCR (n = 3) (* $p < 0.05$, ** $p < 0.01$).

LEVs significantly reduced mitochondrial function in the cells [44]. Overall, this study, in conjunction with existing literature, proposes a potential disease mechanism (**Figure 5**): primary diseases lead to mitochondrial dysfunction in platelets and endothelial cells, resulting in elevated levels of miR-4485-5p within intracellular [13), 45)-48)]. This accompanies with the release of a substantial number of LEVs containing this miRNA into the bloodstream. The presence of miR-4485-5p contributes to the inhibition of tPA, a key component of the fibrinolytic system, in endothelial cells, thus creating a hypercoagulable environment conducive to the formation of DVT.

The study suggests that miR-4485-5p in LEVs could serve as a promising biomarker for DVT. Compared to traditional tests like the blood D-dimer test, miR-4485-5p in LEVs exhibited better specificity [9]. Furthermore, it provides a more stable measurement than ultrasonography of the lower limbs, which can vary in diagnostic performance based on the examiner and equipment [9]. The potential utility of measuring miR-4485-5p is seen in its ability to overcome the limitations of existing tests and improve the diagnosis of DVT.

Our study acknowledges several limitations. The small number of cases analyzed calls for further studies with a larger number of DVT cases. The prevalence of both cancer and DVT in most patients makes it challenging to determine the individual contributions of each disease to the results. The study also points out the need for further research to specify the origin of the identified miRNAs within LEVs and to elucidate detailed underlying mechanisms. In particular, since CD31 is highly expressed in both vascular endothelium and platelets, it is necessary to determine whether the LEVs are of vascular endothelial or platelet origin [34]. Currently, there is no consensus on which cell type predominantly contributes to the high CD31 expression on LEVs. Furthermore, it is important to determine whether miR-4485-5p-rich LEVs are derived from vascular endothelium or platelets.

In conclusion, the study highlights the clinical significance of DVT diagnosis, especially considering that 10% of unidentified VTEs (uVTE) are diagnosed as cancer within a year [49]. A substantial portion (more than 60%) of cancers of unknown primary origin is diagnosed shortly after the identification of uVTE [49]. This suggests that latent DVT might be an early indicator of cancer. Recognizing the importance of early DVT diagnosis from a cancer perspective, the study emphasizes the need to establish biomarkers that can enhance the diagnostic performance of DVT. miR-4485-5p in LEVs is proposed as a potential biomarker that could fulfill this role.

Funding

This study was funded by the Japanese Society of Laboratory Medicine Fund for the Promotion of Scientific Re-

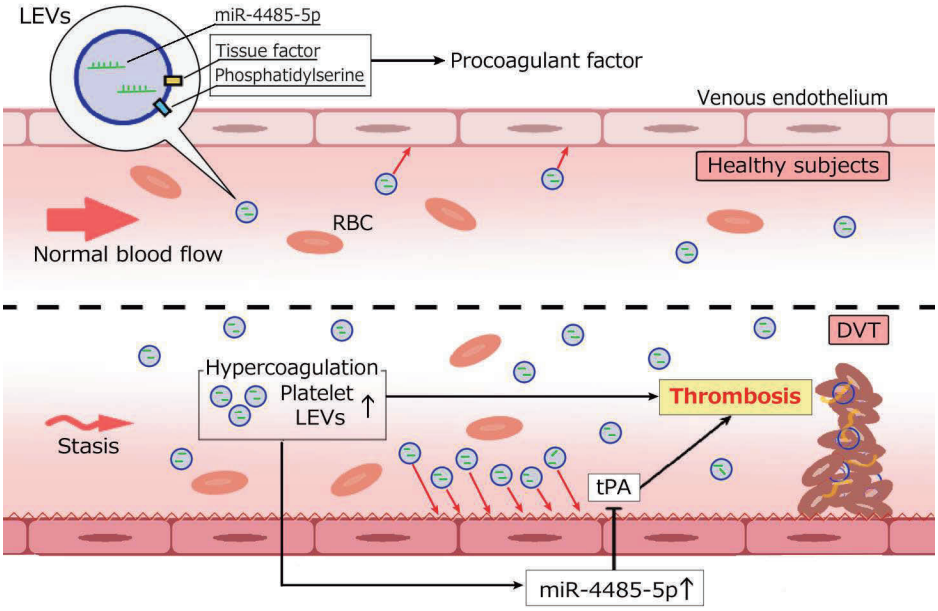

Figure 5 Pathogenesis of DVT involving LEVs and miR-4485-5p.
Schematic summary of our study. Activation of platelets due to cancer and other pathogenic conditions via blood flow stasis increases platelet-derived LEVs that contain miR-4485-5p. The miR-4485-5p is incorporated into endothelial cells, leading to the suppression of tPA. This causes further hypercoagulability status, which leads to the formation of thrombosis.

search and JSPS KAKENHI Grant Number JP 19K16954 and JP 23K06930.

Acknowledgements

We thank Mr. Shinichi Mizuno for the management of personal information, Mr. Hiroshi Shigeto for the support of English editing and suggestions, Ms. Aya Higashi for assisting blood sample storage, and Ms. Kazue Akita for the clerical work.

Author Contributions

Conceptualization: HM, HS., Formal analysis: HS., Funding acquisition: HM, SS, TU, HS., Investigation: HS, SS, MR., Methodology: HM, TU, HS., Project administration: HM, KT., Resources: DS, MN, HU., Software: HS, MR., Supervision: HM, KT, TU., Validation: HS, SS, MR., Writing – original draft: HS, HM., Writing – review & editing: HM, HS, DS, KT.

Competing Interest

The authors have declared that no competing interests exist.

Reference

1) Cushman M, Barnes GD, Creager MA, et al. American Heart Association Council on Peripheral Vascular Disease; Council on Arteriosclerosis, Thrombosis and Vascular Biology; Council on Cardiovascular and Stroke Nursing; Council on Clinical Cardiology; Council on Epidemiology and Prevention; and the International Society on Thrombosis and Haemostasis, Venous Thromboembolism Research Priorities: A Scientific Statement From the American Heart Association and the International Society on Thrombosis and Haemostasis. Circulation 2020; 142 (6) : e85-94. doi:10.1161/CIR.0000000000000818.

2) Stone J, Hangge P, Albadawi H, et al. Deep vein thrombosis: pathogenesis, diagnosis, and medical management. Cardiovasc Diagn Ther 2017; 7 (Suppl 3) : S276-84. doi:10.21037/cdt.2017.09.01.

3) Akinbo DB, Ajayi OI. Thrombotic Pathogenesis and Laboratory Diagnosis in Cancer Patients, An Update.Int J Gen Med 2023; 16: 259-72. doi: 10.2147/IJGM.S385772.

4) Hisada Y, Mackman N. Cancer-associated pathways and biomarkers of venous thrombosis. Blood 2017; 130 (13) : 1499-506. doi: 10.1182/blood-2017-03-743211.

5) Sakamoto J, Yamashita Y, Morimoto T, et al. cancer-associated venous thromboembolism in the real world - from the COMMAND VTE registry. Circ J 2019; 83 (11) : 2271-81. doi: 10.1253/circj. CJ-19-0515.

6) Blom JW, Doggen CJM, Osanto S, et al. Malignancies, prothrombotic mutations, and the risk of venous thrombosis. JAMA 2005; 293 (6) : 715-22.

7) Razak NBA, Jones G, Bhandari M, et al. Cancer-associated thrombosis: An overview of mechanisms, risk factors, and treatment. Cancers (Basel) 2018; 10 (10) : 380. doi: 10.3390/cancers10100380.

8) Ferlay J, Colombet M, Soerjomataram I, et al. Cancer statistics for the year 2020: An overview. Int J Cancer 2021; 149: 778-89. doi: 10.1002/ijc.33588.

9) Lim W, Gal GL, Bates SM, et al. American Society of Hematology 2018 guidelines for management of venous thromboembolism: diagnosis of venous thromboembolism. Blood Adv 2018; 2 (22) : 3226-56. doi: 10.1182/bloodadvances.2018024828.

10) Kelly J, Rudd A, Lewis RR, et al. Plasma D-dimers in the diagnosis of venous thromboembolism. Arch Intern Med 2002; 162 (7) : 747-56. doi: 10.1001/archinte.162.7.747.

11) Kwietniak M, AI-Amawi T, Błaszkowski T, et al. The usefulness of D-dimer in diagnosis and prediction of venous thromboembolism in patients with abdominal malignancy. Pol Przegl Chir 2017; 89 (3) : 27-30. doi: 10.5604/01.3001.0010.1018.

12) Mooberry MJ, Key NS. Microparticle analysis in disorders of hemostasis and thrombosis. Cytometry A 2016; 89 (2) :111-22. https://doi: 10.1002/cyto.a.22647.

13) Konkoth A, Saraswat R, Dubrou C, et al. Multifaceted role of extracellular vesicles in atherosclerosis. Atherosclerosis. 2021; 319: 121-31. doi: 10.1016/j.atherosclerosis.2020.11.006.

14) Chirinos JA, Heresi GA, Velasquez H, et al. Elevation of endothelial microparticles, platelets, and leukocyte activation in patients with venous thromboembolism. J Am Coll Cardiol 2005; 45 (9) : 1467-71. doi: 10.1016/j.jacc.2004.12.075.

15) Nazari M, Javandoost E, Talebi M, et al. Platelet microparticle controversial role in cancer. Adv Pharm Bull 2021; 11 (1) : 39-55. doi: 10.34172/apb.2021.005.

16) Oyabu C, Morinobu A, Sugiyama D, et al. Plasma platelet-derived microparticles in patients with connective tissue diseases. J Rheumatol 2011; 38 (4) : 680-4. doi: 10.3899/jrheum.100780.

17) Fink K, Moebes M, Vetter C, et al. Selenium prevents microparticle-induced endothelial inflammation in patients after cardiopulmonary resuscitation. Crit Care 2015; 19 (1) : 58. doi: 10.1186/s13054-015-0774-3.

18) Nomura S. Microparticle and atherothrombotic diseases. J Atheroscler Thromb 2016; 23 (1) : 1-9. doi: 10.5551/jat.32326.

19) Date K, Hall J, Greenman J, et al. Tumour and microparticle tissue factor expression and cancer thrombosis. Thromb Res 2013; 131 (2) :109-15. doi: 10.1016/j.thromres.2012.11.013.

20) Almeida VH, Rondon AMR, Gomes T, et al. Novel Aspects

of Extracellular Vesicles as Mediators of Cancer-Associated Thrombosis. Cells 2019; 13 (8) ; 716. doi: 10.3390/cells8070716.

21) O'Brien J, Hayder H, Zayed Y, et al. Overview of microRNA biogenesis, Mechanisms of Actions, and Circulation. Front Endocrinol (Lausanne) 2018; 9: 402. doi: 10.3389/fendo.2018.00402.

22) Katoh M. Cardio-miRNAs and onco-miRNAs: circulating miRNA-based diagnostics for non-cancerous and cancerous diseases. Front Cell Dev Biol 2014; 2: 61. doi: 10.3389/fcell.2014.00061.

23) Wang J, Chen J, Sen S. MicroRNA as Biomarkers and Diagnostics. J Cell Physiol. 2016; 231 (1) : 25-30. doi: 10.1002/jcp.25056.

24) Jiang Z, Ma J, Wang Q, et al. Combination of circulating miRNA-320a/b and D-Dimer improves diagnostic accuracy in deep vein thrombosis patients. Med Sci Monit 2018; 24: 2031-7. doi: 10.12659/msm.906596.

25) Kearon C, Akl EA, Ornelas J, et al. Antithrombotic Therapy for VTE Disease: CHEST Guideline and Expert Panel Report. Chest. 2016; 149 (2) : 315-52. doi: 10.1016/j.chest.2015.11.026.

26) Théry C, Witwer KW, Aikawa E, et al. Minimal information for studies of extracellular vesicles 2018 (MISEV2018) : a position statement of the International Society for Extracellular Vesicles and update of the MISEV2014 guidelines. J Extracell Vesicles. 2018; 7 (1) : 1535750. doi: 10.1080/20013078.2018.1535750.

27) Chen JJ, Tsai CA, Tzeng S, et al. Gene selection with multiple ordering criteria. BMC Bioinformatics. 2007; 8: 74. doi: 10.1186/1471-2105-8-74.

28) Rácz GA, Nagy N, Tóvári J, et al. Identification of new reference genes with stable expression patterns for gene expression studies using human cancer and normal cell lines. Sci Rep 2021; 11 (1) :19459. doi: 10.1038/s41598-021-98869-x.

29) Zimmerman DW. A note on preliminary tests of equality of variances. Br J Math Stat Psychol 2004; 57 (Pt 1) : 173-81. doi: 10.1348/000711004849222.

30) Fagerland MW, Sandvik L, Mowinckel P, et al. Parametric methods outperformed non-parametric methods in comparisons of discrete numerical variables. BMC Med Res Methodol 2011; 11: 44. doi: 10.1186/1471-2288-11-44.

31) Robin X, Turck N, Hainard A, et al. pROC: an open-source package for R and S^{+} to analyze and compare ROC curves. BMC Bioinformatics 2011; 12: 77. doi: 10.1186/1471-2105-12-77.

32) Lazar S, Goldfinger LE. Platelets and extracellular vesicles and their cross talk with cancer. Blood 2021; 137 (23) : 3192-200. doi: 10.1182/blood.2019004119.

33) Snir O, Wilsgård L, Latysheva N, et al. Plasma levels of platelet-derived microvesicles are associated with risk of future venous thromboembolism. J Thromb Haemost 2022; 20 (4) : 899-908. doi: 10.1111/jth.15638.

34) El-Gamal H, Parray AS, Mir FA, et al. Circulating microparticles as biomarkers of stroke: A focus on the value of endothelial -and platelet- derived microparticles. J Cell Physiol 2019; 234 (10) : 16739-54. doi: 10.1002/jcp.28499.

35) Dweep H, Gretz N, Sticht C. miRWalk database for miRNA-target interactions. Methods Mol Biol 2014; 1182: 289-305. doi: 10.1007/978-1-4939-1062-5_25.

36) Uhlen M, Ponten F. Antibody-based proteomics for human tissue profiling. Mol Cell Proteomics 2005; 4 (4) : 384-93. doi: 10.1074/mcp.R500009-MCP200.

37) Wojta J, Hoover RL, Daniel TO. Vascular origin determines plasminogen activator expression in human endothelial cells. Renal endothelial cells produce large amounts of single chain urokinase type plasminogen activator. J Biol Chem 1989; 264 (5) : 2846-52. PMID: 2492525

38) Diamond SL, Eskin SG, Mclntire LV. Fluid flow stimulates tissue plasminogen activator secretion by cultured human endothelial cells. Science 1989; 243 (4897) :1483-5. doi: 10.1126/science.2467379.

39) Bianchessi V, Badi I, Bertolotti M, et al. The mitochondrial lncRNA ASncmtRNA-2 is induced in aging and replicative senescence in Endothelial Cells. J Mol Cell Cardiol 2015; 81: 62-70. doi: 10.1016/j.yjmcc.2015.01.012.

40) Fitzpatrick C, Bendek MF, Briones M, et al. Mitochondrial ncRNA targeting induces cell cycle arrest and tumor growth inhibition of MDA-MB-231 breast cancer cells through reduction of key cell cycle progression factors. Cell Death Dis 2019; 10 (6) : 423. doi: 10.1038/s41419-019-1649-3.

41) Burzio VA, Villota C, Villegas J, et al. Expression of a family of noncoding mitochondrial RNAs distinguishes normal from cancer cells. Proc Natl Acad Sci USA 2009; 106 (23) : 9430-4. doi: 10.1073/pnas.0903086106.

42) Borgna V, Villegas J, Burzio VA, et al. Mitochondrial ASncmtRNA-1 and ASncmtRNA-2 as potent targets to inhibit tumor growth and metastasis in the RenCa murine renal adenocarcinoma model. Oncotarget 2017; 8 (27) : 43692-708. doi: 10.18632/oncotarget.18460.

43) Farfán N, Sanhueza N, Briones M, et al. Antisense noncoding mitochondrial RNA-2 gives rise to miR-4485-3p by Dicer processing in vitro. Biol Res 2021; 54 (1) : 33. doi: 10.1186/s40659-021-00356-0.

44) Burger D, Kwart DG, Montezano AC, et al. Microparticles induce cell cycle arrest through redox-sensitive processes in endothelial cells: implications in vascular senescence. J Am Heart Assoc 2012; 1 (3) : e001842. doi: 10.1161/JAHA.112.001842.

45) Zhou B, Tian R. Mitochondrial dysfunction in pathophysiolo-

gy of heart failure. J Clin Invest 2018; 128 (9) : 3716-26. doi: 10.1172/JCI120849.

46) Thaler J, Koder S, Kornek G, et al. Microparticle-associated tissue factor activity in patients with metastatic pancreatic cancer and its effect on fibrin clot formation. Transl Res 2014; 163 (2) : 145-50. doi: 10.1016/j.trsl.2013.06.009.

47) Branchford BR, Carpenter SL. The Role of inflammation in venous thromboembolism. Front Pediatr 2018; 6: 142. doi: 10.3389/fped.2018.00142.

48) Signorelli SS, Conti GO, Fiore M, et al. Platelet-derived microparticles (MPs) and thrombin generation velocity in deep vein thrombosis (DVT) : Results of a case-control study. Vasc Health Risk Manag 2020; 16: 489-95. doi: 10.2147/VHRM.S236286.

49) Carrier M, Langner AL, Shivakumar S, et al. SOME Investigators, Screening for occult cancer in unprovoked venous thromboembolism. N Engl J Med 2015; 373 (8) : 697-704. doi: 10.1056/NEJMoa1506623.